2004

An Experimental and Theoretical Investigation fo Axially Symmetric Wave Propagation In Thick Cylindrical Waveguides

Anthony Puckett

AN EXPERIMENTAL AND THEORETICAL INVESTIGATION OF AXIALLY SYMMETRIC WAVE PROPAGATION IN THICK CYLINDRICAL WAVEGUIDES

By

Anthony Puckett

B.S. Colorado State University, 1998

M.S. Colorado State University, 2000

A THESIS

Submitted in Partial Fulfillment of the

Requirements for the Degree of

Doctor of Philosophy

(in Mechanical Engineering)

The Graduate School

The University of Maine

May, 2004

Advisory Committee:

Michael L. Peterson, Associate Professor of Mechanical Engineering, Advisor

Donald A. Grant, Chairman and Richard C. Hill Professor of Mechanical Engineering

Senthil Vel, Assistant Professor of Mechanical Engineering

John Vetelino, Professor of Electrical and Computer Engineering

George T. Gray III, Fellow, Los Alamos National Laboratory, Outside Reader

AN EXPERIMENTAL AND THEORETICAL INVESTIGATION OF AXIALLY SYMMETRIC WAVE PROPAGATION IN THICK CYLINDRICAL WAVEGUIDES

By Anthony Puckett

Thesis Advisor: Dr. Michael L. Peterson

An Abstract of the Thesis Presented
in Partial Fulfillment of the Requirements for the
Degree of Doctor of Philosophy
(in Mechanical Engineering)
May, 2004

Solid circular cylinders as waveguides for the propagation of longitudinal elastic waves are used primarily as buffer rods in high temperature nondestructive evaluation (NDE), and are also found in the split Hopkinson pressure bar (SHPB). Experiments are typically designed so that only the nondispersive range of the first mode propagates. Design constraints sometimes require larger waveguides and higher frequencies that propagate multiple dispersive modes, which can add considerable complexity to the signal.

This thesis presents an analytical model for multiple mode wave propagation in a finite solid cylindrical waveguide as a means of interpreting the complex signals and possibly removing the complexity. The model uses the phase velocities and normal stresses of the axially symmetric modes calculated by the Pochhammer-Chree equations to calculate a transfer function for each of the propagating modes. The sum of the transfer functions of the propagating modes is the transfer function of the waveguide, which can be used to predict the change of a signal in the waveguide.

The ability of the model to accurately capture the general physics of multiple mode wave propagation is demonstrated in the time, frequency and joint time-frequency domain. In the time-reversal domain the calculated dispersed signal for a dispersive multi-mode waveguide is shown to produce a signal with compact support in the time domain. A range of diameter to wavelength ratios is considered for these comparisons, which show the limitations of the model for wavelengths less than the radius.

The transfer functions generated by the model indicate which modes are dominant over a particular range of frequencies and which modes have a much smaller magnitude. The transfer functions further indicate that broadband signals are composed of multiple modes. It is found that observed trailing

pulses contain energy from multiple propagating modes, and it is the superposition of the modes that creates the trailing pulses. The information from the transfer functions is also used to show the conditions for a sufficiently narrow band signal to excite a single higher order mode with little dispersion.

ACKNOWLEDGMENTS

This research was sponsored by the Missile Defense Agency through Dr. Y. D. S. Rajapakse of the Office of Naval Research. Additional support was provided by the National Science Foundation (NSF) GK-12 "Sensors!" grant at the University of Maine. The assistance of S. Vel on the least squares method expansion is also appreciated.

The author is deeply grateful to his wife, Leslie, for her encouragement and putting up with three Maine winters during the completion of the dissertation.

TABLE OF CONTENTS

LIST OF TABLES

LIST OF FIGURES

CHAPTER 1: INTRODUCTION

1.1. Motivation

The use of solid circular cylindrical rods as waveguides generally falls into two major areas: ultrasonic nondestructive analysis and the split-Hopkinson pressure bar. In both areas, acoustic signals propagated through the waveguides are occasionally of sufficiently high frequency to excite multiple dispersive modes. These signals are highly complex and information carried by the signals is difficult to extract. This research is primarily motivated by the need for an analytical model to interpret these signals and to provide a more complete basic understanding of multiple mode axially symmetric wave propagation in finite cylindrical waveguides. For this research only linearly elastic, isotropic, homogeneous cylindrical bars are considered.

1.1.1. Split Hopkinson Pressure Bar

In 1914 B. Hopkinson developed a technique for determining the pressure pulse from bullets and high explosives by measuring the momentum trapped in a cylindrical bar. A modified version of the technique, known as the split-Hopkinson pressure bar (SHPB), Davies bar (Davies 1948), or Kolsky bar (Kolsky 1949), is used extensively today to determine the strain rate dependency of elastic properties of materials. For a general review of SHPB see the manuscript by Gray (2000). The theory used to determine the elastic properties from the SHPB is often based on one-dimensional wave theory in the transmission bars. At higher strain rates the assumption of one-dimensional theory introduces greater error. The fast rise in the pulse necessary for high strain rates requires energy at higher frequencies. These higher frequencies excite not only the first mode in the dispersive range but can also excite the second mode (Tyas 2000). If only the first mode is excited a dispersion correction is often used to improve results (Gong, Malvern, and Jenkins 1990). Determination of the elastic properties with confidence under dispersive conditions is more difficult. An analytical model of axially symmetric waves in the solid cylindrical transmission bars for high frequency ranges can provide additional insight into the interpretation of the one-dimensional theory and the effects of typical simplifications.

1.1.2. Nondestructive Evaluation

In nondestructive evaluation (NDE) solid cylindrical waveguides are typically used as buffer rods to isolate ultrasonic transducers from hostile environments (Jen et al. 1991, Jen et al. 1997, Peterson 1994). As with the SHPB the excitation and propagation of only the first mode in the nondispersive frequency range is desired. However, due to design constraints it is often not possible to use a waveguide that is sufficiently thin to propagate only the first axially symmetric mode. In sensor applications a number of approaches have been taken to eliminate the propagation of multiple modes, including the bundling of thin waveguides, cladding of buffer rods and introduction of surface roughness to eliminate spurious signals (e.g., Thurston 1978, Jen et al. 1990). However, in some cases design constraints make the use of a multi-mode waveguide necessary (Peterson 1994). The propagation of multiple modes causes a signal that is compact in the time domain to have a large time signature after propagating through the waveguide, Fig 1.1. As a result, if the acoustic signal is propagated through a specimen, as well as a buffer rod, phase velocity and attenuation information about the specimen are difficult to extract. While a number of approaches have been considered to solve this problem, the processing is highly complex (Peterson 1999).

There are two specific applications of direct interest that utilize the multiple mode waveguide. The first is the determination of elastic constants of materials or other properties at high temperatures, over 200 °C and up to 2000 °C. Multiple mode solid cylindrical waveguides are used as buffer rods in a through transmission configuration or a pulse echo configuration to couple a high temperature material to a room temperature transducer. At high temperatures, ultrasound is currently the only method to measure shear modulus accurately. This is also the most accurate method available for measuring the Young's modulus (Hearmon 1984). A new motivation is a novel sensor for measuring the glass transition temperature of polymers and specifically composites to determine the extent of curing. For this application the temperature is swept from –40 °C to over 200 °C, and the wave speed is measured. A thick cylindrical waveguide is used as a buffer rod to isolate the transducer from the at temperature sample, in a pulse echo configuration. While this technique has only seen limited application, it has the potential to eliminate problems with boundary conditions in conventional dynamic mechanical thermal analysis (DMTA).

The disadvantage of the complexity of the signal from a multiple mode waveguide can be removed by the use of time reversal, which has been developed during the last ten years (Fink 1997). Time

reversal allows a signal with compact support in the time domain to be created in a multiple mode waveguide by modifying the excitation signal. The appropriate signal is easily found in a pulse-echo configuration where the same transducer excites and receives the ultrasonic signal. It is more difficult to determine the required excitation in a through transmission configuration. The analytical model presented in this work is one method of finding the required excitation.

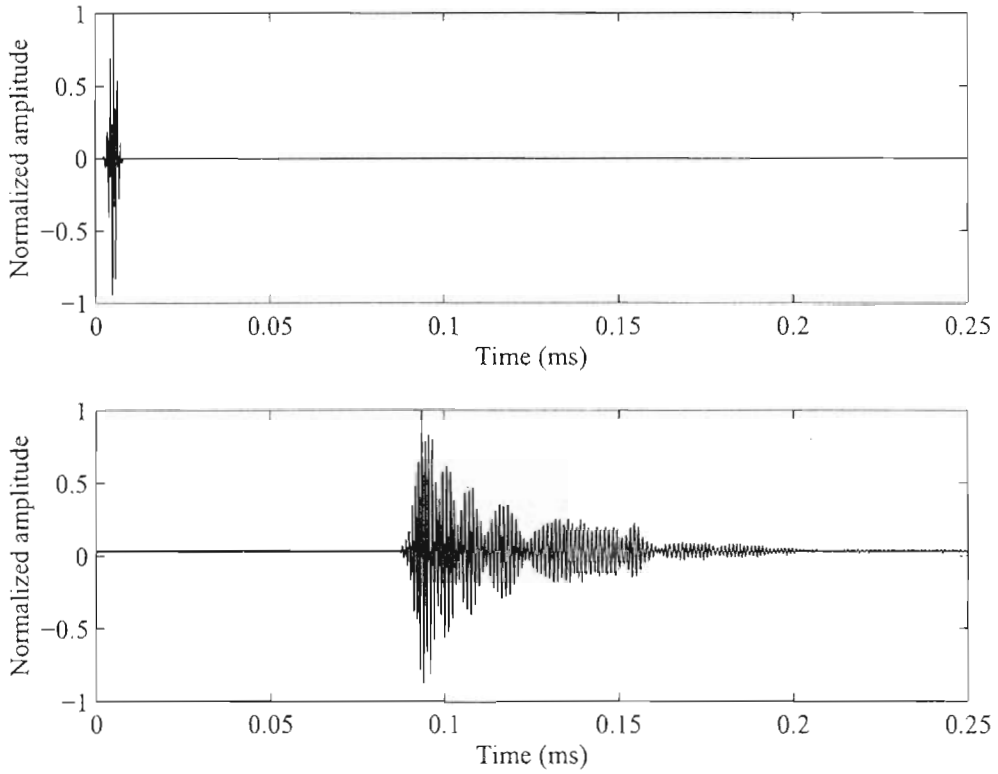

Fig. 1.1. Illustration of dispersion in a cylindrical waveguide. The top graph is the original signal with compact time domain. The bottom graph is the original signal after propagating through the cylindrical waveguide used in this research.

1.1.3. Basic Science

Research on wave propagation in circular cylindrical waveguides was at first a purely academic exercise in elasticity with no driving application. Mathematical equations were developed that described the propagation of waves with little, if any, physical understanding. Since then circular cylindrical waveguides have been explored extensively analytically and experimentally. The analytical models typically agree with the experiments; however, except for a couple of cases the comparisons are not

explored extensively. As such, the relation between the Pochhammer-Chree theory and what physically happens in a waveguide is not fully understood. The successive development and evaluation of an analytical model with experiments will improve the basic understanding of axially symmetric wave propagation in cylindrical waveguides, specifically regarding trailing pulses and the role of higher order modes.

1.2. Scope of Dissertation

Research on wave propagation in cylindrical bars spans more than a century with hundreds of contributions. The most pertinent contributions to this research are presented and discussed, so that a general understanding of axially symmetric wave propagation in infinite cylindrical rods is accessible. The contributions on the development of an analytical model for transient wave propagation in semi-infinite and finite cylindrical bars are also presented.

For the case of axially symmetric wave propagation in a finite cylindrical bar, an analytical model is developed to improve the understanding of the physics of cylindrical waveguides. The two primary experimental ultrasonic configurations involving cylindrical waveguides are the through transmission and pulse echo configurations. The configurations and experimental considerations are discussed along with the theory of time reversal in solid cylindrical waveguides.

The primary focus of this dissertation is the development and validation of an analytical model for wave propagation in finite solid cylindrical waveguides. The analytical model uses the phase velocities and stress functions from the Pochhammer-Chree theory to determine the shape of a dispersed signal. The model considers the interactions in a common experimental configuration that uses cylindrical waveguides. The excitation of the waveguide from the ultrasonic transducer, the propagation of the waves, and the reception of the waves of the receiving transducer are each considered.

The ability of the model to accurately capture the physics of multiple mode wave propagation is validated by considering several different domains. In the time domain and the frequency domain the dispersed signals calculated by the analytical model are compared to the experimentally measured dispersed signals for the same waveguide. In the time-reversal domain the calculated dispersed signal is shown to produce a signal with compact time domain in a dispersive waveguide using a time-reversal mirror. In the time-frequency domain the spectrograms of the analytical and experimental signals

demonstrate the presence of the same modes in each signal. In all three domains it is shown that the model captures the physics of multiple mode wave propagation in cylindrical waveguides. The comparisons between the analytical signals and the experimental signals are extended to a range of diameter-to-wavelength ratios, d/λ_L, from 0.5 to 20, where λ_L is calculated using the longitudinal wave speed, c_L. For both ends of the range the model demonstrated results comparable to the experiments.

The nature of the model allows each individual mode to be considered, so that the signal generated by a single mode can be determined. Thus, an observed experimental signal can be understood in terms of the individual propagating modes. The experimentally observed trailing pulses are interpreted in terms of the propagating modes of the Pochhammer-Chree theory. Information provided by the analytical model is used to demonstrate the conditions for the propagation of a single higher order mode in a cylindrical bar.

1.3. Thesis Statement

An analytical model of axially symmetric wave propagation in a multiple mode cylindrical waveguide is developed and validated to extend the use of multiple mode waveguides as a useful diagnostic tool.

CHAPTER 2: BACKGROUND

The propagation of waves has been a topic of interest in mathematics and mechanics for over 200 years. The general behavior of the propagation of elastic waves in solids was extensively developed during the 19th century. Only in the last part of the 20th century has wave propagation in cylindrical rods been extensively investigated. The rich area of research that has developed in this area is considered in this section. The main focus of this section is the research concerning the propagation of axially symmetric waves in circular cylindrical rods.

The first derivations of the equations for three-dimensional longitudinal wave propagation in a solid cylinder were developed independently by Pochhammer in 1876 and Chree in 1889. The full Pochhammer-Chree theory describes the axially symmetric, torsional, and flexural wave propagation in an infinite solid circular cylinder with traction free surfaces. Torsional modes are characterized by a circumferential displacement that is independent of the circumferential angle. Axially symmetric modes are also independent of the circumferential angle but are characterized by axial and radial displacements. The displacements of flexural modes, however, are dependent on the circumferential angle. For anisotropic materials, an axially symmetric excitation of a cylindrical bar will excite flexural modes in addition to the axially symmetric modes. However, this research is focused on linearly elastic isotropic solid cylinders and the propagation of axially symmetric waves.

After the development of the Pochhammer-Chree theory continuing research on axially symmetric wave propagation in cylinders was concerned with three areas. One area of research was furthering the understanding of the Pochhammer-Chree frequency equation and exploring the equation numerically. Despite the completeness of the wave equation few analytical results were developed in the beginning because of the complexity of the relationships in the Pochhammer-Chree theory. A second area of research was the exploration of one-dimensional approximations to the Pochhammer-Chree frequency equation. As the understanding of the Pochhammer-Chree theory increased, a third area of research emerged that focused on developing exact and approximate transient solutions for axially symmetric wave propagation in semi-infinite bars. Additional efforts were focused on the use of solid cylinders as delay lines and waveguides.

This thesis is concerned with the first and last areas of research; exploration and understanding of the Pochhammer-Chree solution and the development of three-dimensional analytical models for axially symmetric wave propagation in finite and semi-infinite cylinders. Previous research in these two areas is discussed in the following sections. For a more complete history of wave propagation in cylindrical waveguides, several review papers provide perspective on practical as well theoretical work. The review paper by Julius Miklowitz (1966) covers the research up until 1964. Al-Mousawi (1986) reviews mainly the experimental side, and Thurston (1978) reviews elastic waves in rods and clad rods through August 1977. The monograph on elastic waveguides was also published by Redwood (1960). The texts by Achenbach (1999) and Graff (1975) cover more generally wave propagation in elastic solids.

2.1. Axially Symmetric Wave Propagation in Infinite Linearly Elastic Isotropic Cylinders

2.1.1. Pochhammer-Chree Theory

The Pochhammer-Chree theory is considered valid for the cases of compressional, flexural and torsional waves in an infinite rod. This thesis is focused on compressional (also known as longitudinal and dilatational) wave propagation referred to as axially symmetric wave propagation in this dissertation. For reference to the background research and other solution techniques, a brief derivation of the Pochhammer-Chree solution for axially symmetric wave propagation in an infinite cylinder with traction free boundaries is presented in conjunction with the background[1].

The derivation of the Pochhammer-Chree frequency equation starts with the displacement equation of motion,

$$\mu\nabla^2\underline{u}+(\lambda+\mu)\underline{\nabla}\underline{\nabla}\cdot\underline{u}=\rho\ddot{\underline{u}}\,, \tag{2.1}$$

where $\underline{u}$ is the displacement vector, ρ is the density, and λ and μ are Lamé constants. The method of potentials is most suited to solving this differential equation. When the displacement vector is of the form,

$$\underline{u}=\underline{\nabla}\varphi+\underline{\nabla}\times\underline{\psi}\,, \tag{2.2}$$

---

[1] This derivation follows Achenbach (1999). A more complete derivation of the Pochhammer-Chree frequency equation is developed in Zemanek (1962).

where φ and $\underline{\psi}$ are the scalar and vector potentials respectively, two differential equations are produced,

$$\nabla^2\varphi = \frac{1}{{c_L}^2}\ddot{\varphi} \qquad c_L = \sqrt{\frac{\lambda + 2\mu}{\rho}}, \tag{2.3}$$

$$\nabla^2\underline{\psi} = \frac{1}{{c_T}^2}\ddot{\underline{\psi}} \qquad c_T = \sqrt{\frac{\mu}{\rho}}, \tag{2.4}$$

where c_L is the velocity of longitudinal waves in an unbounded medium and c_T is the velocity of transverse waves in an unbounded medium. For axially symmetric wave propagation in cylindrical coordinates the two solutions are:

$$\varphi = AJ_0(pr)\exp[i(kz - \omega t)] \qquad p^2 = \frac{\omega^2}{{c_L}^2} - k^2 \tag{2.5}$$

$$\psi_\theta = CJ_1(qr)\exp[i(kz - \omega t)] \qquad q^2 = \frac{\omega^2}{{c_T}^2} - k^2. \tag{2.6}$$

where J_0 and J_1 are Bessel functions of the first kind of order zero and one respectively. r and z define the radial and axial coordinates respectively. The wavenumber, k, is equal to ω/c where ω is the circular frequency, and c is the phase velocity. a is the radius of the cylinder. In terms of the potentials, the radial and axial displacements, respectively, are expressed as,

$$u = \frac{\partial\varphi}{\partial r} - \frac{\partial\psi_\theta}{\partial z} \text{ and } w = \frac{\partial\varphi}{\partial z} + \frac{\psi_\theta}{r} + \frac{\partial\psi_\theta}{\partial r}. \tag{2.7}$$

The circumferential displacement, v, is zero because of the symmetry. The displacements define the stresses through the relations,

$$\sigma_{zz} = \lambda\left(\frac{\partial u}{\partial r} + \frac{u}{r} + \frac{\partial w}{\partial z}\right) + 2\mu\frac{\partial w}{\partial z}, \ \sigma_{rr} = \lambda\left(\frac{\partial u}{\partial r} + \frac{u}{r} + \frac{\partial w}{\partial z}\right) + 2\mu\frac{\partial u}{\partial r}, \ \sigma_{rz} = \mu\left(\frac{\partial u}{\partial z} + \frac{\partial w}{\partial r}\right). \tag{2.8}$$

The substitution of the solutions, Eqs. (2.5) and (2.6) into the displacements, Eq. (2.7), and the displacements into the stress equations, Eq. (2.8) and the application of the traction free boundary conditions at the surface ($r = a$) produces the frequency equation,

$$\frac{2p}{a}\left(q^2 + k^2\right)J_1(pa)J_1(qa) - \left(q^2 - k^2\right)J_0(pa)J_1(qa) - 4k^2pqJ_1(pa)J_0(qa) = 0. \tag{2.9}$$

The frequency equation describes the modes of both longitudinal vibration and transient wave propagation and provides the relation between the wavenumber, k, and the frequency, ω (Miklowitz 1966). In

particular, the dispersive nature of the waves for all propagating modes in the three-dimensional cylinder is described. The frequency equation is often the point at which the analysis ends. However, the frequency equation of the Pochhammer-Chree theory is a purely mathematical concept without a link to the physical understanding of axially symmetric wave propagation in a solid cylinder. When the original work was performed this physical interpretation did not exist. Due to the complexity of the equation, numerical exploration of the solution was limited until the advent of the digital computer.

Early research exploring the Pochhammer-Chree theory does not provide significant insight for this work. However, the work of these early authors (i.e. Field 1931, Bancroft 1941) did pave the way for future research. The first significant contribution to the understanding of axially symmetric wave propagation in cylindrical waveguides and the Pochhammer-Chree theory was an extensive manuscript by Davies (1948). Davies performed extensive analytical calculations of the Pochhammer-Chree theory as well as numerous experiments. From numerical calculations of the frequency equation (Eq. 2.9) he plotted the phase velocity of the first three modes as well as the group velocity of the first two modes. An example of the dispersion curves and the group velocity curves appear in Fig. 2.1. Davies also demonstrated that for each mode the magnitude of the stress and displacement vary across the radius of the bar and vary with frequency, see Fig. 2.2.

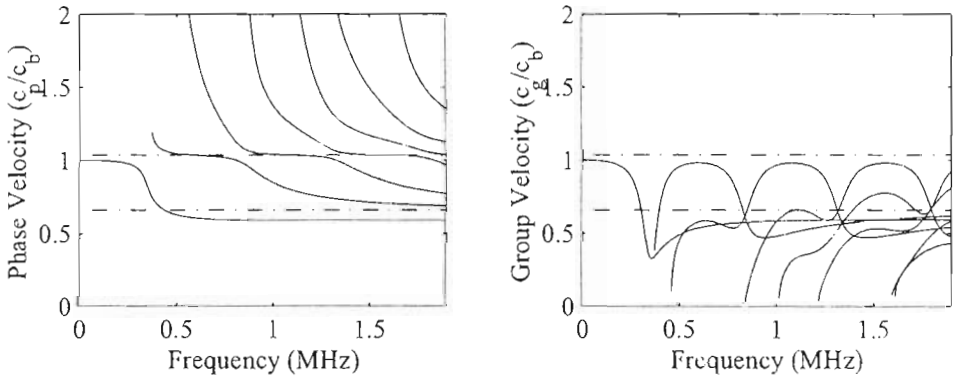

Fig. 2.1. Example of phase velocity and group velocity curves for a 10 mm solid cylindrical quartz waveguide.

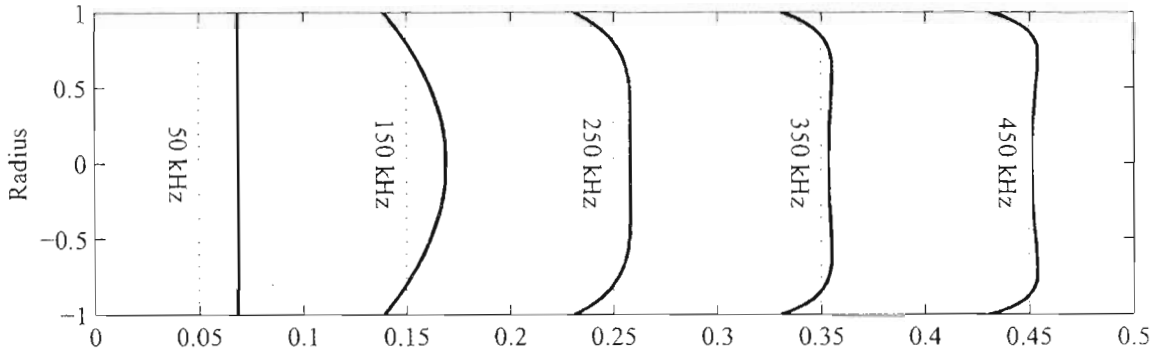

Fig. 2.2. Example of frequency dependence of normal stress for the 1st mode of a 10 mm solid cylindrical quartz waveguide. The normalized normal stress is plotted at different frequencies. The vertical dashed lines represent zero stress.

Some of the significance of Davies work is also a result of improved experimental techniques. Davies introduced a way to measure the axial and radial displacements separately on a circular bar. He produced experimental results using a Hopkinson bar, which were in good agreement with the Pochhammer-Chree theory and confirmed the phenomenon of dispersion experimentally (Al-Mousawi 1986). Davies research was a major contribution to the field and marked the beginning of a surge of research on wave propagation in solid cylinders that lasted about two decades.

The next major step was the recognition of the need for and the prediction of complex roots to the frequency equation. At low frequencies there is only a single propagating mode whose stress is a function of radius and frequency. At higher frequencies there is still only a finite number of propagating modes. However, for an arbitrary pressure distribution on the end of the bar it is necessary to be expand over an infinite number of stress functions that result from an infinite number of modes. Curtis (1953) is generally credited with recognizing and predicting the complex roots of the frequency equation, and an exploration of the frequency equation by Adem (1954) found the required infinite number of modes (Zemank 1972). Onoe, McNiven, and Mindlin (1962) presented an extensive mapping of the relation between the frequency and propagation constant (i.e. nondimensional phase velocity) from the Pochhammer-Chree frequency equation. Real, imaginary and complex propagation constants were calculated for a large frequency spectrum. The influence of Poisson's ratio was also explored. The work by Onoe, McNiven, and Mindlin produced a better understanding of the roots of the frequency equation but little physical interpretation.

Using the recent research of Onoe, McNiven and Mindlin, Zemanek's Ph.D. dissertation (1962) extended the work by Davies. Zemanek extensively explored the higher order modes numerically, and made some key observations of the properties of the Pochhammer-Chree theory. First, the maxima of the group velocity curves of higher order modes approach the wave speed of longitudinal waves in an infinite medium. Secondly, the axial displacement of the higher order modes is in phase near the maximum group velocity. At frequencies not associated with the maximum group velocity the axial displacement along the radius is out of phase and the average displacement approaches zero. An additional contribution of Zemanek was the experimental verification of the theoretical dispersion curves.

A number of experimental observations were also made during the same period. Tu, Brennan, and Sauer (1955) and Oliver (1957) also reproduced experimentally the theoretical developments of the Pochhammer-Chree theory, although primarily the first mode. McSkimm (1956) and Redwood (1959) observed trailing pulses in experiments with sine burst excitations. Meitzler (1960 and 1965) performed experimental work on the propagation of elastic pulses in cylinders.

2.1.2. General Understanding

Between the experimental research and the research of Davies, Onoe et al., and Zemanek a foundation is provided for the understanding of the Pochhammer-Chree theory and the behavior of elastic wave propagation in cylindrical waveguides. A brief review of the general understanding of the Pochhammer-Chree theory is advantageous for future discussions.

The Pochhammer-Chree theory is a time-harmonic solution that describes wave propagation in an infinite isotropic homogeneous solid circular cylinder. The solutions assume a loss free material and do not consider viscous effects. Despite the loss free assumption, the behavior of the solution is quite complex. Evaluation of the frequency equation is one of the key elements of the problem since the frequency equation provides the multiple solutions that are available.

Frequency Equation

The frequency equation is a transcendental equation that relates the frequency to a propagation constant such as the wavenumber, k, or phase velocity, c. At any frequency there are an infinite number of roots that satisfy the frequency equation. Each root is associated with a single mode. At the lowest frequencies there is only one root that is real, the others being imaginary and complex. This one real root

corresponds to the first propagating mode, and it is the only mode that propagates at the low frequencies. As the frequency is increased complex roots of the frequency equation become real, so at higher frequencies there is more than one propagating mode. The frequency where a root first becomes real is the cutoff frequency. The second and third modes are an exception and become real before the second and third cutoff frequencies respectively (for example Meiztler 1965). The cutoff frequency is the frequency at which the wave number is equal to zero, and thus the phase velocity is infinite. The cutoff frequencies can be found by simplifying the frequency equation for $k \rightarrow 0$. At frequencies greater than a mode's cutoff frequency the mode the propagation constant is real and the mode propagates. Below the cutoff frequency a mode is either evanescent, with a complex wavenumber, or nonpropagating with an imaginary wavenumber. Since the time harmonic solution is of the form $exp[ikx]$, when the wavenumber becomes imaginary, $k \rightarrow ik$, the solution becomes $exp[-kx]$, which attenuates and does not propagate. At each frequency all of the modes have associated stresses and displacements.

Stress and Displacement Functions

The radial displacement, $u^{(j)}$, and the axial displacement, $w^{(j)}$, in cylindrical coordinates, associated with mode j, referred to later as displacement functions, are defined as:

$$u^{(j)} = -[pJ_0(pr) + iC^{(j)}k^{(j)}J_1(qr)], \tag{2.10}$$

$$w^{(j)} = ik^{(j)}J_0(pr) + C^{(j)}qJ_1(qr), \tag{2.11}$$

$$\text{where } C^{(j)} = \frac{-2ik^{(j)}pJ_1(pa)}{(q^2 - (k^{(j)})^2)J_1(qa)} \tag{2.12}$$

and $k^{(j)}$ is the wavenumber (Fraser 1975). The axial (normal) stress, $\sigma^{(j)}_{zz}$, and shear stress, $\sigma^{(j)}_{rz}$, associated with mode j, referred to later as stress functions, are defined as:

$$\sigma^{(j)}_{zz} = -J_0(pr)[\lambda(p^2 + (k^{(j)})^2) + 2\mu(k^{(j)})^2] + 2\mu C^{(j)}iqk^{(j)}J_0(qr), \tag{2.13}$$

$$\text{and } \sigma^{(j)}_{rz} = -\mu[2ik^{(j)}pJ_1(pr) + C^{(j)}(q^2 - (k^{(j)})^2)J_1(qr)]. \tag{2.14}$$

The radial normal stress is not of interest for this problem. The factor $exp(ik^{(j)}z - i\omega t)$ that appears in the potential solutions, Eqs. 2.5 and 2.6, has been suppressed. The stresses and displacements are a function of both radius and frequency as shown in Fig. 2.2.

The fact that the stress and displacement functions change with frequency makes it necessary to obtain the functions at each frequency in the analytical model. The stress and displacement functions are complex valued. Thus, the axial stress, $\sigma^{(j)}_{zz}$, of a mode at each point across the radius has a complex value. If the stress is represented as a magnitude (positive valued) and phase angle it will be seen that for the propagating modes the stress along the radius is in phase or pi radians out of phase. At the frequency nears the maximum group velocity of a mode the stress of all of the points become in phase acting more like a "piston". This was observed by Zemanek (1962). Redwood and Lamb (1957) also observed this phenomenon when the phase velocity of a mode is nearest to the longitudinal wave speed the stress function of that mode is in phase. A comparison of the phase velocity curves and the group velocity curves in Fig. 2.1 shows that plateaus of the individual modes near the longitudinal wave speed in the phase velocity curves correspond to the maximum group velocity, which is also near the longitudinal wave speed.

Evanescent Modes

The evanescent modes with complex propagation constants behave differently than the propagating modes. The real component indicates the mode propagates, and the imaginary component indicates the mode attenuates spatially. However, this represents a loss of energy. Pilant (1960) explained that a pair of the complex modes, one traveling in the +z direction, one traveling in the –z direction, are always generated simultaneously with propagation constants that are negative complex conjugates (Zemanek 1972). These two traveling waves form a standing wave, which decreases in amplitude spatially. Standing waves do not represent a transport of energy, so the evanescent modes do not represent a transport of energy.

The evanescent modes are important for problems involving finite and semi-infinite waveguides because the evanescent modes are required to satisfy the boundary conditions on the end of the bar. For low frequencies with only a single propagating mode, the mode shape of the first mode is not sufficient to satisfy an arbitrary stress function on the end of the bar. The shapes of the infinite number of evanescent modes allow an arbitrary stress function to be represented by an expansion over the modes.

Phase Velocity

Each mode has a phase velocity and a group velocity at each frequency. The phase velocity of a mode approaches infinity at the cutoff frequency. This is equivalent to a wavenumber that is equal to zero.

Even at frequencies above the cutoff frequency the phase velocity is greater than the wave speed of either a longitudinal wave or a shear wave in an infinite medium. This is not unreasonable because the phase velocity represents the propagation of constant phase. To visualize a phase velocity greater than a material's wave-speed, the propagation of plane waves oblique to a plane is used, Fig. 2.3. Lines of constant phase travel a distance $d/cos\theta$ along the waveguide during the same time the wave front travels a distance d. As θ approaches pi/2 the distance and therefore the phase velocity approaches infinity.

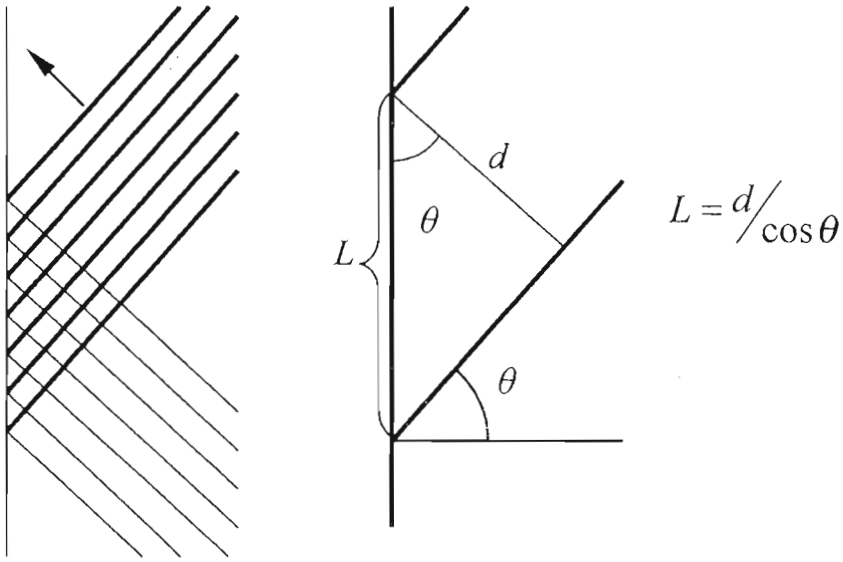

Fig. 2.3. Plane wave illustration of phase velocity

Group Velocity

It can also be seen that the energy of the wave front has only moved a distance $dcos\theta$ along the length of the waveguide, Fig. 2.4. This is the group velocity, which represents the propagation of the energy. For θ equal to zero the energy propagates at the wave speed, as does the phase velocity. As θ approaches $\pi/2$ the group velocity approaches zero. The group velocity can also be calculated from the roots of the Pochhammer-Chree frequency equation by finding the derivative $d\omega/dk$. The consideration of plane waves illustrates why the phase velocity is never slower than the transverse wave speed and why the group velocity is never greater than the longitudinal wave speed in Fig. 2.1. For θ equal to zero, the lines of constant phase and the energy travel the same distance in the same time, and therefore have the same wave speed. As θ increases the distance the lines of constant phase travel increases and the distance the energy travels decreases corresponding to an increase in the phase velocity and a decrease in the group

velocity. Therefore the fastest group velocity is associated with longitudinal plane waves at θ equal to zero, and the slowest phase velocity is associated with transverse plane waves at θ equal to zero.

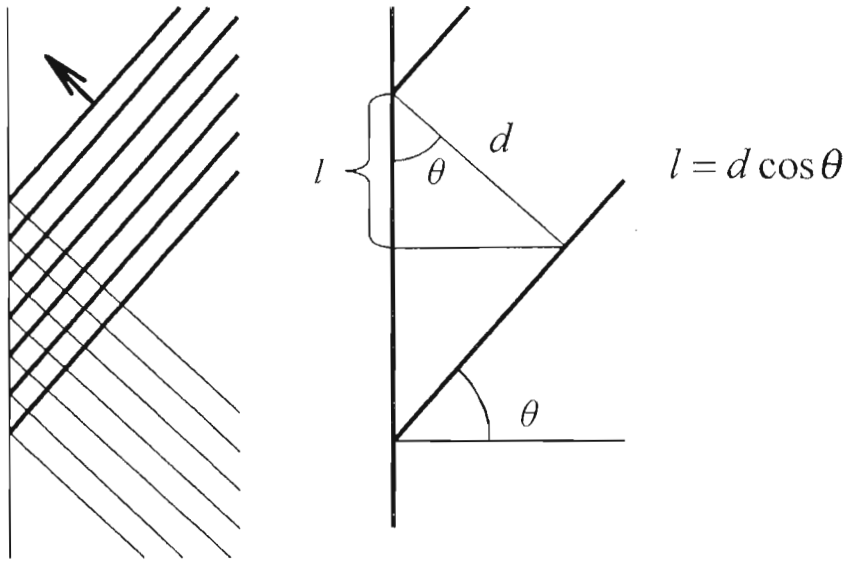

Fig. 2.4. Plane wave illustration of group velocity

Plane Wave Representation

Besides the phase and group velocity, the consideration of plane wave propagation in cylinders can also be used to understand the cylinder's dispersive nature. There are two phenomena of plane waves that explain the various arrival times of waves consistent with a signal exhibiting geometrical dispersion. First, there are multiple paths from one end of the waveguide to the other due to reflections, Fig 2.5 (top). Two sets of plane waves traveling at different angles will travel different length paths from one end of the cylinder to the other. Two sets of plane waves with the same wave speed will arrive at different moments in time. Additionally, at the free boundary a longitudinal wave will excite a longitudinal wave and a transverse wave to satisfy the traction free boundary conditions, Fig. 2.5 (bottom) (i.e. Graff 1975). A transverse wave will reflect a transverse wave and may also excite a longitudinal wave. The slower wave speed of the transverse wave also contributes to the varied arrival times of the waves.

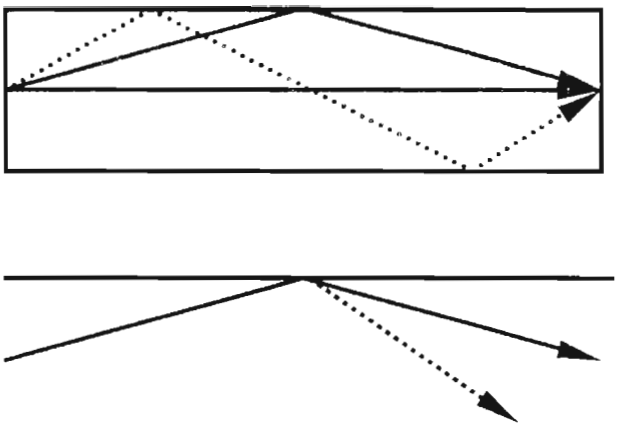

Fig. 2.5. Plane wave description of dispersion illustrating multiple paths (top) and wave excitation.

The plane wave solutions can be related to the solutions of the differential equations by considering an infinite number of plane waves. The cylindrical geometry of the system produces Bessel functions in the solutions to the differential equations. A cylindrical wave with the shape of a Bessel function can be synthesized from an infinite number of plane longitudinal waves by using Sommerfeld's integral to integrate a plane wave solution over 360° (Redwood, 1960; Peterson 1994). A Bessel function is also synthesized from an infinite number of plane transverse waves. The functions that describe the stress and displacement across the radius for a mode contain two terms. One term is a Bessel function that represents the superposition of plane longitudinal waves, and the other term is a Bessel function that represents the superposition of plane transverse waves.

2.2. Wave Propagation in Semi-infinite and Finite Cylinders

The Pochhammer-Chree theory describes the solutions for wave propagation in an infinite cylindrical waveguide. However, from an experimental point of view, a solution that predicts the shape of a signal after propagating through a finite cylinder is more advantageous and useful. But the addition of a face to the cylinder and the associated boundary condition complicates the problem.

A separation-of-variables technique can be used to solve the differential equations, Eq. 2.3 and Eq. 2.4. The solutions to the ordinary differential equations in time, t, and the axial coordinate, z, are exponential in form, Eq. 2.5 and 2.6. The ordinary differential equation in the radial coordinate, r, is a form of Bessel's equation. Bessel's equation has the form of a Sturm-Liouville problem. However, the

stress free boundary conditions at the surface are functions of the second derivative of the potential, which do not satisfy the boundary conditions specified by the Sturm-Liouville (for example, Greenberg 1978). The application of the boundary conditions still produces a characteristic equation (the Pochhammer-Chree frequency equation), which defines the eigenvalues (propagation constant such as the wavenumber). However, the eigenvalues are complex, which indicates the differential operator is non-self-adjoint. The properties of the Sturm-Liouville theory, including the orthogonality conditions, are only applicable to self-adjoint operators. Thus, axially symmetric wave propagation in finite and semi-infinite cylindrical waveguides is considerably more complicated than Sturm-Liouville problems.

Two approaches have been taken to develop three-dimensional analytical solutions to the problem of axially symmetric wave propagation in a semi-infinite isotropic elastic cylinder. The first approach uses the phase velocities (eigenvalues) and stress functions (eigenfunctions) of the Pochhammer-Chree theory to predict the propagation of a signal. The second method solves the boundary value problem for a semi-infinite cylindrical rod subjected to an initial condition. An integral transform technique is used to solve these equations. In both cases there are difficulties and approximations are required.

2.2.1. Integral Transform Technique

The integral transform technique has been used by a number of authors for different initial conditions. Skalak (1957) considered an infinite cylinder, solving the differential equations for a set of boundary conditions that modeled the collision of two semi-infinite cylinders. Skalak considered the cylinders just after impact, and assumed the two cylinders behaved as a single, solid, infinite cylinder. The solution consisted of the superposition of two parts. The first part of the solution modeled the impact with the additional constraint that the lateral displacement be equal to zero everywhere. The wave from the impact is nondispersive and will travel at the longitudinal wave speed. For the second part the lateral restraint required for zero lateral displacement is calculated from part one and applied as an outward radial traction that travels with the wave. The superposition of these two parts produces a traction free bar. The solution for part two used a double integral transform technique with a Laplace transform in time and a Fourier integral transform in the axial coordinate, z. The differential equations were transformed and a solution in the transformed space was found. To find the actual displacement the inverse transforms are applied to the transformed solution. The integrals are evaluated by Cauchy's residue theorem. Two poles

are determined from the loading conditions, and the remaining poles are determined from the roots of the Pochhammer-Chree frequency equation, which appears in the denominator of the integral. Due to the difficulty of the transform inversions, an approximate solution was found for large time using the first two terms of the expansion of the phase velocity about $k=0$ for the first mode. The calculated shape of the wave front at large time agreed well with Davies (1948) approximate solution.

Vales *et al.* (1996) completed the exact solution started by Skalak. With 40 years of progress in computer technology, Vales *et al.* were able to extend Skalak's decomposition to the near field with extensive numerical calculations. Evidence of von Schmidt waves from a glancing incidence plane wave was observed in the numerical calculations. This solution however is only valid for the specific case of the impact of two bars.

Not long after Skalak, Folk *et al.* (1957) developed a solution for a semi-infinite bar loaded with a step pressure function at the end. A uniform pressure was applied to the end of the bar, and the end of the bar was constrained from displacing laterally. The mixed end conditions were used to uncouple the equations of motion. The proper combination of transforms was chosen to provide solutions of the differential equations as well as "ask" for the appropriate initial and boundary conditions. Again the inverse transforms are evaluated using the Cauchy residue theorem, with all of the poles defined by the Pochhammer-Chree frequency equation. Asymptotic solutions were obtained to solutions valid at large time.

Fox and Curtis (1957) showed experimentally that the mixed end condition solution introduced by Folk *et al.* predicted accurately the main features of a step function excitation in a semi-infinite bar with pure end conditions for distances larger than 20 diameters. Jones and Norwood(1967) used the method of Folk *et al.* to investigate the axially symmetric longitudinal response of a semi-infinite elastic bar to a pressure step end loading and to a velocity impact end loading. They found at distances greater than 20 diameters the approximate solutions were within one percent of each other. Although, no experimental comparisons were made. They discussed this small difference in terms of a dynamic Saint-Venant's principle. Kennedy and Jones (1969) further explored the effects of different radial distributions on the response of a waveguide to a pressure step end loading. Again it was found the difference in peak values

was insignificant at distances over 20 diameters, and the difference in average values was insignificant at distances of 5 diameters. Again, only analytical results were considered.

Goldberg and Folk (1993) extended the method of Folk *et al.* to solve the pure-end-condition problem. Goldberg and Folk obtained the solution to two mixed-end-condition problems, and used these solutions to solve the pure-end-condition problem. These results also agree well with the experimental work of Curtis and Fox. For large distances the approximate solutions for wave propagation in cylindrical waveguides developed by the integral transform method are representative of the step function experiment of Fox and Curtis (1957).

2.2.2. Pochhammer-Chree Solutions

A number of analytical models have been developed from the Pochhammer-Chree solutions to predict aspects of axially symmetric wave propagation in finite and semi-infinite cylindrical bars. Davies (1948) used the phase velocities from the frequency equation and a Fourier decomposition to predict the change in shape of a trapezoidal (first mode only) excitation in a finite cylindrical bar; however, no experimental comparison was made. In a similar method Follansbee and Frantz (1983) calculated a dispersion correction for signals measured in the split Hopkinson pressure bar (SHPB).

Zemanek (1962) considered the stresses of the modes to determine the reflection of the first mode incident on the free end of a cylindrical bar. In addition to the fundamental mode, modes with complex wave numbers were considered in an expansion to satisfy the stress free boundary conditions. Reflection coefficients were calculated from a system of equations equal to the number of modes considered, and an end resonance was observed. Gregory and Gladwell (1989) also considered the reflection of the first mode but calculated the coefficients in the expansion using an integral formulation of least squares. The resonant frequency observed by both Zemanek and Gregory and Gladwell was very close to the experimental frequency measured by Oliver (1957). However, this was the only experimental comparison in either case.

The orthogonality conditions are typically used to determine the coefficients in an expansion; however, the orthogonality conditions for a cylinder with stress free lateral boundary conditions are quite complicated. The orthogonality conditions have been developed for the elastostatic case by Power and Childs (1971) and more completely by Fama (1972). Fraser (1975) extended Fama's solutions to the

elastodynamic case. The complexity of the orthogonality conditions makes alternate methods desirable for determining the coefficients.

Peterson (1999) combined the techniques of Davies and Zemanek. A system of equations was used to determine the coefficients of the propagating modes in a finite cylindrical waveguide with a broadband excitation, and a Fourier decomposition was used to determine the phase shift of each mode. Peterson's model predicted the shape generally fairly well. Puckett and Peterson (2002) refined the model by calculating the relative mode amplitudes at each frequency; however, the receiving end conditions were still not modeled. Calculated signals were similar to experimental signals though.

2.3. Background Discussion

Investigations of axially symmetric wave propagation in cylindrical bars have focused mainly on the numerical exploration of the Pochhammer-Chree theory, and the comparison of experiments to the theory. A general understanding has emerged, and the theory generally agreed with experiments. Transient solutions were developed to extend the comparison of the theory to experiments. Two models were developed to predict the transient solutions. The models based on integral transform techniques and the models based the Pochhammer-Chree solutions each have benefits and drawbacks.

Integral transform models predict well the response of a waveguide to a step function excitation. A step function excitation was chosen because of the simplicity of the transforms and of the interest experimentally in modeling the Split Hopkinson Pressure Bar (SHPB). However, an analytical model is needed for acoustic signals used in ultrasonic nondestructive evaluation. These signals are arbitrary broadband signals that are not easily described by analytical functions.

The techniques based on the Pochhammer-Chree theory lend themselves more easily to end conditions with arbitrary stress functions in both time and space and are the basis for the semi-analytical model developed in this research. The techniques can be implemented to represent standard ultrasonic testing configurations using cylindrical waveguides, and will allow more extensive experimental comparisons, which have not previously been made.

CHAPTER 3: EXPERIMENTAL SYSTEM

There are a number of ways to generate and measure ultrasonic waves in solid materials. The piezo-electric transducer is the most common method. A piezo-electric material subjected to a stress will generate an electric potential difference between the faces of the material. Similarly, an electric potential difference applied to faces of the piezo-electric material will cause a strain in the piezo-electric material. Contact transducers typically use a polarized ceramic cut specifically to generate longitudinal or shear waves. Coupling fluids are used to help transmit the elastic waves generated by the strain of the piezo-electric material into specimen being evaluated. Piezo-electric transducers are used for this research.

Another means of contact ultrasound is the electromagnetic acoustic transducer (EMAT). EMATs are used with metals and generate a surface stress via the Lorentz magnetic force (Papadakis et al. 1999). EMATs are not as efficient as piezo-electric transducers for converting an electrical signal into elastic waves and are primarily used in special circumstances to generate elastic modes that are difficult to generate with other means. EMATs are especially good in situations were a couplant is prohibitive.

A non-contact alternative to piezo-electric transducers and EMATs is laser generation and measurement of ultrasonic waves, known as interferometry (for example, Scruby and Drain 1990). Laser interferometry has the added benefits of high spatial and temporal resolution; however, there can be problems with rough and poor reflecting surfaces. Also, the equipment for laser ultrasonics is expensive in comparison to other ultrasonic techniques.

3.1. Experimental Configuration

In contact ultrasonics there are primarily two experimental configurations, through transmission and pulse-echo. The nature of an experiment often requires one configuration of the ultrasonic system, but other times either configuration can be used. For solid circular waveguides both configurations are useful, and both are considered here.

3.1.1. Through-Transmission

The through-transmission configuration uses two transducers, one to excite the ultrasonic signal at one end of the waveguide and a second to receive the ultrasonic signal at the opposite end. High

temperature through-transmission experiments with solid cylindrical waveguides use two waveguides to isolate a sample that is at an elevated temperature. One waveguide is used to couple each transducer to the sample, one on either side of the sample. This research is focused on the wave propagation in the waveguide, so for the experiments only a single waveguide is considered.

The basic experimental setup is illustrated in Fig. 3.1. A pulser sends an electrical pulse to one of the transducers. The transducer converts the electrical pulse into an acoustical pulse, which propagates down the waveguide. The other transducer measures the signal and converts the received acoustical pulse into an electrical signal. This signal is amplified by a preamplifier and displayed on an oscilloscope. Ideally the received signal still has the shape of a pulse, so that if a sample is placed between two waveguides then information about the sample can be extracted from the signal easily.

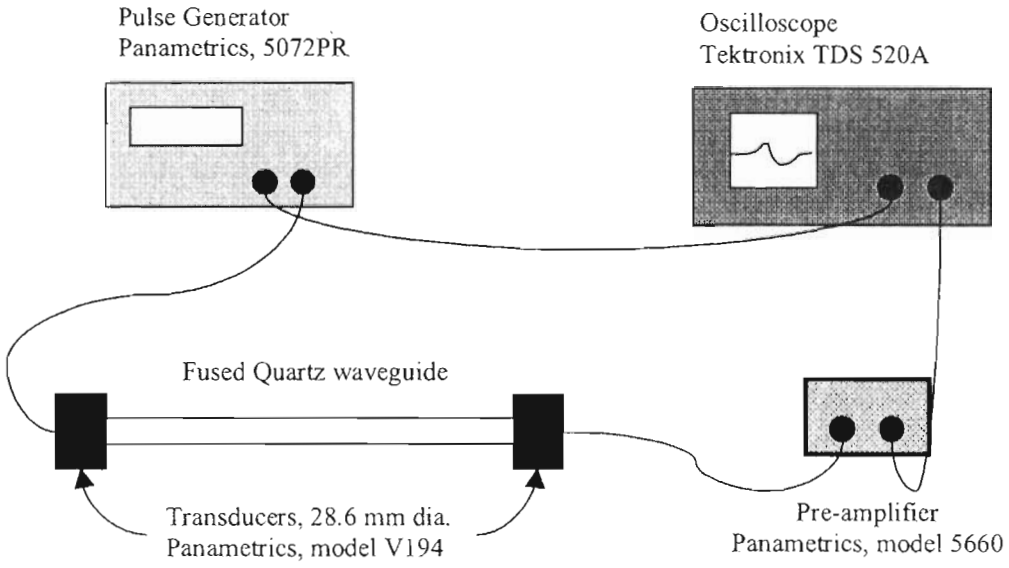

Fig. 3.1. Diagram of the through transmission experimental setup.

3.1.2. Pulse-Echo

The pulse-echo configuration uses the same equipment as the through-transmission configuration, but a single transducer is used for both the excitation and the reception of the ultrasonic signal. In this configuration a single waveguide is always used, so the signal travels twice the length of the waveguide, down and back.

The basic pulse-echo experimental setup, Fig. 3.2, is similar to the through transmission. A pulser sends an electrical pulse to the transducer. The transducer converts the electrical pulse into an acoustical pulse, which propagates down the waveguide. Part of the signal reflects off the end of the waveguide and part of the signal transmits into the specimen at the end of the waveguide. Reflections from within the specimen are transmitted back into the waveguide. The transducer measures all of the reflected signals and converts the received acoustical pulse into an electrical signal. This signal is amplified by a preamplifier and displayed on an oscilloscope. Ideally the signal maintains its shape as it propagates through the waveguide, so that information can be extracted from the signal easily.

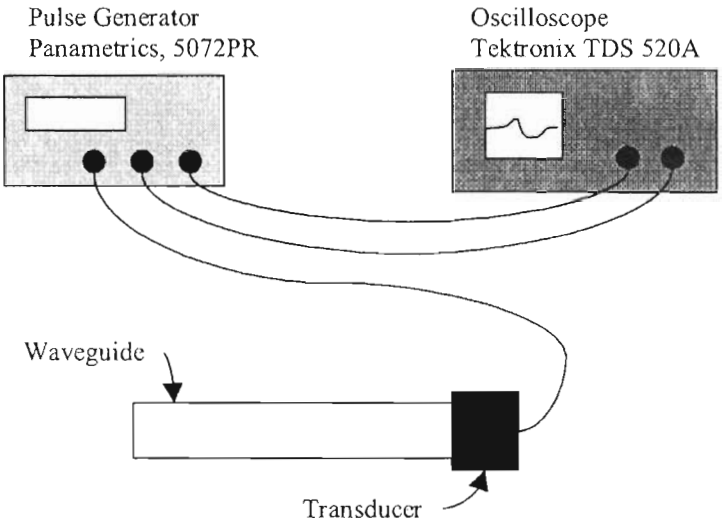

Fig. 3.2. Diagram of the pulse-echo experimental setup.

3.1.3. General Considerations

In both experimental configurations adequate understanding of the experimental system is essential for interpreting the experimental signals and gathering meaningful data. There are two primary systems in the experimental configuration, the electrical system and the acoustical system (Schmerr 1998). The electrical system consists of all of the components that propagate the electrical signal including the pulser, amplifier and the transducers. The acoustical system consists of all of the components that propagate the acoustical signal including the waveguides, the specimen, and any other acoustical paths in the experimental configuration. Both the electrical and acoustical systems influence the received signals to

varying degrees, and the total experimental system can be represented as a series of linear time-shift invariant systems each of which has an impulse response function (Schmerr 1998).

Each component in the electrical system has an impulse response function that is a function of frequency (Schmerr 1998). The response functions of the transducers typically have the narrowest bandwidth of the experimental system, so the transducers will dictate the frequency spectrum of the excitation signal. However, if the amplitude of the electrical signal to the transducers is too high the transducers will have a nonlinear response. In this range the transducer is converting some of the electrical signal to heat, which can eventually damage the transducer.

Amplifiers also have a limited linear response. A preamplifier is typically used to amplify the signal generated by the receiving transducer. The preamplifiers have a maximum output voltage. In the linear range there is an input voltage associated with the maximum output voltage. Any increase in the input voltage will also produce the maximum output voltage. This is known as clipping. Reducing the amplification will remove this effect. Power amplifiers are also sometimes used in ultrasonic systems to drive the transmitting transducer. Understanding the response functions of the electrical system ensures better accuracy in the measurements.

Each part in the acoustical system also has a response function, which may need to be considered either with deconvolution or modeling. However, in the system considered the main concern with the acoustical system is the propagation of the elastic waves along multiple paths and the multiple arrival times of these signals. At interfaces between two materials, such as the interface between a waveguide and a sample (see section 3.2.3) part of the acoustical signal is transmitted and part is reflected generating some of the multiple arrival times of these signals. Typically there is only one path that is of interest, so the arrival time of this path must be determined to extract information from the signal. For both the through transmission and pulse-echo configurations an understanding of the acoustical system is necessary to determine the signal with the correct arrival time.

3.2. Time Reversal

In both the through transmission and pulse-echo configurations, design constraints may require thick cylindrical waveguides, which propagate multiple dispersive modes. The propagation of multiple modes causes a signal that is compact in the time domain to have a large time signature after propagating

through the waveguide, Fig 1.1. As a result, if the signal is propagated through a specimen, as well as a waveguide, phase velocity and attenuation information about the specimen are difficult to extract. A time-reversal mirror is capable of reducing the complexity of the received signal.

3.2.1. Background

Time-reversal mirrors (TRM) have been developed based on the property of time-reversal invariance (Fink 1997). A time-reversal mirror experiment consists of three steps. In the case of a cylindrical rod, first, an acoustic signal is excited by a source at one end of the rod. The acoustic signal propagates through the rod, and the altered signal is recorded at the opposite end. Second, the recorded signal is reversed in time. Finally, the receiver is excited with the reversed signal. The reversed signal propagates through the rod, and a new signal is recorded at the source. If time invariance is satisfied, this new signal is the same as the original acoustic signal. This ability of the TRM can be used to produce a compact time signal from a dispersive system. This technique has been shown to be effective in eliminating the dispersion of Lamb waves for plate inspection (Ing and Fink 1998).

Time reversal in a solid circular waveguide has been demonstrated recently in an application to concentrate acoustic energy at a point in a fluid (Montaldo *et al.* 2001). Multiple transducers on the end of a solid circular waveguide were excited by a 1-bit digitized time-reversed signal to create a high amplitude pulse in a fluid near the opposite end of the waveguide instead of the dispersed multi-mode signal. In this application and the applications mentioned previously, only the axially symmetric longitudinal modes are excited. Thus, at most, an annular array of transducers would be required to reconstruct the general displacement field on the end of a cylinder. However, a single element, cylindrical transducer is most commonly used in sensor applications with cylindrical waveguides (Jen *et al.* 1991, Peterson 1994). The time reversal technique has been shown to be effective when only the first two axially symmetric modes are excited in a solid circular waveguide using a single transducer (Puckett and Peterson 2003). However, the ability to extend time reversal to a cylindrical waveguide for which a large number of axially symmetric modes propagate using only the information from a single transducer is of primary interest.

The stress and displacement of an axially symmetric mode may be regarded as having two components. One component is the contribution from the superposition of plane longitudinal waves. The second component is the contribution from the superposition of plane transverse waves (Redwood 1960).

As the frequency increases, there are frequencies where both the longitudinal and transverse components are strong. There are also frequencies where one component dominates, including frequencies where the mode is predominately the result of the superposition of plane transverse waves. These changes are exhibited in all of the axially symmetric modes.

A single transducer is capable of exciting multiple axially symmetric modes in a circular waveguide. For a transducer that is much larger than the waveguide (in this case about 4 times greater in diameter than the waveguide), the pressure distribution across the face of the waveguide is approximately constant with radius. Although the pressure is nearly constant with radius, all of the modes with cutoff frequencies within the spectrum of the signal will propagate. These real modes, along with some imaginary modes and an infinite number of attenuating complex modes are excited to satisfy the boundary conditions on the end of the waveguide (Zemanek 1972). The multiple propagating modes are evident in the large time signature in the bottom signal of Fig. 1.1, which is from a 10 mm diameter fused quartz rod excited by a 28.6 mm diameter transducer. The frequency spectrum of the top signal in Fig. 1.1 and the dispersion curves of the waveguide appear in Fig. 3.3. From Fig. 1.1 and Fig. 3.3, it is evident that multiple dispersive modes are excited and propagated through the waveguide by a single transducer.

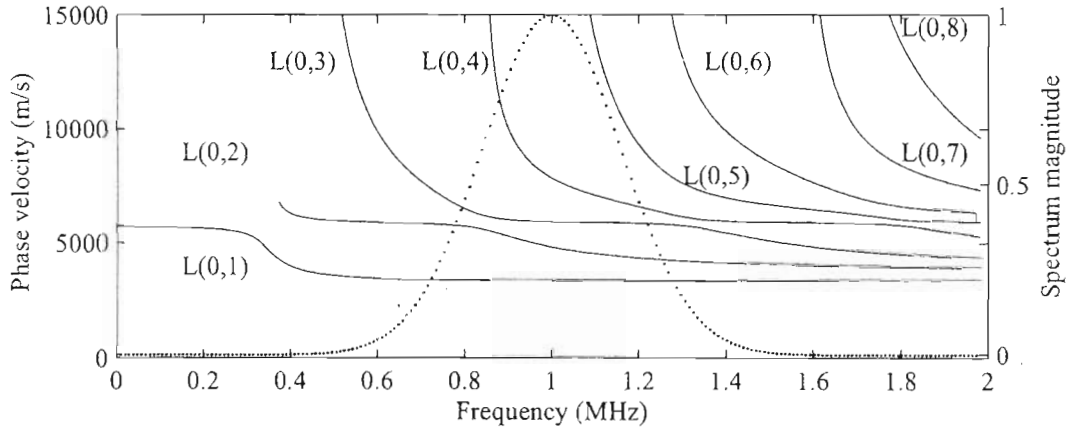

Fig. 3.3. Dispersion curves for the cylindrical waveguide used in the TRM experiments and the normalized frequency spectrum (dashed) of the signal used to excite the waveguide. The label L(0,N) represents the N^{th} axially symmetric mode.

The signal from a single transducer should include sufficient information from a multi-mode signal to perform an accurate time reversal. As the signal propagates along the waveguide, the modes

separate in time, and the complex modes attenuate to negligible amplitude. Thus, the pressure distribution on the receiving end of the waveguide is not constant with radius. The actual pressure distribution on the end of the waveguide at a particular time is the superposition of the normal stress of all of the modes and frequencies present. Additionally, the transducer has only the ability to measure the average pressure across the face. The transducer does not record the shear stress of any of the modes present. It is reasonable though, to assume that the most important information are the phase components of the frequencies that are present in the received signal and the relative amplitudes of those frequencies. This is the information that is time-reversed and used to excite the transducer.

Thus, the ability of a TRM with a single transducer that is only capable of sensing the average normal stress even though the transducer can excite the modes that are associated with the superposition of plane transverse waves is explored. A TRM experiment was conducted using single element, longitudinal contact transducers on either end of a solid fused quartz rod. The original excitation signal was compared to the final signal from the TRM experiment to determine the ability of the TRM to reconstruct the original input signal.

3.2.2. Through-Transmission

The configuration used for the through transmission experiments had a slightly different setup and is shown in Fig. 3.4. The waveguide consisted of a 10 mm diameter, fused quartz cylindrical rod, 485 mm in length. An amorphous material was chosen for the waveguide because linear elastic and homogeneous assumptions are well satisfied. Fused quartz has a Young's modulus, E, of 72 GPa, a density, ρ, of 2200 kg/m^3, and a Poisson's ratio, ν, of 0.162 (General Electric Advanced Materials 2004).

Two transducers were used for the experiments. Both transducers were 28.6 mm diameter, 1 MHz broadband, longitudinal contact transducers [Panametrics, model V194, Waltham, MA]. The transducers had a bandwidth corresponding to a 6 dB drop in amplitude between 0.5 MHz to 1.5 MHz. A coupling fluid was used between the transducers and the waveguide [Sonotech, Inc. UT-30, State College, PA].

An arbitrary waveform generator [Agilent 33250A, Palo Alto, CA] produced the signal to drive the transducer. A radio frequency power amplifier [ENI A-300, Rochester, NY] with a gain of 55 dB was used to amplify the signal to the transducer. The received signal was recorded by a digital storage

oscilloscope [Tektronix TDS 520A, Wilsonville, OR] after amplification of the signal by an ultrasonic pre-amplifier [Panametrics model 5660C, Waltham, MA] with a gain of 40 dB.

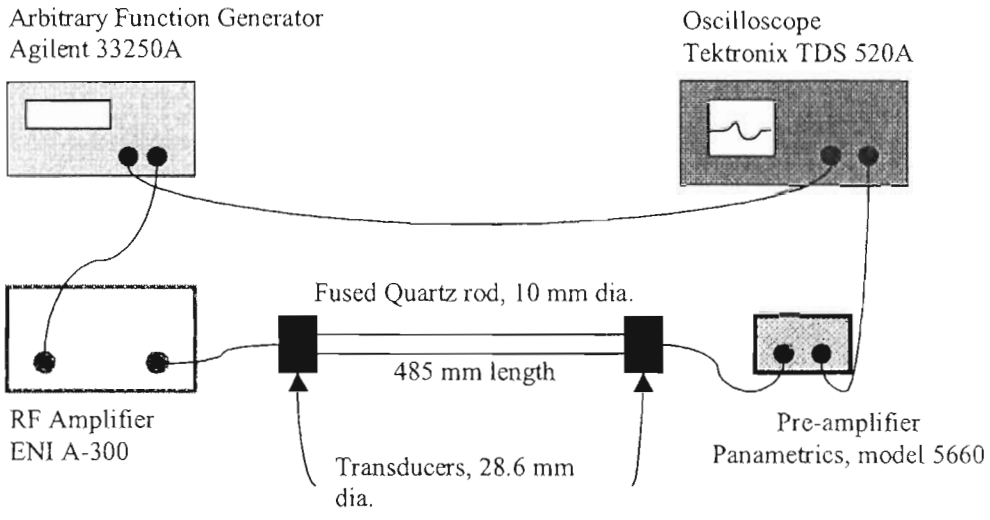

Fig. 3.4. Diagram of the experimental setup.

The acoustic signal used in the TRM experiments was a broadband signal. The signal had a frequency spectrum with a 6 dB drop in amplitude at 0.5 and 1.5 MHz and a central frequency of 1 MHz (Fig. 3.3). For the geometry of the waveguide and the frequency spectrum, six propagating axially symmetric modes were excited in the waveguide, with a component of each mode being the superposition of plane transverse waves. Fig. 3.3 shows the dispersion curves calculated for the waveguide used in the experiments.

To ensure the correct signals were recorded, the time window was chosen to include only the initial propagated signal and no end reflections. The excitation signals were repeated at a frequency of 10 Hz to ensure that reflections from previous signals were sufficiently attenuated and were not included in the recorded signal. The recorded signals were averaged over 20 signals to remove noise. Finally, since the waveguide is symmetric about its length, the received signal that is reversed can be excited from the source transducer instead of the receiving transducer to produce the same results. So, for the experiments, all signals were sent from the same end of the waveguide using the same experimental set up.

It was necessary to include the experimental frequency response of the apparatus in the comparison of the original excitation signal to the final signal of the TRM, so the ability of the single

element TRM in the waveguide could be determined more accurately. The frequency response includes an amplitude factor and a phase shift for each frequency. However, since the original excitation signal is compared to the final signal of the TRM the phase shift does not need to be known, due to the reversal of the signal in the second step of the TRM experiment. For example, if a signal that propagates through the system is altered by a phase shift of $\varphi(\omega)$, then the reversed signal will have a negative phase shift, $-\varphi(\omega)$. When the system is excited by the reversed signal, the phase shifts will cancel. Since the signal was always propagated from the same source for the TRM experiments, the phase shift was always the same. Therefore, only the amplitude of the frequency response was required to account for the equipment response.

The frequency response of each piece of equipment (RF amplifier, transducers, and ultrasonic pre-amplifier) was measured. The system response function is the convolution of the amplitude factors of each piece of equipment. The ability of the TRM in the waveguide is determined by the comparison of the final signal in the TRM experiment with the original excitation signal convolved with the system response function. For this convolution, the system response was squared because the original excitation signal was propagated through the experimental system twice before becoming the final signal.

The signals from the TRM experiments are compared in Fig. 3.5. All of the signal amplitudes have been normalized, and the signals are plotted with the same time scale. The original excitation signal convolved with the system response function is shown as the top signal of Fig. 3.5. The bottom four signals in Fig. 3.5 are the signals from the TRM experiments in the waveguide. The second signal from the top in Fig. 3.5 is the dispersed signal recorded at the receiving transducer after the excitation signal has propagated through the waveguide. The dispersed signal was reversed in time, as shown in the third signal in Fig. 3.5, and was used to excite the ultrasonic transducer. The signal second to the bottom in Fig. 3.5 is the signal recorded at the receiving transducer after the reversed signal is propagated through the waveguide. The bottom signal in Fig. 3.5 is the previous signal reversed in time for comparison with the first signal. A closer comparison of these two signals appears in Fig. 3.6.

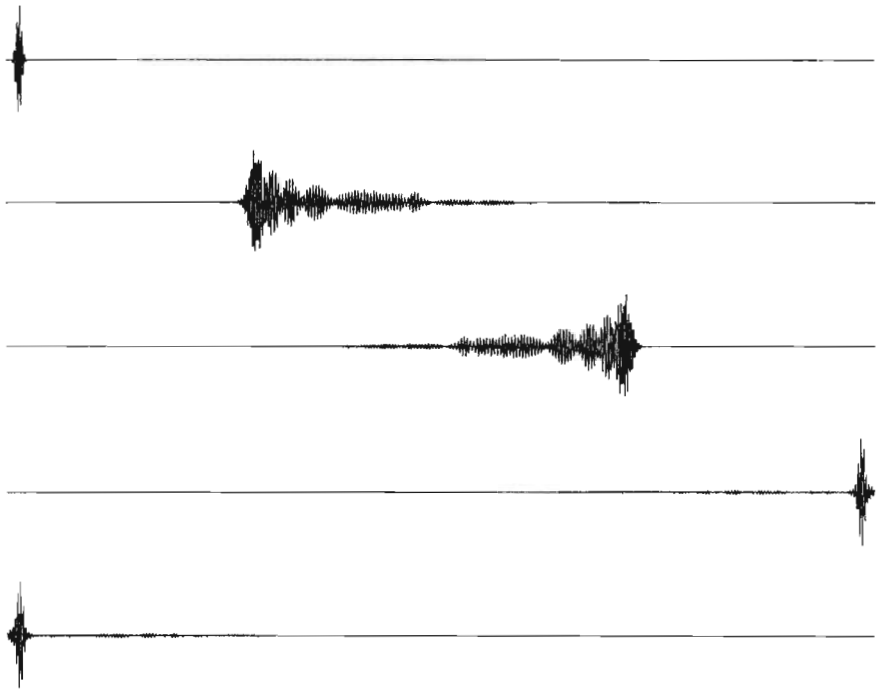

Fig. 3.5. TRM experiment in a solid multi-mode waveguide. The signals are normalized and plotted on the same time scale. The signals are, from top to bottom, the original signal convolved with the system response, the dispersed signal, the reversed dispersed signal, the final signal created from the propagation of the reversed dispersed signal, and the final signal reversed in time.

The two signals in Fig. 3.6 are very similar, with additional noise evident in the experimental signal. The ability of a TRM to reconstruct the original excitation signal using the limited information of a single, longitudinal contact transducer appears to be very good. It was shown earlier that a single, longitudinal contact transducer excited multiple modes in a cylindrical waveguide, including the axially symmetric modes that result from the superposition of plane transverse waves. The experimental signal in Fig. 3.6 implies that a single longitudinal contact transducer appears to be capable of reconstructing a compact time signal from a solid circular waveguide. Thus, the effects of the pressure distribution on the end of the waveguide and the lack of information about the shear stress appear to be minimal.

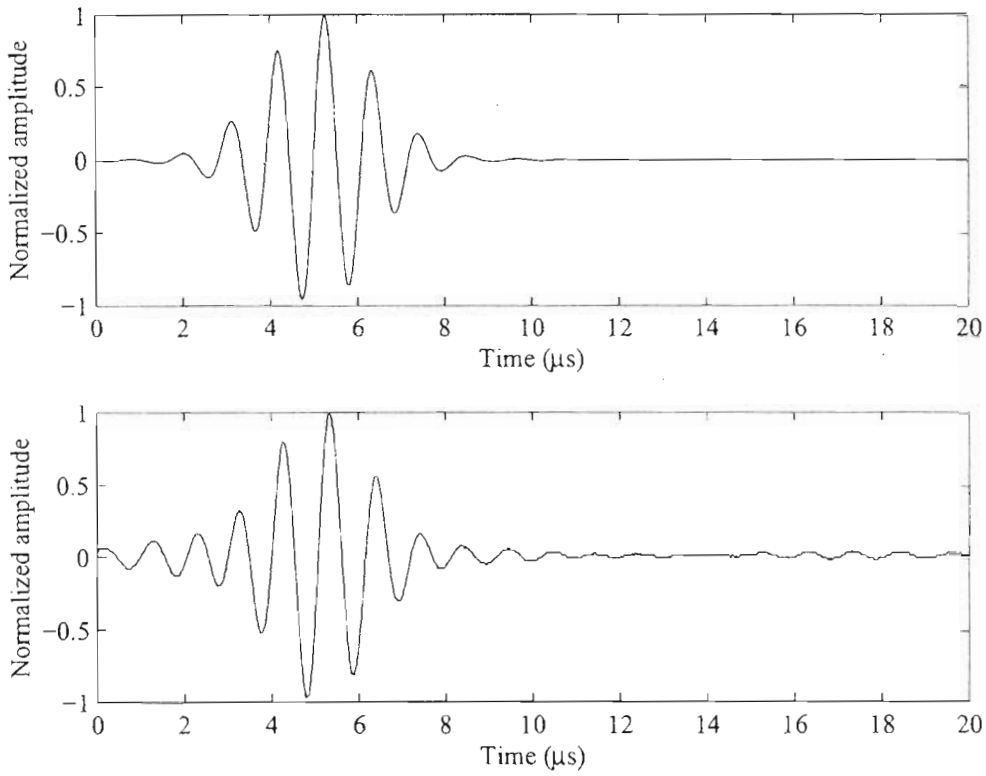

Fig. 3.6. Comparison of the original signal (top) to the final signal from the TRM experiment (bottom). The original signal has been convolved with system response function.

The most important characteristic of the resulting experimental signal in Fig. 3.6 is the compact time signature. By using the time-reversed signal as the excitation signal, the dispersive properties of the waveguide can be negated. This capability allows the use of a dispersive solid circular waveguide as a low cost sensor. The compact time domain signal greatly simplifies signal analysis that was previously used (Peterson 1994).

For a practical application with a single waveguide, the signal that will cancel the dispersive effects of the waveguide is easily determined from the TRM experiment. For more complex configurations where significant changes with time are expected [Jen *et al.*, 2001], either modeling or more extensive experiments are required. Future work remains to be done to show that measurements can be made in-situ and to develop appropriate models.

3.2.3. Pulse-Echo

Time-reversal has also been effectively demonstrated in the pulse echo configuration. For these experiments the pulse-echo configuration also required a slightly different setup, Fig. 3.7. The waveguide consisted of a 25.4 mm diameter fused quartz cylindrical rod, 228 mm in length. An amorphous material was chosen for the waveguide because linear elastic and homogeneous assumptions are well satisfied. Fused quartz has a Young's modulus, E, of 72 GPa, a density, ρ, of 2200 kg/m^3, and a Poisson's ratio, ν, of 0.162 (General Electric Advanced Materials 2004).

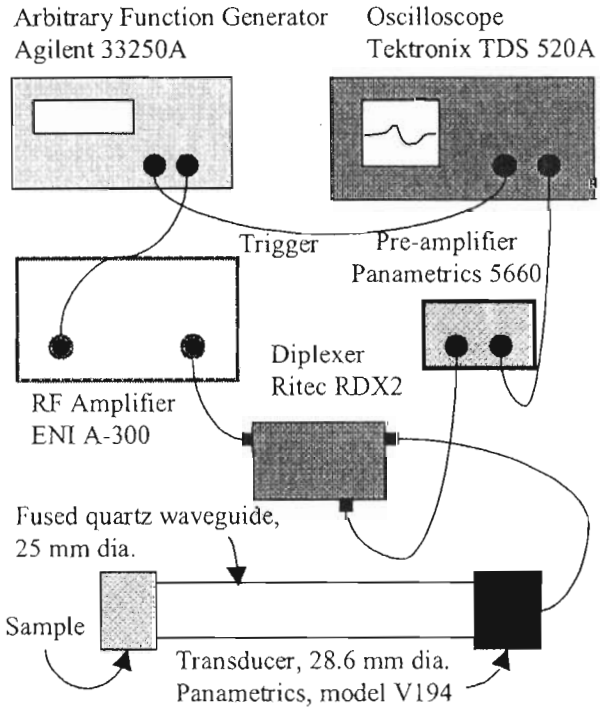

Fig. 3.7. Diagram of the experimental setup.

The pulse-echo configuration uses a single transducer that acts as the source and the receiver. The transducer used in the experiment was a 28.6 mm diameter, 1 MHz broadband longitudinal contact transducer [Panametrics, model V194, Waltham, MA]. A coupling fluid was used between the transducer and the waveguide and between the waveguide and the sample [Sonotech, Inc. UT-30, State College, PA].

A pulser [Panametrics, 5072PR, Waltham, MA] was used to generate a pulse to the transducer. The dispersed signal was recorded and reversed in time. An arbitrary waveform generator [Agilent 33250A, Palo Alto, CA] produced the time-reversed signal to drive the transducer. A radio frequency

power amplifier [ENI A-300, Rochester, NY] with a gain of 55 dB was used to amplify the signal to the transducer. The received signal was recorded by a digital storage oscilloscope [Tektronix TDS 520A, Wilsonville, OR] after amplification of the signal by an ultrasonic pre-amplifier [Panametrics, model 5660, Waltham, MA] with a gain of 40 dB. In order to use the transducer in pulse-echo mode with the arbitrary waveform generator a transformer diplexer [Ritec Inc., model RDX2, Warwick, RI] was placed between the transducer, the ultrasonic pre-amp, and the power amplifier.

The TRM proved to be effective in the pulse echo configuration. The time-reversed signal was used to excite the transducer, and the echoed signal received by the transducer was a pulse, top graph in Fig. 3.8. The most important characteristic of this experimental signal is the compact time signature. By using the time-reversed signal as the excitation signal, the dispersive properties of the waveguide can be negated. This capability allows the use of a dispersive solid circular waveguide as a low cost sensor. The compact time domain signal greatly simplifies signal analysis that was previously used (Peterson 1994).

To explore the ability of this technique as a sensor, a 25.4 mm aluminum cube was placed at the free end of the waveguide. The same time-reversed signal was used to excite the transducer. The received signal includes both front and back wall reflections from the aluminum cube, bottom graph Fig. 3.8. The first peak corresponding to the reflection at the end of the waveguide was attenuated compared to the peak from the reflection from the free end of the waveguide. The attenuation results from transmission into the finite impedance material. Also a second peak was generated from the reflection of the back wall of the sample. The time delay between the two peaks correlates to the bulk wave speed in aluminum and the thickness of the cube.

From these experiments the technique is promising as a means to detect changes in impedance or wave speed in an actual application. For a practical application with a single waveguide, the signal that will cancel the dispersive effects of the waveguide is easily determined from the TRM experiment. For more complex configurations where significant changes with time are expected either modeling or more extensive experiments is required (Schmerr 1998). Future work remains to be done to show that measurements can be made in-situ.

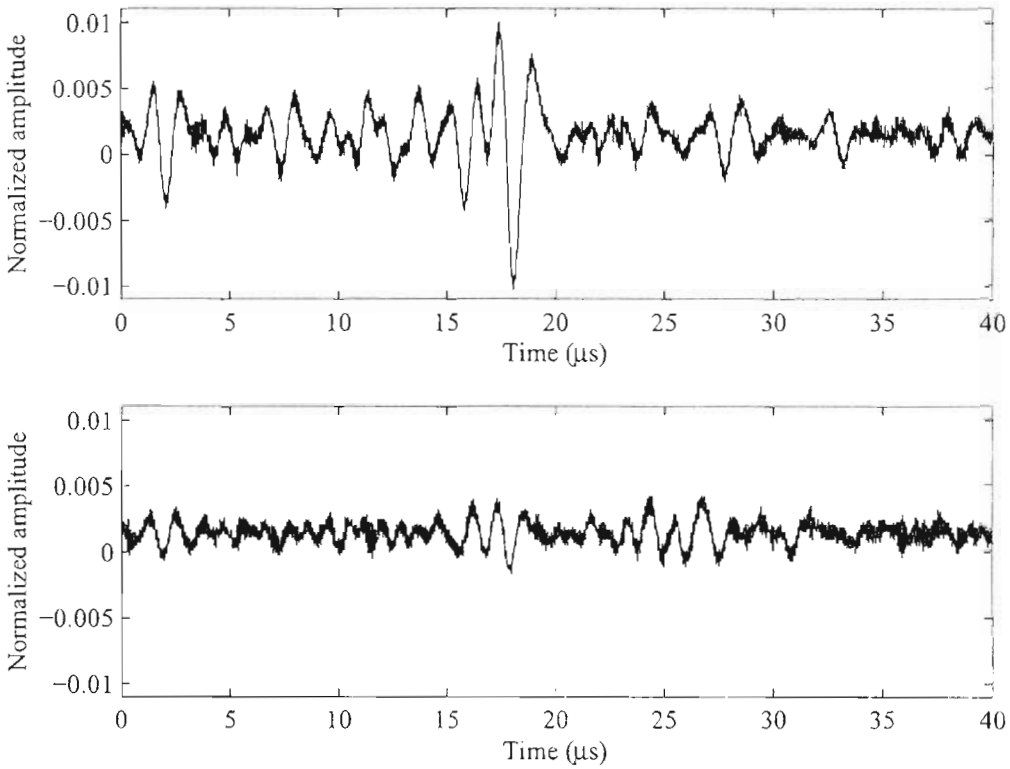

Fig. 3.8. Comparison of received signals.

3.3. Transducer Characteristics

Contact ultrasonic transducers that generate longitudinal waves in a solid are used in many experimental applications besides time reversal mirrors. Typical applications range from determining the elastic properties of materials to locating cracks or inclusions in materials (Krautkramer 1983). To accurately interpret the results for these applications, analytical models are often required (Schmerr 1998). In a number of cases analytical models need to include the effects of the transducer on the measurement system. The main attributes of the transducer are the frequency response, which is easily determined experimentally, and the pressure distribution across the face of the transducer. It is possible to assume a uniform pressure across the face of the transducer, but often this is not adequate (Lerch 1998). For example, the beam profile of the transducer must be well understood for sizing of cracks, a key nondestructive evaluation task. If the pressure decreases towards the edge of the transducer, the near field becomes more uniform than a transducer with a uniform pressure distribution. Therefore, measurement of the pressure distribution across the face of the transducer may be required (Bacon 1993).

3.3.1. Methods

A circular cylindrical waveguide sensor is another application where the pressure distribution on the transducer is required (Peterson 1999). Waveguides are used primarily to isolate contact transducers from a specimen that is at an extreme temperature and/or pressure. However, the relationship between the frequencies required for the experiments and the diameter of the waveguide results in dispersion and the propagation of multiple modes. An analytical model to determine the dispersion of the signal through the waveguide can be developed based on propagating modes. The relative amplitudes of the modes are determined by the boundary conditions on the end of the waveguide (Zemanek 1972). In order to evaluate the boundary conditions, the pressure distribution across the face of the longitudinal contact transducer that is in contact with the waveguide must be known.

The technique described makes it possible to determine the pressure distribution across the face of a transducer using a standard commercial immersion scanning system or off-the-shelf optical components. This apparatus provides a low cost alternative to laser based methods for verification and testing. The experimental setup and procedure are described. Potential difficulties are discussed as well as the necessary remedies.

The schematic of the system used for the measurement technique is illustrated in Fig 3.9. The arrangement consists of two parts; the sensor and the transducer to be characterized (the unknown transducer). The sensor consists of a longitudinal contact transducer (receiving transducer), a stepped waveguide, and a housing fixture to hold the waveguide in contact with the receiving transducer. The stepped waveguide allows a measurement to be performed over a small area of the unknown transducer while still providing sufficient energy to the receiving transducer. The unknown transducer is mounted facing the end of the waveguide. In order to take measurements at multiple locations, the sensor is able to move independent of the unknown transducer in two axes of the plane normal to the waveguide.

The ultrasonic signal received by the sensor is indicative of the pressure on the transducer. The unknown transducer is excited by a pulse, a square wave, or an arbitrary function such as a sine burst or chirp. The ultrasonic signal propagates through the air and the sensor receives the signal. The sensor is moved across the face of the unknown transducer, and at each point the signal is recorded. The change in

amplitude of the signal received by the tip of the waveguide across the unknown transducer is representative of the pressure distribution across the unknown transducer.

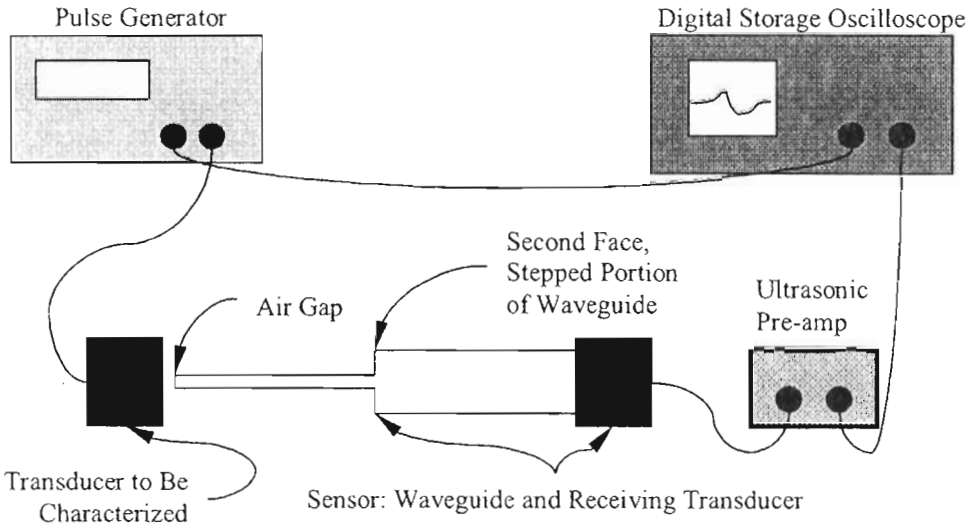

Fig. 3.9. Schematic diagram of the setup for the experimental technique.

This technique takes advantage of the difference in wave speed between the waveguide and the air to isolate the ultrasonic signal received by the tip of the waveguide. Since the velocity of the wave is much higher in the waveguide (aluminum in this case) than in air, the path through the waveguide will represent the first arrival in the signal. The fastest path in this configuration is through the tip of the aluminum waveguide, which is closest to the transducer. The first signal arrival is thus recorded and corresponds to the signal received by the tip of the waveguide. This signal is used to determine the pressure distribution across the transducer. A second signal is received later corresponding to the larger face on the stepped portion of the waveguide. Fig 3.10 illustrates this phenomenon.

Air is used as the coupling fluid to ensure that the coupling between the waveguide and the unknown transducer is the same at all points across the unknown transducer. Liquid coupling such as water is not possible for contact transducers. For normal contact ultrasonic methods, such as the use of coupling gel, if the coupling is not the same at all points the amplitude of the signal may be affected by the coupling.

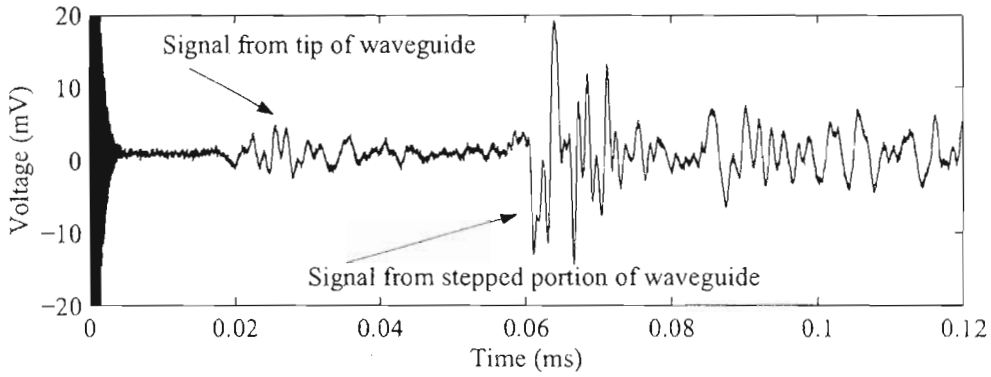

Fig. 3.10. Experimental signal showing portion received by tip and stepped portion of waveguide.

However, air is difficult to use as a couplant since the ultrasonic signal is highly attenuated by the air. The attenuation of the ultrasonic signal in air is highly frequency dependent (Pierce 1981). The high attenuation at normal ultrasonic frequencies of 1 MHz to 10 MHz requires that the sensor and face of the transducer be aligned as closely as possible to the plane defined by the two axes of motion. A change in the air gap across the unknown transducer will change the amplitude of the received signal as the sensor moves across the unknown transducer. However, the distance between the unknown transducer and the waveguide will also change the time delay of the received signal. Therefore, the alignment of the face of the unknown transducer and the consistency of the air gap can be verified by the measured time delay. The accuracy of the time delay is a function of the sampling rate of the signal (Peterson 1994).

3.3.2. Results

An example of the pressure distribution measurement is shown for a 28.6 mm (1.125 in.) diameter, 1 MHz, longitudinal contact transducer (Panametrics, model V194, Waltham, MA). The sensor used a 1.0 MHz nominal center frequency, 12.7 mm (0.5 in.) element diameter immersion transducer (Panametrics, model V303, Waltham, MA). A higher or lower frequency transducer can be used for the sensor if a matched transducer is not present. Transducers with matched center frequencies will produce a higher signal to noise ratio, but a reasonable amplitude response is possible even with unmatched transducers. The waveguide was made of aluminum with a narrow section 16 mm long and 3 mm in diameter and a wide section 52 mm long and 9 mm in diameter. An air gap of approximately 1 mm was used between the tip of the waveguide and the 1 MHz contact transducer. An ultrasonic square wave generator (Ritec Inc.,

model SP-801, Warwick, RI) was used to generate a square wave pulse excitation signal to the 1 MHz contact transducer. Signals were recorded at multiple points along the face of the transducer. The apparatus is shown in a picture in Fig. 3.11.

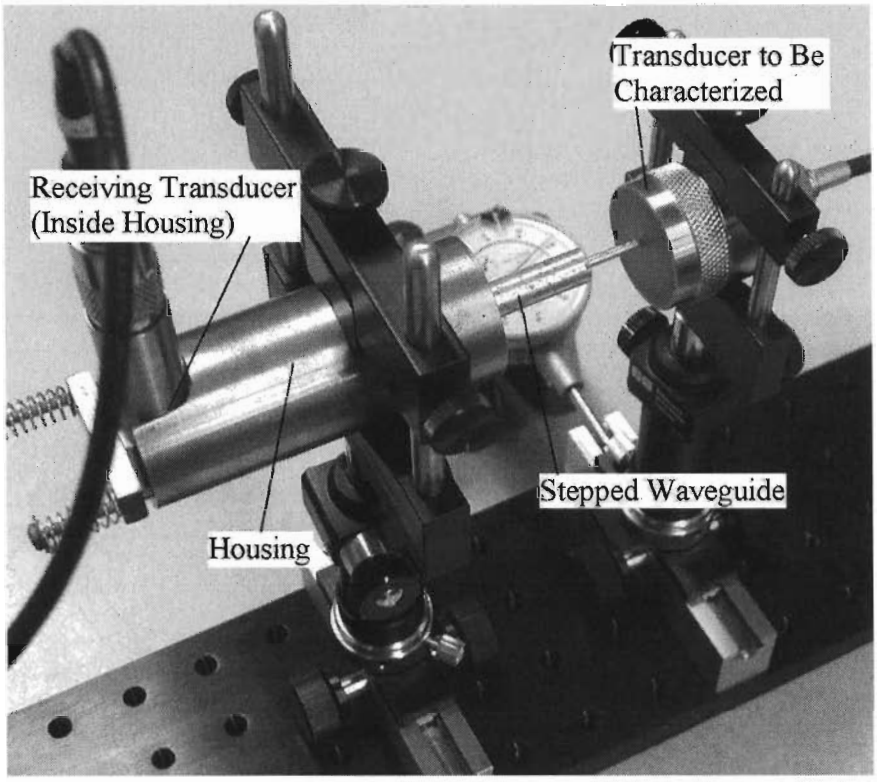

Fig. 3.11. Picture of the sensor and the transducer to be characterized with waveguide, transducers and alignment fixture.

An example of a recorded signal and the same signal after filtering appear in Fig 3.12. Filtering was used to remove all of the frequencies above the 40 dB upper bandwidth limit of the 1 MHz transducer. These frequencies in the signal represent little transmitted signal and mostly noise. For the measurements, the variation of the shape of the received signal at all points was minimal. Therefore, the cross-correlation technique was used to determine the relative amplitude and time delay at each location across the transducer (Peterson 1997). A signal recorded at the center of the transducer was used as the reference signal for the cross-correlation. The relative amplitude across the transducer is of interest, so any of the signals recorded near the center of the transducer can be used as the reference signal. The relative amplitude and the difference in time delay for the 1 MHz contact transducer appears in Fig 3.13. Three

signals were acquired at each location. Error bars represent the range of the three samples, and a line connects the mean at each location.

The difference in time delay can also indicate the misalignment, if any, of the transducer by multiplying the difference in time delay by the velocity of sound in air, 330 m/s. The right side of the graph displaying the time delay shows the relative distance. It is apparent from the results in Fig. 3.13 that one side of the transducer was about 50 μm closer to the waveguide than the other. The misalignment is seen as a slight decrease in amplitude across the transducer, indicative of the attenuation of the ultrasonic signal in air. For the purpose of this experiment, the "smoothness" of the transducer is of interest, so a slight misalignment is not an issue.

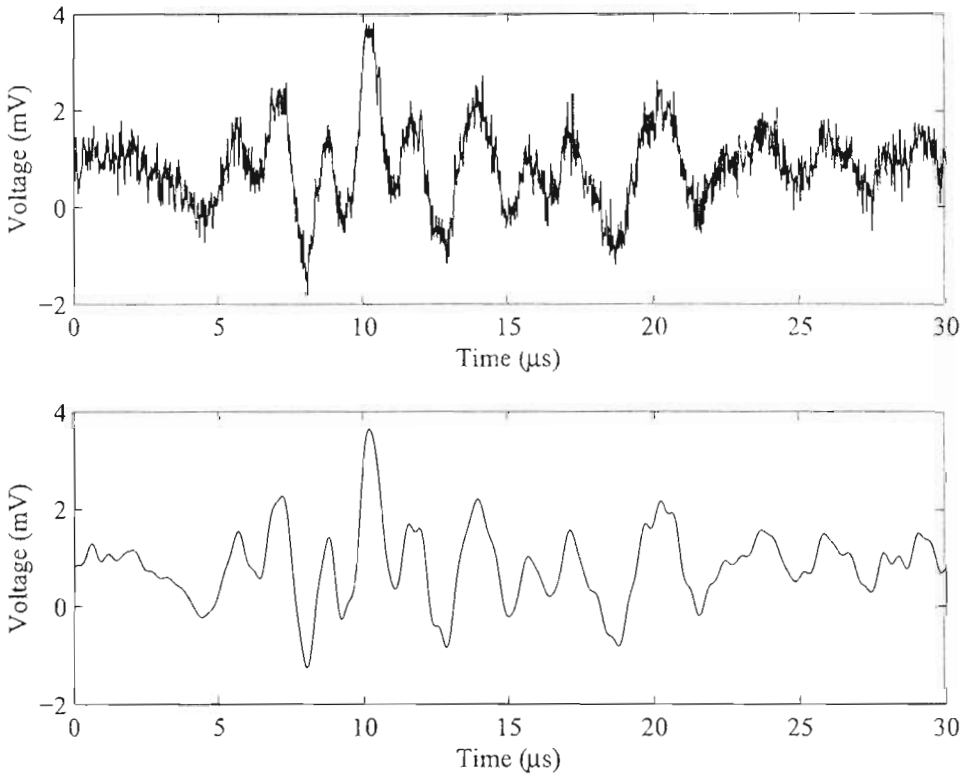

Fig. 3.12. Portion of the experimental ultrasonic signal (1 MHz) received at the tip of the waveguide, before (upper graph) and after filtering (lower graph) to remove frequencies above 40 dB upper limit bandwidth of transducer (2 MHz).

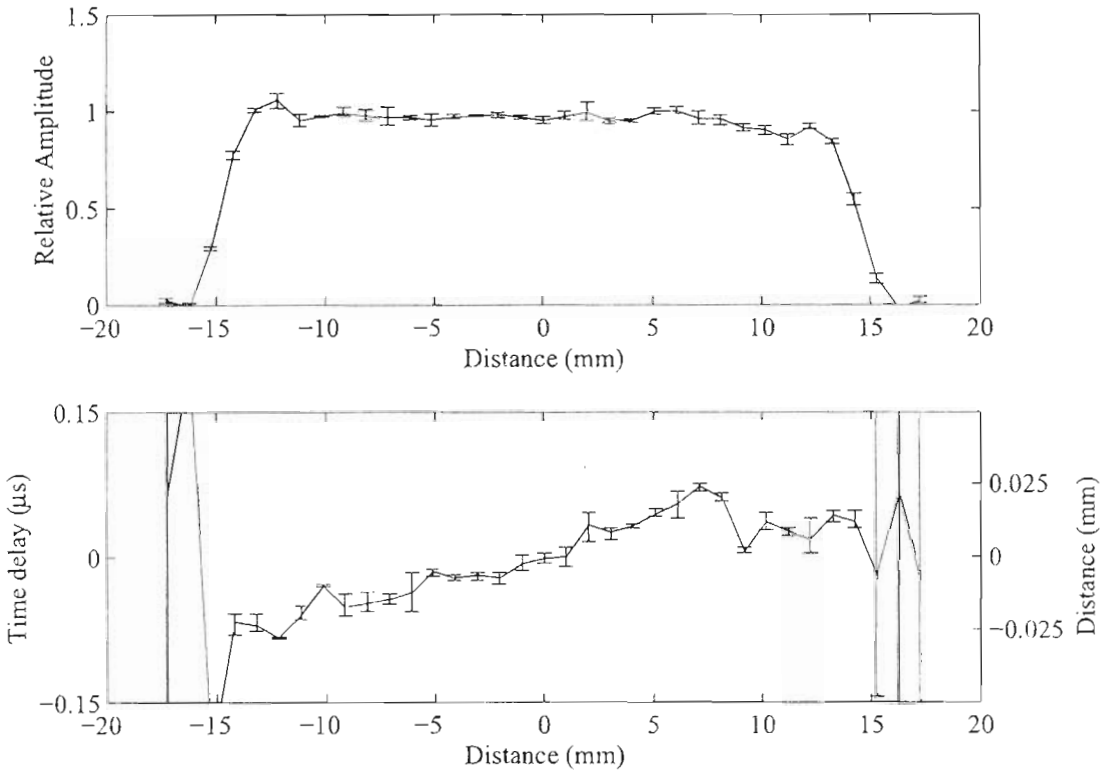

Fig. 3.13. Experimental results for a 1 MHz longitudinal contact transducer. Upper graph shows mean amplitude versus radius for three measurements (errorbars indicate limits). Lower graph shows corresponding time delays and a 50 μm misalignment of the transducer that corresponds to a small slope in the amplitude results.

3.3.3. Discussion and Conclusion

Most of the difficulties with the technique are associated with the signal acquired during testing. High frequency noise is apparent in the signal in Fig. 3.10 and Fig. 3.12 (upper graph). Appropriate filtering can be used to remove the noise; however, the cross-correlation will not be greatly affected by the noise. The signal to noise ratio also can be maximized by using narrow band excitation.

In addition to the noise, the signal also contains multiple arrivals, each arrival corresponding to a different cross section of the waveguide. Therefore, care must be taken in analyzing the correct arrival. The second arrival corresponds to the signal received by the larger diameter stepped portion of the waveguide, which has a longer ultrasonic path in air. This arrival has a larger amplitude because the larger area receives more energy.

Since the energy is directly related to the received cross sectional area of the waveguide, the geometry of the waveguide is critical. The waveguide must have a sufficiently small tip so that the measurement can be made over a small area of the transducer. For a more accurate determination of the pressure distribution, a smaller waveguide tip would be used. However, the smaller tip will result in a reduction of the amplitude in the received signal. Alternatives, such as narrow band excitation can help overcome these difficulties.

These difficulties are commonly found in other ultrasonic applications, so the difficulties should not be new to most users. This technique is a simple cost-effective way of determining the pressure distribution of a contact ultrasonic transducer, which may be useful for accurately modeling a transducer.

3.4. Experimental Discussion

For both the through-transmission configuration and the pulse echo-configuration, the propagation of axially symmetric waves in cylindrical bars produces complex signals. The complexity of the signals can be removed by employing time reversal even with only a single acoustic element. The use of time reversal allows a simple signal with compact support in the time domain to be generated in a dispersive waveguide. However, it may not be possible to experimentally acquire the necessary time-reversed signal, such as in a though transmission configuration with a sample between two waveguides. For these cases an analytical model could calculate the necessary signal to generate a signal with compact support in the time domain.

For an accurate model that is representative of experiments, the experimental configuration must be well understood. For the through-transmission configuration the primary piece of experimental equipment that will affect the results is the piezo-electric transducer. The transducers interact directly with the waveguide, so the spectral and spatial attributes of the transducers must be understood. The technique presented for mapping the transducer face provides the necessary spatial information about the transducer, and the spectral information is easily found using standard ultrasonic techniques. The other parts of the experimental system must also be considered but are not as influential as the transducers in an analytical model.

CHAPTER 4: ANALYTICAL MODEL FOR AXIALLY SYMMETRIC WAVE PROPAGATION

The semi-analytical model presented is designed as a tool for predicting and interpreting experimental signals, so the model is based on a general experimental configuration. The experimental setup associated with the waveguide consists of an ultrasonic contact transducer for exciting the ultrasonic signal in the waveguide, the waveguide, and a second ultrasonic contact transducer for receiving the signal. The excitation, propagation, and reception of the ultrasonic signal are each described by a part of the model using the Pochhammer-Chree solutions for an infinite cylindrical bar. For a given input signal, the model predicts the measured dispersed output signal at the opposite end of a specific length waveguide.

4.1. Parts of the Model

The frequency dependence of the Pochhammer-Chree solutions compels that the operations of the analytical model be performed in the frequency domain. All operations are conducted in the frequency domain unless noted otherwise. The time representation of the dispersed signal, $x_d(t)$, that has propagated through the waveguide can be represented as the inverse Fourier transform of the frequency spectrum of the dispersed signal, $X_D(\omega)$, Eq. (4.1) (Peterson 1999).

$$x_d(t) = \int_{-\infty}^{\infty} X_D(\omega) \exp(i\omega t) d\omega \tag{4.1}$$

The dispersed signal can be represented by the input reference signal, $X_R(\omega)$, multiplied by a dispersion function, $F_D(\omega)$, Eq. (4.2).

$$X_D(\omega) = X_R(\omega) F_D(\omega) \tag{4.2}$$

The dispersion function is a transfer function that represents the dispersion in the waveguide. The dispersion function contains the effects of all of the modes and is equal to the sum of the transfer functions of the modes.

The transfer function of each mode is determined from the three parts of the experimental setup: the transmission from the exciting transducer to the waveguide, the propagation through the waveguide, and the transmission from the waveguide to the receiving transducer. The phase information of the transfer function is dictated by the propagation of the mode through the waveguide, and the amplitude is provided by the boundary conditions on both ends of the cylindrical rod.

4.1.1. Excitation

The excitation on the end of the waveguide determines the relative amplitudes of the modes. An ultrasonic contact transducer excites the ultrasonic signal into the waveguide, so the characteristics of the transducer determine the boundary conditions on the end of the cylindrical bar. The transducer exhibits a pressure, $P(r)$, on the end of the cylinder, which specifies the normal stress boundary condition. This boundary condition is a function of radius and can be represented by an expansion over the normal stress function, $\sigma^{(j)}_{zz}$.

$$P(r) = \sum_j A^{(j)} \sigma^{(j)}_{zz}(r) , \tag{4.3}$$

where $A^{(j)}$ and $\sigma^{(j)}_{zz}$ are associated with the wave number $k^{(j)}$ of mode j. Previous authors have made compelling arguments that the stress functions of the modes form a complete set (Gregory and Gladwell 1989, Fama 1972). The coefficients in the expansion, $A^{(j)}$, are equal to the amplitudes of the modes.

Either the shear stress or the radial displacement specifies the second boundary condition on the end of the bar. The shear stress, $\sigma^{(j)}_{rz}$, is assumed to be zero because a viscous fluid coupling is used between the transducer and the bar. Therefore, the amplitudes of the modes must also satisfy an expansion over the radial shear stress functions,

$$0 = \sum_j A^{(j)} \sigma^{(j)}_{rz}(r) . \tag{4.4}$$

These two expansions are usually written as a single expansion (for example Zemanek 1972 and Gregory and Gladwell 1989).

There are a number of approaches to calculating the coefficients, $A^{(j)}$, in the expansion. The first choice is to use the orthogonality relations of the functions, if available. These relations have been developed by Fama (1972) for the elastostatic case, and Fraser (1975) demonstrated that the relations also applied to the elastodynamic case. The orthogonality relation for a cylinder with a stress free lateral surface is expressed as:

$$\int_0^a (w^{(j)} \sigma^{(l)}_{zz} - \sigma^{(j)}_{rz} u^{(l)}) r dr = 0 \qquad j \neq l \qquad \text{(Fraser 1975, Eq. 17).} \tag{4.5}$$

For the case of pure stress end conditions this relation does not provide a direct solution for the coefficients (Fama 1972, Eq. 10). However, Fama shows there is a unique solution for the coefficients in the pure end condition problem.

Zemanek (1972) used a simple method to solve for the coefficients, a system of equations. The number of equations was dictated by the number of modes of interest and the desired accuracy. The same number of points were considered along the radius, and for each point an equation was generated from either, Eq. (4.3) or Eq. (4.4). This technique works well when a large number of modes are being considered. However, at the lowest frequencies there is only one propagating mode, so evanescent modes must be considered for better accuracy.

Gregory and Gladwell (1989) used an integral formulation of least squares to evaluate the coefficients. In the present model the expansion is evaluated at discrete points using a least squares technique to solve the coefficients. This technique is more accurate than the system-of-equations and allows more points to be evaluated since the system of equations is overdetermined. Additionally, the least squares relation can be derived directly from the expansion, Eq. (4.3), by rewriting the equation to include a residual error, e:

$$P(r) = \sum_j A^{(j)} \sigma_{zz}^{(j)}(r) + e \text{, or } \quad \{P\} = [\sigma]\{A\} + \{e\}. \tag{4.6}$$

When the sum of the squares of the residuals is minimized the coefficients can be expressed in matrix notation as:

$$\{A\} = \left[[\sigma]^T [\sigma]\right]^{-1} [\sigma]^T \{P\}. \tag{4.7}$$

In the limit as the residual error approaches zero the coefficients are the exact solution. This equation provides the amplitudes of the modes.

The main issue with the least squares method and any collocation method is the number of modes to consider in the expansion. For any number of modes in the expansion the accuracy of the coefficients can be found by summing the series, Eq. (4.3) and Eq. (4.4), and comparing the value to the applied pressure excitation, *P(r)*, at points along the radius. An increase in the number of modes considered in the expansion will increase the accuracy even if only slightly. At the lowest frequencies where only a small number of modes propagate, evanescent modes must be considered for an accurate value of the amplitudes

to be calculated. At higher frequencies only the propagating modes may be sufficient to accurately calculate the coefficients in the expansion. The number of modes considered in the expansion is discussed in the experimental comparisons.

4.1.2. Propagation

Each of the propagating modes has a different phase velocity, which varies with frequency. The phase velocity provides a phase shift in the transfer function of the mode. The length of the waveguide divided by the phase velocity is the time for a point of constant phase in a continuous harmonic wave to travel the length of the waveguide. This time delay is a phase shift in the frequency domain. The phase shift is represented as:

$$\Phi^{(j)}(\omega) = \exp\left(i\omega L / c^{(j)}\right), \tag{4.8}$$

where $c^{(j)}$ is the phase velocity of mode j at frequency ω. This technique has also been used by Kohl, Datta and Shah (1992) in semi-infinite hollow cylinders and by Peterson (1999) whose model is refined here. The evanescent modes are not considered in the propagation because the modes have at least 40 dB of attenuation at a distance of 20 diameters, and at 5 diameters the effects are negligible.

4.1.3. Reception

The transmission from the waveguide to the receiving transducer adds another amplitude factor to the transfer function of each mode. Ideally this interface is modeled as a reflection problem, with the stresses and displacements continuous at the interface, to determine the reflected and transmitted energy. Experimentally, a viscous fluid coupling is used between the waveguide and the transducer, so it is assumed that no shear stress is transmitted. However, the normal stress excites the normal modes of the piezo-electric transducer. A more rigorous interpretation of the interface would consider the slight viscosity of the coupling fluid, which transmits some shear energy. However, the shear energy transmitted into the coupling fluid attenuates considerably, and any shear energy transmitted to the transducer does not excite any of the normal modes of the piezo element (Schmerr 1998). The experimental signals shown in this research represent the excitation of the normal modes of the piezo element of the transducer.

The contact transducer is modeled as an immersion transducer, which has a response that is proportional to the average normal pressure over the face of the transducer (Schmerr 1998). The average

pressure exhibited on the transducer by a single mode is calculated by integrating the normal stress of the mode, $\sigma^{(j)}_{zz}$, over the area of the bar and dividing by the area. The average pressure is an additional amplitude factor in the transfer function of a mode, and it is only calculated for the propagating modes.

4.2. Final Model

The combination of the three parts of the model gives the final form of the dispersion function, which is the sum of the transfer functions of the propagating modes, Eq. (4.9).

$$F_D(\omega) = \sum_j A^{(j)}(\omega) \cdot \Phi^{(j)}(\omega) \cdot \frac{2}{a^2} \int_0^a r\sigma_{zz}^{(j)}(\omega, r) dr \cdot \tag{4.9}$$

The transfer function of each propagating mode contains a relative amplitude term from the excitation, $A^{(j)}(\omega)$, a phase shift term from the propagation, $\Phi^{(j)}(\omega)$, and an additional amplitude term representing the average normal stress. It should be noted that if the phase velocity was the same for all of the modes and did not change with frequency, then the phase shift, $\Phi^{(j)}(\omega)$, would be the same for all of the modes at each frequency. This would allow the phase shift to move outside the summation, and therefore the dispersion function would reduce to a term consisting of the phase shift times the average pressure of the excitation. This is the case for a thin bar where only the first mode propagates and the phase velocity is equal to the bar velocity, $c_b = \sqrt{E/\rho}$.

4.2.1. Discretization

The complexity of the Pochhammer-Chree theory and the arbitrary nature of the ultrasonic signals that are considered dictate that the calculations be best made numerically and thus at discrete frequency intervals. A discrete Fourier transform (DFT) pair, Eqs. (4.10) and (4.11), is used to transform between the time domain and the frequency domain. A lowercase letter is used to denote the time domain and an upper case letter is used to denote the frequency domain.

$$F\{x(n)\} \Rightarrow X[m] = \sum_{n=0}^{N-1} x[n] \exp\left(-inm(2\pi/N)\right) \qquad m = 0,1,\ldots,N-1. \tag{4.10}$$

$$F^{-1}\{X(m)\} \Rightarrow x[n] = \frac{1}{N} \sum_{m=0}^{N-1} X[m] \exp\left(inm(2\pi/N)\right) \qquad n = 0,1,\ldots,N-1, \tag{4.11}$$

where the index n corresponds to time, the index m corresponds to frequency, and N is the number of points in the DFT.

The substitution of the dispersion function into Eq. (4.2) and Eq. (4.2) into the discrete version of Eq. (4.1) yields the final form of the model,

$$x_d(n) = \frac{1}{N}\sum_{m=0}^{N-1}\left[\sum_j A^{(j)}(m)\cdot\Phi^{(j)}(m)\cdot\frac{2}{a^2}\int_0^a r\sigma_{zz}^{(j)}(m,r)dr\cdot X_R(m)\right]\exp(inm(2\pi/N))\cdot \tag{4.12}$$

The phase shift is represented discretely as:

$$\Phi^{(j)}(m) = \exp\left(-im\left(L/c^{(j)}(m)/\Delta t\right)(2\pi/N)\right), \tag{4.13}$$

where $c^{(j)}(m)$ is the phase velocity of mode j at frequency m, and Δt is the time step. The operations within the square brackets of Eq. (4.12) are calculated at each frequency.

4.2.2. Discussion

This model calculates the change of a signal after propagating through a finite length cylindrical bar. The lengths of interest, greater than 5 diameters, are sufficiently in the far field, so only the propagating modes need to be considered for the propagation and reception portions of the model. However, at the lowest frequencies only a small number of modes propagate. The consideration of only these modes may provide insufficiently accurate results in the expansion to determine the amplitudes of the modes. To ensure sufficient accuracy, evanescent modes should also be considered in the expansion. Thus, an area of concern with the model is the number of modes to consider in the calculations.

The least squares method of solving the coefficients in the expansion is quite robust, so the results do not typically change much with an increase in the number of modes. Transfer functions of the first four modes were calculated using various numbers of modes in the expansion, including just the real modes and up to nine modes. It was found that the difference in the calculated transfer functions of the individual modes was typically less than two percent of the maximum value except for the range of frequencies before the second mode cutoff frequency where the difference was larger. However, it was found that at high frequencies with a large number of propagating modes, considering nine modes in the expansion provided good results.

Similar results were also observed when only the normal stress was considered in the expansion. This is also a result of considering bars with lengths that are in the far field. From an experimental standpoint the negligible effects of the second boundary condition can be thought of in terms of a dynamic Saint-Venant's principle.

The evaluation of the expansion at a discrete number of points along the radius produces some obvious erroneous calculations at some frequencies. It was often found that just above a mode's cutoff frequency the amplitude of the mode would often spike along with one of the lower modes. The nature of the mode shapes required large offsetting amplitudes to satisfy the boundary conditions. However, it was found that if the number of modes considered was limited, the errors disappeared. The algorithm that provided the best results considered a fixed number of modes on either side of the mode with the largest average normal stress.

A number of additional steps were used to simplify the model and minimize numerical problems. The stress functions of the modes are complex valued at any given radius, so the coefficients in the expansion are complex as well. However, the phase shift of each stress function can be calculated to eliminate the imaginary part of the stress function. The real form of the stress functions simplifies both the matrix operations and the integration and produces a real coefficient.

The amplitudes of the stress functions change with frequency; therefore, it is prudent to also normalize the real form of the stress functions to help prevent the matrix from becoming singular. This also ensures that the stresses are the same order of magnitude as the applied excitation pressure. It is necessary that the same form of the stress functions be used in the expansion and the integration, so that there are no erroneous phase or amplitude terms added to the transfer functions.

4.3. Experimental Comparison of Analytical Model

A number of experiments in a through-transmission configuration were performed for comparison to the analytical model. The signals and the size of the waveguides used in the experiments are representative of ultrasonic NDE experiments (e.g. Jen *et al.* 1997, Peterson 1994). The application of the analytical model is discussed in the description of the experiments.

The experiments used two 28.6 mm diameter, 1 MHz broadband, longitudinal contact transducers [Panametrics, model V194, Waltham, MA] to excite and receive the ultrasonic signals. The transducers

had a bandwidth, corresponding to a 6 dB drop in the peak amplitude of the spectrum, of 0.4 MHz to 1.1 MHz. The pressure distribution over the area of the transducers was nearly uniform (Puckett and Peterson 2003). Therefore, the pressure distribution, *P(r)*, used in the analytical model was prescribed as having a value of unity at all radii and for all frequencies.

Signals were provided by two different sources depending on the experiment. For one of the experiments a pulser/reciever [Panametrics, 5072PR, Waltham, MA] was used to generate a pulse and amplify the received signal. For the other experiments an arbitrary waveform generator [Agilent 33250A, Palo Alto, CA] was used to generate more complex signals to drive the transducer. With this configuration a radio frequency power amplifier [ENI A-300, Rochester, NY] with a gain of 55 dB was used to amplify the signal to the transducer, and the signal generated by the receiving transducer was amplified by an ultrasonic pre-amplifier [Panametrics model 5660C, Waltham, MA] with a gain of 40 dB. For both setups the amplified signal was averaged to remove noise and recorded by a digital storage oscilloscope [Tektronix TDS 520A, Wilsonville, OR].

Waveguides of 10 mm and 25 mm diameter fused quartz cylindrical rods were used. An amorphous material was chosen for the waveguide because linear elastic and homogeneous assumptions are well satisfied. The properties of the fused quartz rods used in the experiments are a Young's modulus, E, of 72 GPa, a density, ρ, of 2200 kg/m^3, and a Poisson's ratio, v, of 0.162 (General Electric Advanced Materials 2004). A coupling fluid [Sonotech, Inc. UT-30, State College, PA] was used between the transducers and the waveguide to improve the transmission of the ultrasonic signal.

4.3.1. Thick Rod

A thick cylindrical rod was considered with narrow band and broad band excitations. The narrow band excitations required the consideration of up to nine modes over a narrow range of frequencies. The broadband excitations considered a similar number of modes but over a much larger range of frequencies.

Narrow Band

The first experiments considered a 0.25 m long, 25 mm diameter, fused quartz waveguide excited by a Gaussian modulated sine wave. Two different frequencies of the sine wave are shown that compare the results of the experiments to the analytical model. The first frequency, at 1 MHz, coincides with the maximum group velocity of the 6th propagating mode. The other frequency, at 1107 kHz, was chosen so

that the group velocities of all of the modes were well below the velocity of a longitudinal wave in an infinite medium, in this case, the dip in the group velocity curves following the maximum group velocity of the 6th mode. Fig. 4.1 displays the group velocity curves for the 25 mm quartz waveguide with the vertical dashed lines defining the two frequencies. For each frequency the signal was propagated through the waveguide experimentally and calculated using the model

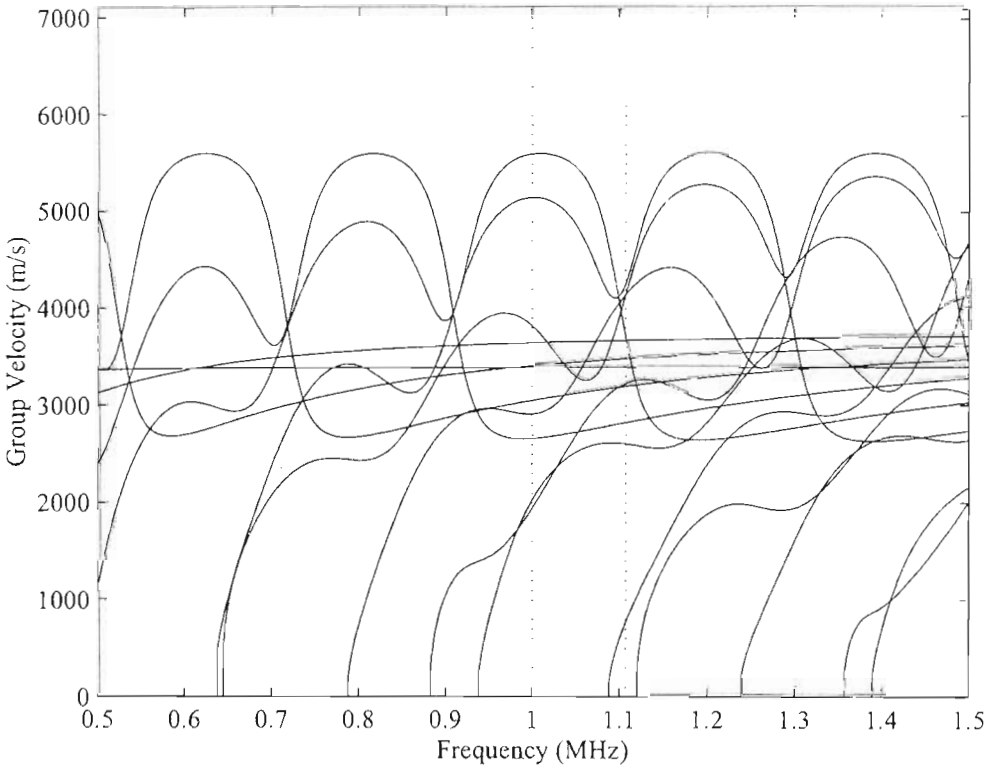

Fig. 4.1. Group velocity curves of a 25 mm diameter fused quartz bar. The vertical dotted lines indicate the frequencies used in the Gaussian excitations.

For the model, the discrete Fourier transform (DFT) of the Gaussian was used as X_R, the reference signal. Dispersion curves (in a wave numbers vs. frequency domain) were calculated for the propagating modes at the appropriate frequencies prior to running the model. At each frequency step the phase velocities and the normal stress functions were used to calculate the complex value of the dispersion function, $F_D(\omega)$. To evaluate the coefficients, $A^{(j)}$, in the expansion, 100 points along the radius were considered. Therefore, in Eq. (4.7) the pressure, $\{P\}$, is a 100×1 column vector, all entries have a value of unity for the constant pressure distribution. The stress, $[\sigma]$, is a $100 \times j$ matrix where j represents the number of modes being considered. Each column of the matrix contains the values of the normal stress

(Eq. 2.11) along the radius for one of the modes being considered. For the two Gaussian signals, all of the energy is in the higher propagating modes, so only the propagating modes were considered in the expansion. For the phase shift, $\Phi^{(j)}(\omega)$, the length of the rod (0.25m) and the phase velocity are used. The phase velocity is calculated from the wave number by $c^{(j)} = \omega/k^{(j)}$. Finally, the average normal stress over the end of the waveguide is calculated for each mode. The coefficient for each mode is multiplied by its phase shift and average pressure. This product is summed with the products calculated for the other modes to produce the value of the dispersion function for that frequency. These calculations are repeated at each frequency step. The inverse DFT of the dispersion function multiplied by the spectrum of the excitation signal is the calculated dispersed signal. This calculated dispersed signal is compared to the measured dispersed signal.

Fig. 4.2 compares the input Gaussian signal (top) to the experimental signal (middle) and the analytical signal (bottom) for the 1 MHz frequency. There is good agreement between the analytical signal and the experimental signal, and both signals exhibit very little dispersion. This is not the case for the second frequency. Dispersion is much more apparent in the comparison of the signals from the 1107 kHz Gaussian excitation, Fig. 4.3. Despite the dispersion, the analytical and experimental signals are still very similar.

Broadband

The ability of the model was also considered with a broadband excitation. For this experiment a pulse excitation of the transducers was used with the 0.5m long 25 mm diameter quartz waveguide. There are 13 modes that have cutoff frequencies below the upper 6-dB limit of the frequency spectrum of the pulse. The same procedure was used for the analytical model, and again only the propagating modes were considered in the expansion because the frequency spectrum of the signal contains very little energy in the first modes.

Fig. 4.4 compares the experimental and analytical signals through a 0.5 m long 25 mm diameter fused quartz waveguide. For this excitation trailing pulses are observed, which are consistent with plane wave theory (Redwood 1960). The general shape between the analytical and experimental signals is very similar, and the arrival times and the amplitudes of the pulses are in good agreement. The analytical model

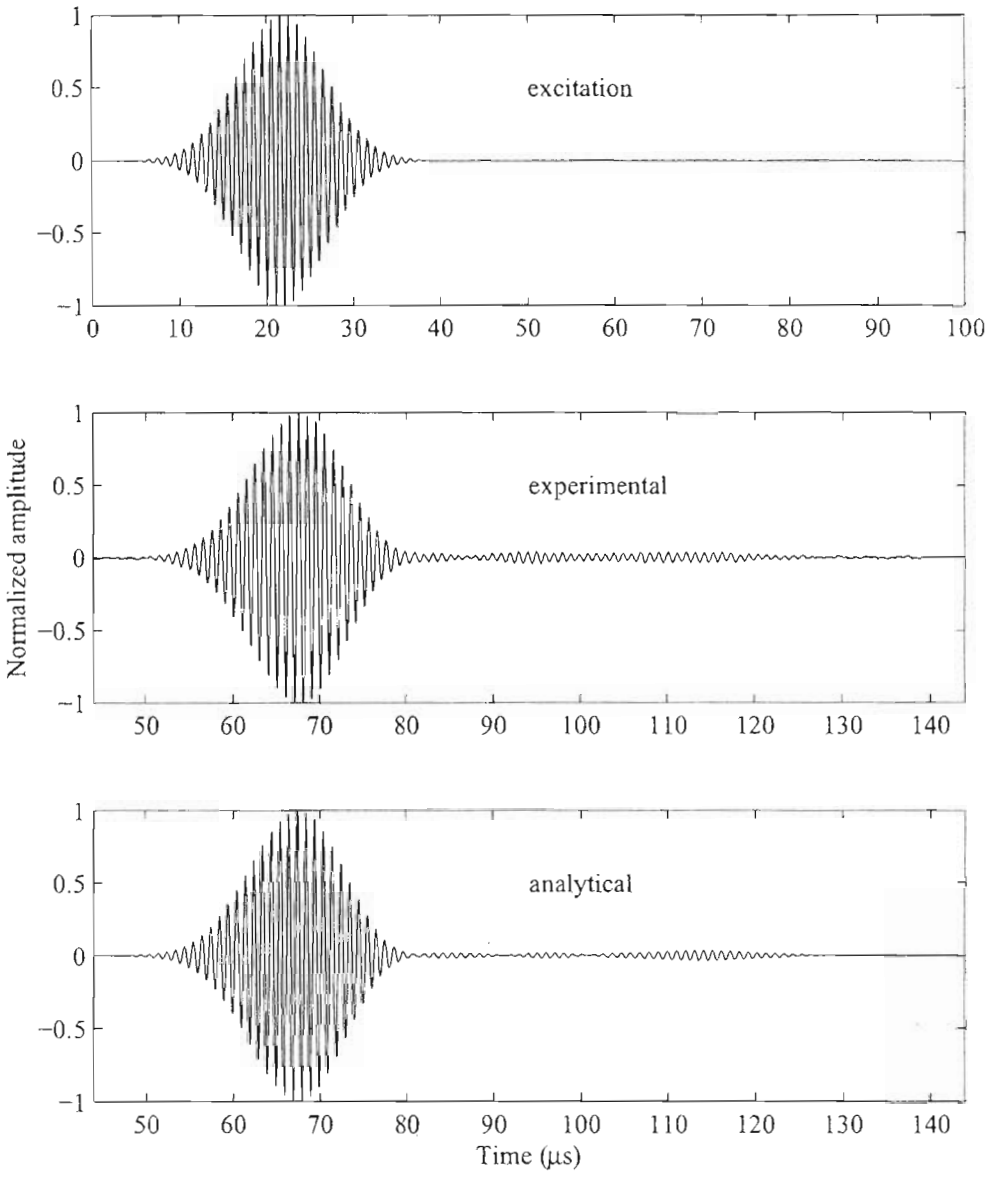

Fig. 4.2. 1 MHz Gaussian excitation of a 0.25m long 25 mm diameter fused quartz waveguide. The excitation signal (top) is compared to the experimental received signal (middle) and the analytical signal (bottom).

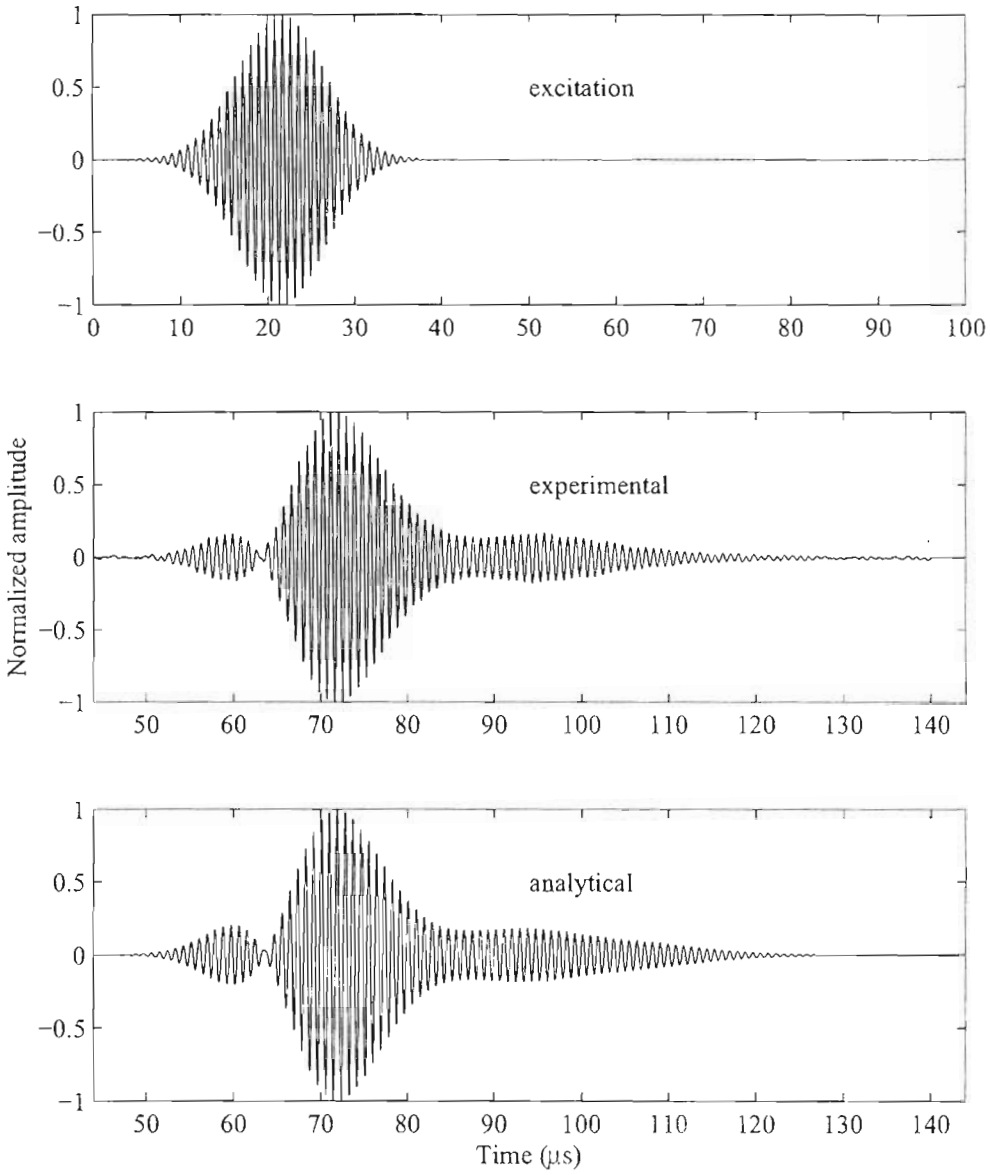

Fig. 4.3. 1107 kHz Gaussian excitation of a 0.25m long 25 mm diameter fused quartz waveguide. The excitation signal (top) is compared to the experimental received signal (middle) and the analytical signal (bottom).

appears to capture nearly all of the physics of the wave propagation in the cylindrical waveguide in this experimental configuration.

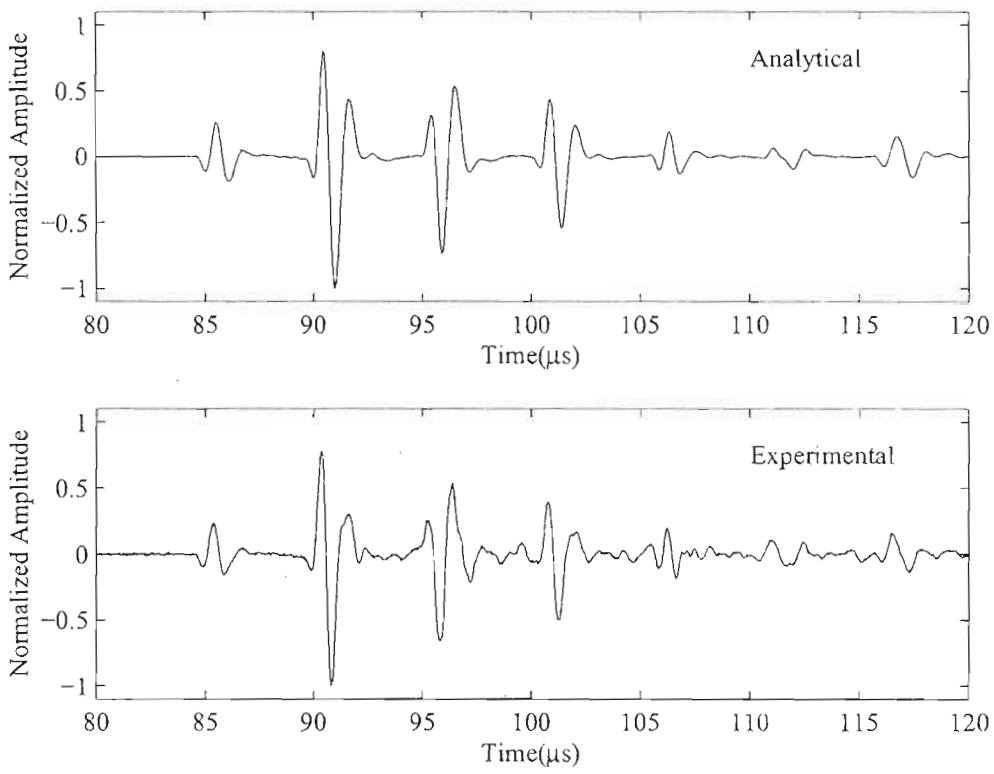

Fig. 4.4. Measured and calculated signals of a pulse propagated through a 0.5 m long 25 mm diameter fused quartz waveguide.

A comparison in the frequency domain indicates similar results. The top graph in Fig. 4.5 is the magnitude of the dispersion function for a 0.2 m long 25 mm diameter quartz bar calculated by the model. There are observed dips in the dispersion function, but these characteristics are also observed experimentally. The lower graph in Fig. 4.5 is the magnitude of the frequency spectrum of an experimental signal measured in the quartz bar. For comparison, the magnitude of the frequency spectrum of the excitation signal is also shown, middle graph Fig. 4.5. Similar dips appear in the frequency spectrum of the measured experimental signal and at the same locations as the dispersion function. These dips are a result of the insensitivity of the receiving transducer to radial variations in the normal stress. It is advantageous to consider the transfer functions of the modes to explain the occurrence of the dips.

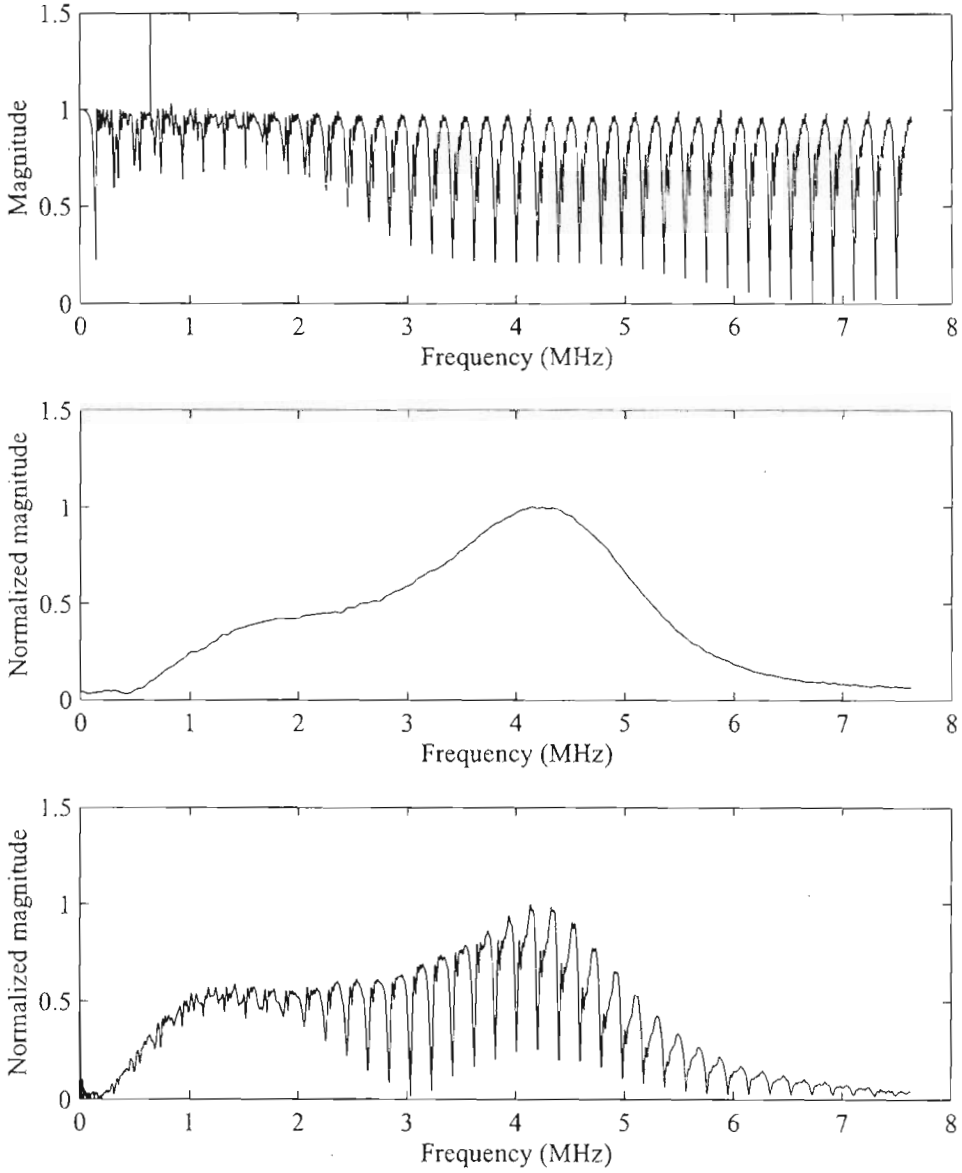

Fig. 4.5. The dispersion function for a 20 cm long, 25 mm diameter fused quartz waveguide (top), the magnitude of the frequency spectrum of an experimental signal before (middle) and after propagating through the waveguide (bottom).

The transfer functions of the 1st, 6th, and 7th modes for the 0.5 m long waveguide are plotted in the lower graph of Fig. 4.6 (other modes are not shown for clarity). The upper graph of Fig. 4.6 shows the dispersion function for this waveguide. A comparison of the two graphs indicates that the large dips in the transfer function of the waveguide appear at frequencies where the magnitudes of the transfer functions of two neighboring modes are equal. The phase velocities of the two modes at these frequencies are different. For certain length bars the modes will be entirely out of phase at the receiving end of the bar, and the magnitudes will cancel each other. Similar effects are observed at other frequencies though not as pronounced. In all cases it is a result of the interaction of the modes. The energy is present; however, the superposition of the normal stress of the modes over the radius is such that the energy is not measured because the response of the transducer is proportional to the average normal stress. It must be stressed though that the model is intended to represent the experiment not mathematical modeling. Similar models that do not include receiving end conditions have been used in theoretical studies and have shown to satisfy energy criteria (Gregory and Gladwell 1989, Rattanawangcharoen, Shah, and Datta 1994).

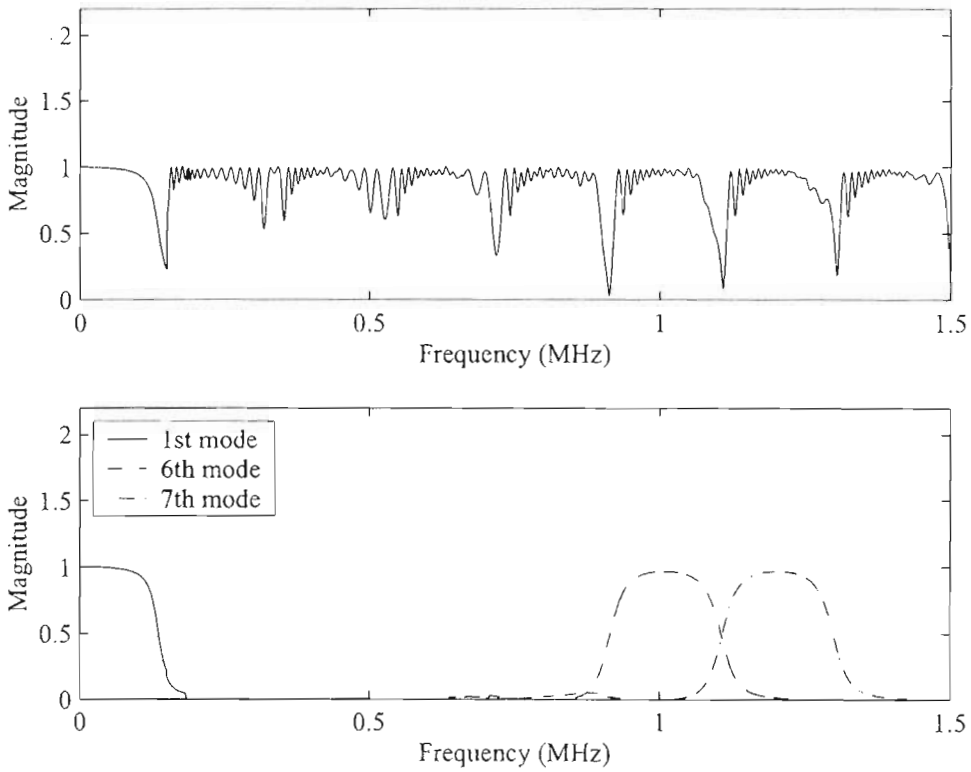

Fig. 4.6. Magnitude of the transfer function of the waveguide (top) and the magnitudes of the transfer functions of the 1st, 6th, and 7th modes (bottom). Other modes are not shown for clarity.

The transfer functions of the modes also illustrate that each mode is dominant over a small frequency range. This is consistent with the observations of Zemanek (1962) who found that the stress function of a mode is entirely in phase when the group velocity is close to the longitudinal wave speed. The experiments and the model used a uniform excitation across the radius of the cylindrical bar, which most excites the modes whose normal stress functions are in phase. The averaging over the area of the normal stress of the receiving transducer further emphasizes the modes that are in phase.

4.3.2. Long Rod

Experiments also considered a 1.22 m long 10 mm diameter fused quartz waveguide with a Gaussian excitation of the transducer for the reference signal. The reference signal and its spectrum appear in Fig. 4.7. At the 1-MHz center frequency the diameter-to-wavelength ratio d/λ_L is 1.7, where is λ_L is calculated using the longitudinal wave speed, c_L. For this geometry waveguide, the first four modes have cutoff frequencies below the upper 6-dB limit of the frequency spectrum of the signal. The analytical model for this waveguide considered the first five modes at every frequency. For the lower frequencies some of the modes were evanescent. At the highest frequencies the five modes consisted of the mode with the largest average normal stress and the two modes above and below.

The same procedure was used for the analytical model with exception of different dispersion curves. The dispersed signal calculated by the analytical model is compared to the measured dispersed signal in Fig. 4.8. The arrival times, the lengths, and the general shape of the two signals are quite similar. There are discrepancies between the two signals in the interference patterns. This is not unexpected. In the frequency range of the signal the model is evaluated at 5000 different frequencies, so a slight error in the phase velocities have a profound effect on signal. Therefore, it is useful to look at several different domains to determine the ability of the model.

One domain in which signals can be compared is a time-reversal mirror (TRM) (Fink 1997). For a regular TRM all of the signals are exited and measured experimentally. A TRM experiment consists of two steps. In the case of a cylindrical rod, first, an acoustic signal is excited by a source at one end of the rod. The acoustic signal propagates through the rod, and the altered signal is recorded at the opposite end. In the second step of the TRM the recorded signal is reversed in time, and the receiver is excited with the

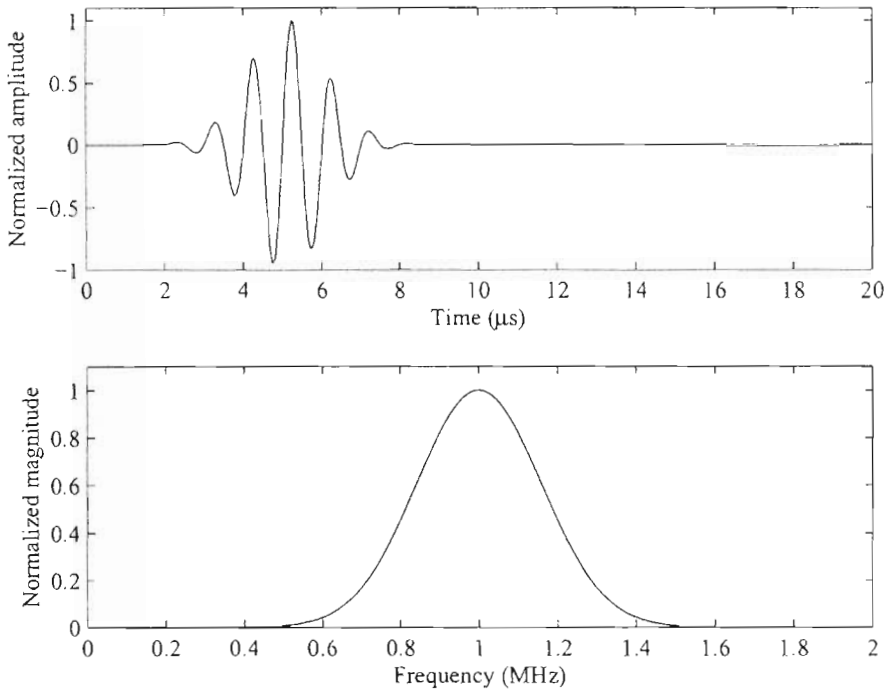

Fig. 4.7. Reference signal used with a 1.22 m long 10 mm diameter fused quartz waveguide. Upper graph is the time domain. Lower graph is the frequency domain.

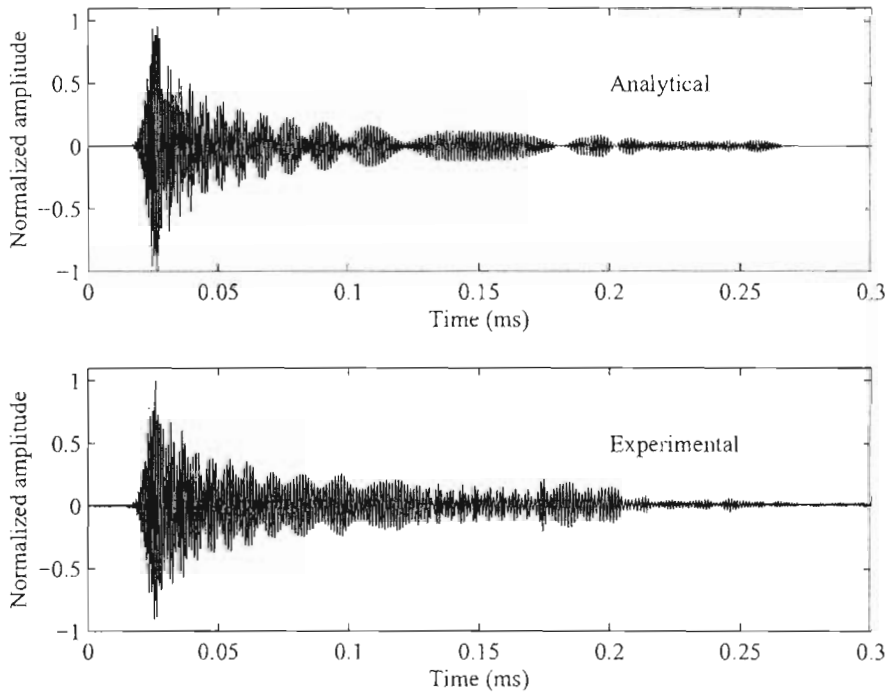

Fig. 4.8. Measured and calculated signals of the reference signal propagated through a 1.22 m long 10 mm diameter fused quartz waveguide.

reversed signal. The reversed signal propagates through the rod, and a new signal is recorded at the source. If time invariance is satisfied, this new signal is the same as the original acoustic signal. This ability of the TRM can be used to produce a compact time signal from a dispersive system. For this experimental setup, time invariance has been demonstrated using a TRM, and a compact signal has been produced in a dispersive waveguide (Puckett and Peterson 2003).

If the analytical model correctly captures the physics of the waveguide then the calculated dispersed signal should also be able to produce a signal with compact support in the time domain. The previously calculated signal was used in place of the experimental signal in a TRM as a means of judging the ability of the analytical model. For the experiment, both the experimentally measured dispersed signal and the calculated dispersed signal were reversed in time and used to excite the transducer in the experimental setup. The measured signals are compared in Fig. 4.9. It can be seen that the experimental signal reproduced the original signal consistent with previously reported experiments. The analytical signal, however, also produces a signal with compact support in the time domain, which when compared with the original dispersed signal is significantly shorter. There are discrepancies between the signals, which again are not unexpected considering the number of calculations. Additionally, if there were a major error in the model then such a compact signal would not have been measured.

A second domain for further comparison of the calculated dispersed signal with experimentally measured dispersed signal is the time-frequency domain. Time-frequency analysis provides an additional means of evaluating the calculated signal. One standard tool to analyze ultrasonic signals is the short-time Fourier transform (STFT) (e.g. Niethammer and Jacobs 2001). The energy density spectrum of the STFT, called a spectrogram, can be used to visualize the results of a STFT. Spectrograms of the dispersed signals appear in Fig. 4.10 and Fig. 4.11 with the analytical curves in black. These curves are the calculated arrival times of the modes based on the group velocity curves. In both spectrograms the individual modes are apparent and follow the analytical curves. Additionally, the same modes appear in both spectrograms. However, there does appear to be slightly more energy in the analytical signal especially in the slower group velocities.

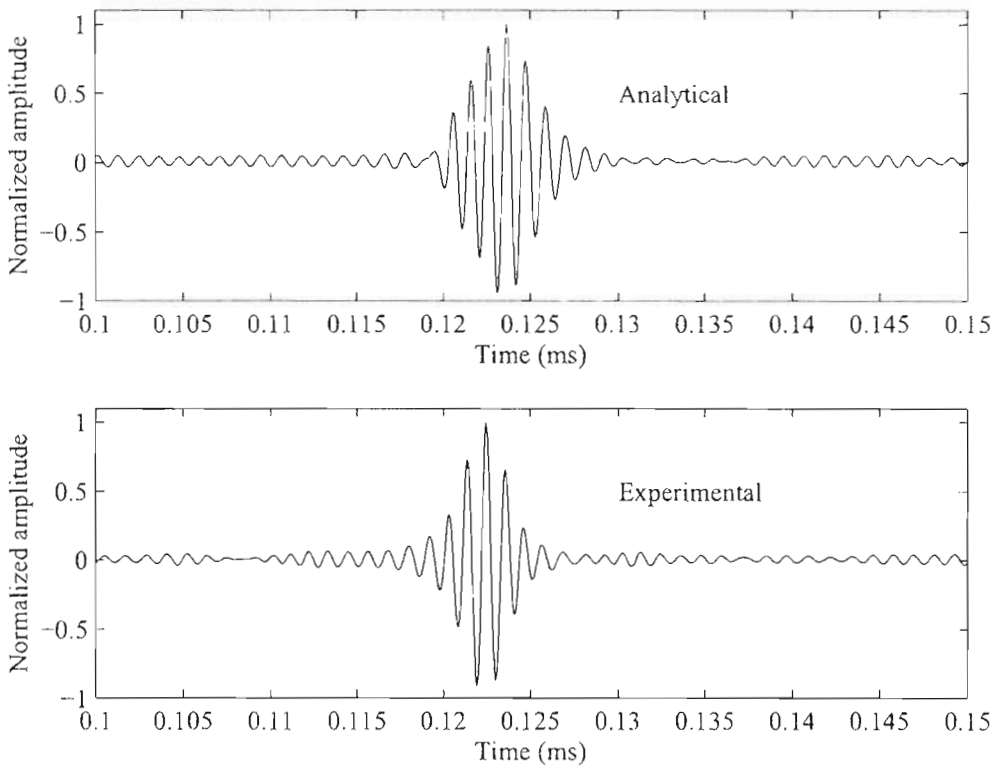

Fig. 4.9. Measured signals recorded in a time-reversal mirror. The top signal represents the signal measured using the excitation of the reversed experimental signal from Fig. 5. The bottom signal represents the signal measured using the excitation of the reversed analytical signal from Fig. 5. Error bars on the experimental signal are negligible and not visible.

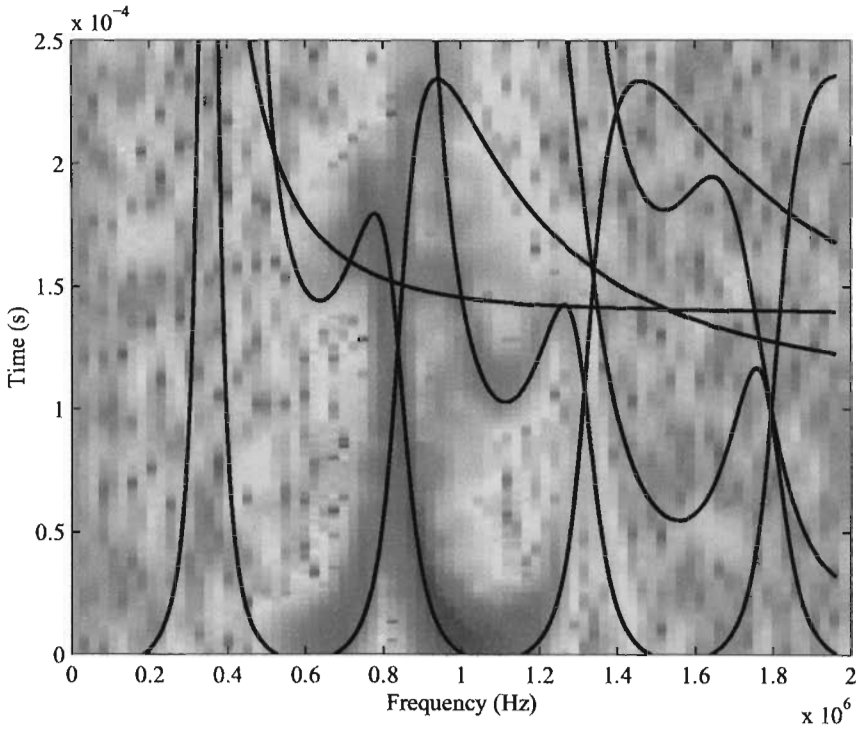

Fig. 4.10. Spectrogram of the measured dispersed signal from Fig. 4.8. Theoretical curves appear in black.

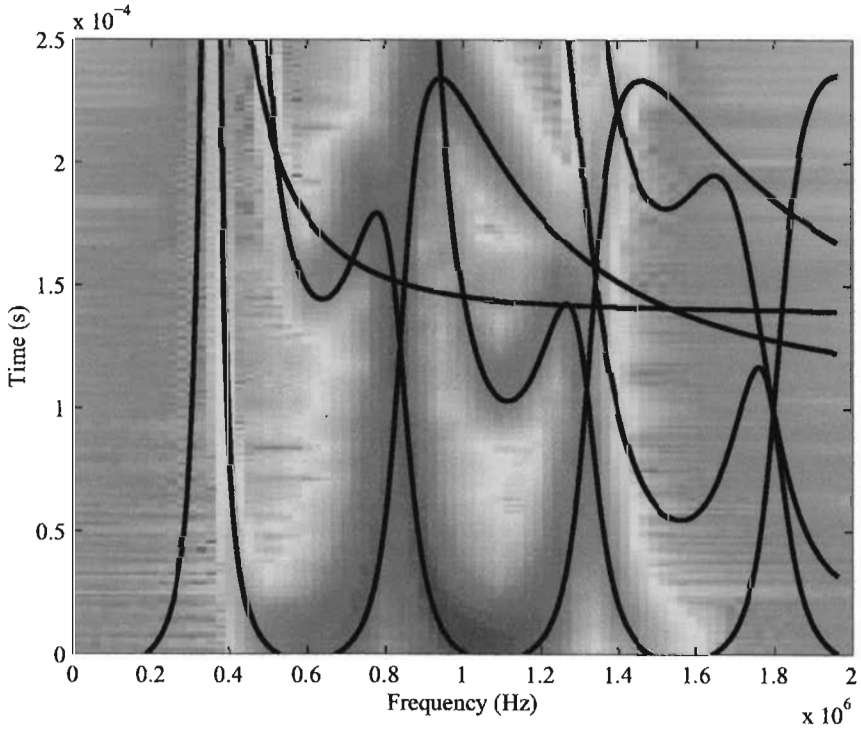

Fig. 4.11. Spectrogram of the calculated dispersed signal from Fig. 4.8. Theoretical curves appear in black.

4.4. Parametric Study

Experimental comparison with the analytical model shows the model adequately captures the physics of the wave propagation for d/λ_L of 1.7 and 4.2. At lower values of d/λ_L there are fewer propagating modes. The analytical model may not be able to capture all of the physics of the wave propagation with only a couple of modes. For values of d/λ_L greater than 4.2 there are more propagating modes, so the model should be capable of capturing the physics of the wave propagation.

4.4.1. Smaller Values of d/λ_L

The 10 mm diameter, 1.22 m long fused quartz waveguide was also excited with a Gaussian broadband signal centered at 250 kHz. The experiments used 500 kHz transducers, the frequency response of which shifted the center frequency of the Gaussian to about 300 kHz. At the 300 kHz center frequency the diameter-to-wavelength ratio, d/λ_L, is 0.51, where is λ_L is calculated using the longitudinal wave speed, c_L. A phase corrected 250 kHz Gaussian signal propagated through a nondispersive aluminum sample provided the signal used for the analytical model.

The same comparisons used to evaluate the 10 mm diameter waveguide at 1 MHz are used to evaluate the 10 mm waveguide at 250 kHz. The dispersed signals are compared, Fig. 4.12. The experimental time-reversal mirror was performed using the analytically calculated and experimentally measured time-reversed dispersed signal, Fig. 4.13. The spectrograms of the dispersed signals were calculated, Fig. 4.14, and Fig. 4.15. Additionally, the frequency spectrums of the analytically calculated and experimentally measured dispersed signals are compared, Fig. 4.16.

From these figures there are mixed results about the ability of the analytical model. The dispersed signal calculated by the analytical model has a noticeably different shape than the measure signal. However, the calculated dispersed signal is almost as effective as the experimentally measured dispersed signal in the TRM experiment. The spectrograms of both the experimental and analytical signals follow the theoretical curves closely and exhibit the same modes. However, the experimental spectrogram indicates that the second mode dominates entirely not long after the second mode cutoff frequency, and there is no power transmitted in the third mode. The spectrogram of the analytical signal shows there is still some power in the first mode at higher frequencies than the experimental signal, and there is power in the third mode as well. Finally, the frequency spectrums of the two signals appear quite different. However, in both

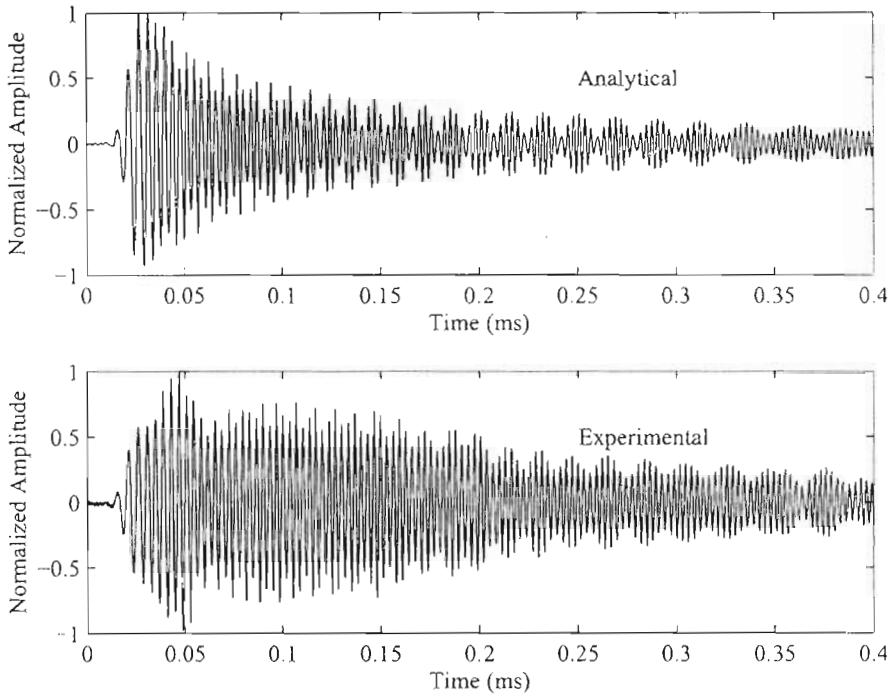

Fig. 4.12. Calculated and measured signals from a 250 kHz Gaussian excitation through a 1.22 m long, 10 mm dia. quartz rod.

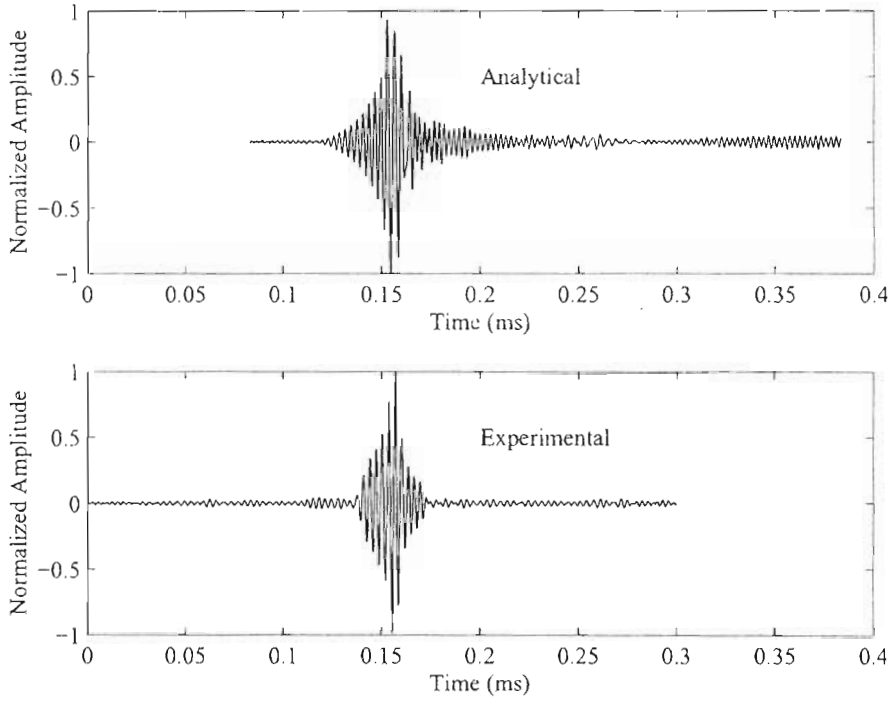

Fig. 4.13. Measured signals from a time-reversal mirror in a 1.22 m long, 10 mm dia. quartz rod. Top and bottom signals were excited by the time-reversed analytical and experimental signals from Fig. 4.12.

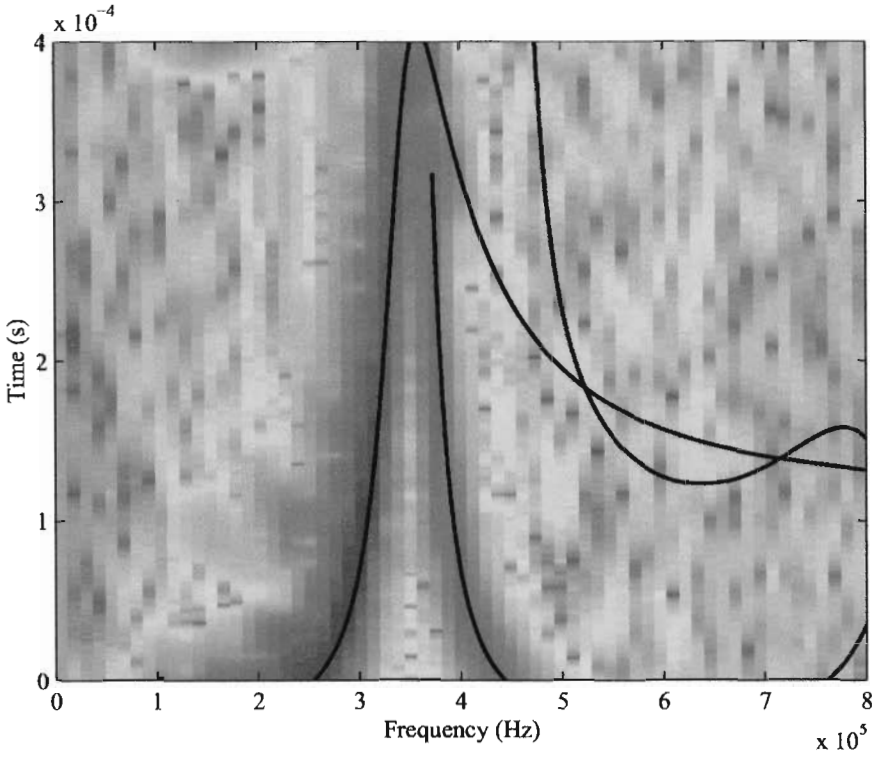

Fig. 4.14. Spectrogram of the measured dispersed signal from Fig. 4.12. Theoretical curves appear in black.

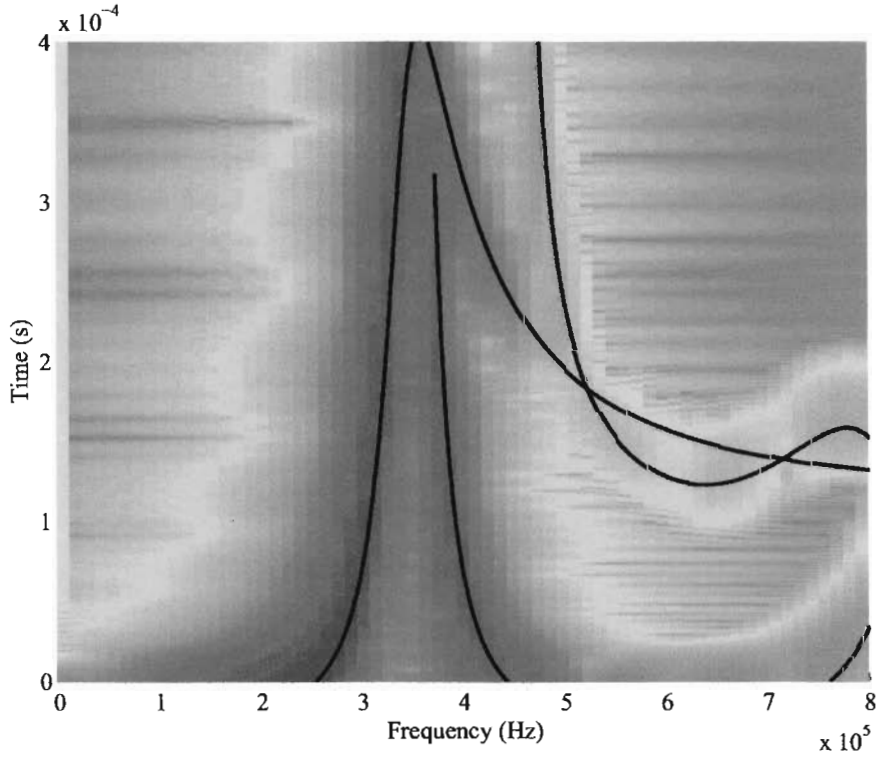

Fig. 4.15. Spectrogram of the calculated dispersed signal from Fig. 4.12. Theoretical curves appear in black.

of the spectrums there is a dip between 300 kHz and 400 kHz, and right after the dip there is "noise" in the spectrum. This "noise" is due to the interaction of the first and second modes.

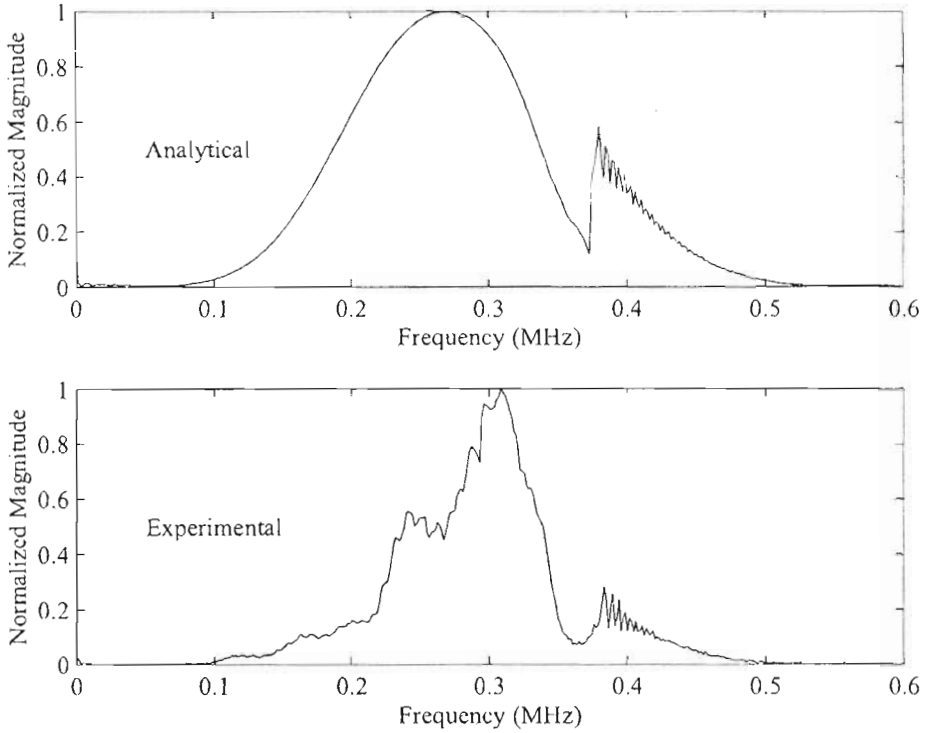

Fig. 4.16. Frequency spectrum of the signals in Fig. 4.12.

It is apparent that the analytical model is capturing some of the physics of the wave propagation; however, there are discrepancies. The poor quality of the experimental time-reversal indicates there may be some issues related to this experimental setup. These issues are also indicated by the frequency spectrum of the experimental system, which does not have the general shape of the excitation like the analytical signal. Problems arise when conducting ultrasonic experiments to excite only the first one or two axially symmetric modes. For a large diameter waveguide a low frequency is needed to excite only the first mode. A low center-frequency contact transducer has a large diameter to accommodate the size of the piezo-electric element. In order to excite the first mode ultrasonically the diameter of the transducer must be much larger than the diameter of the cylinder. However, for good experimental results, the size of the transducer and the diameter of the bar should be comparable. This experimental scenario is on the outer limits of ultrasonic uses, and will be rarely encountered.

4.4.2. Large Values of d/λ_L

A fused quartz waveguide 25 mm in diameter was used to consider values of d/λ_L up to 20. A pulse excitation was used with 5 MHz center-frequency transducers. At 5 MHz the diameter-to-wavelength ratio, d/λ_L, is near 21. The dispersed signal calculated by the model was compared to the experimentally measured dispersed signal in a 0.2 m long waveguide, Fig. 4.17. Consistent with the 1 MHz pulse the signal calculated by the model compares well to the experiment. Although the exact shapes of the signals are only similar, the arrival times and relative amplitudes are very accurate for all of the trailing pulses. Note that the vertical scales of the lower graphs are smaller than the vertical scale of the top graph. The frequency spectrum of the experimental signal is compared to the dispersion function in Fig. 4.5

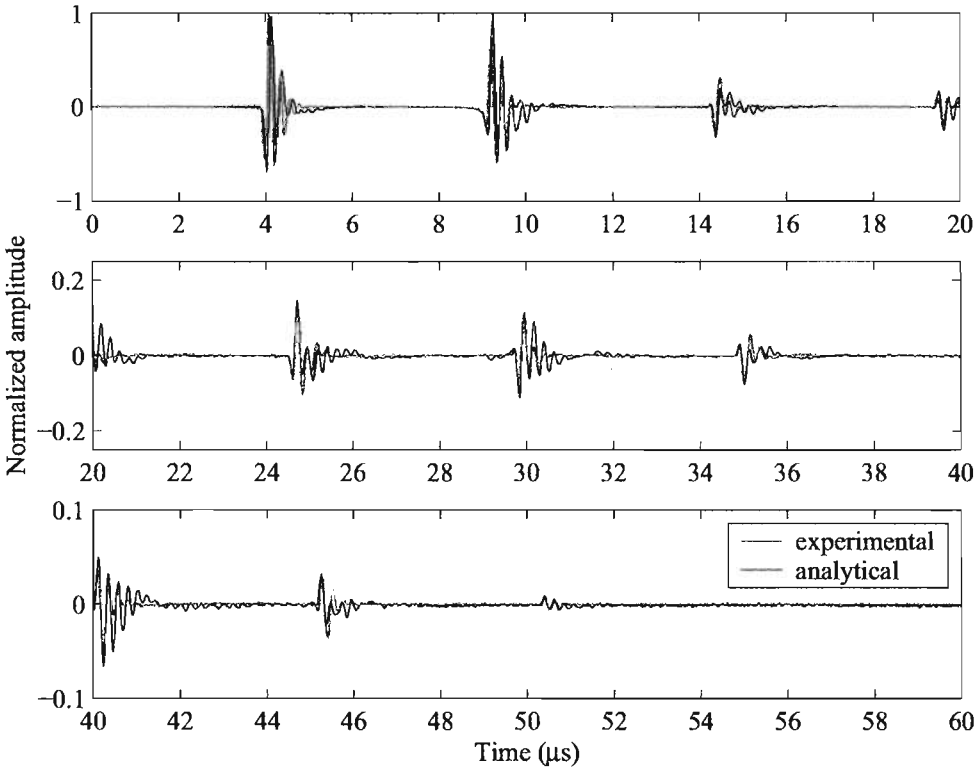

Fig. 4.17. Comparison of the experimental and analytical signals in a 200 mm long, 25 mm diameter fused quartz waveguide excited by a 5 MHz pulse.

4.5. Discussion of Experiments

The comparisons made for a number of experimental conditions demonstrate the ability of the model. Within those experimental conditions the model produced consistent results. The experimental

comparisons indicate the analytical model captures the general physics of multiple mode wave propagation in cylindrical waveguides. The ability of the model was demonstrated in four different domains. In the time and frequency domain the dispersed signals calculated by the analytical model were found to be similar to the experimentally measured dispersed signals for the same waveguide. In the time-reversal domain the calculated dispersed signal was able to produce a signal with compact time domain in a dispersive waveguide using a time-reversal mirror. In the time-frequency domain the spectrograms of the analytical and experimental signals demonstrated the presence of the same modes in each signal. In all the domains it was shown that the model captures the general physics of multiple mode wave propagation in cylindrical waveguides. However, there were some slight discrepancies between the signals calculated by the analytical model and the experimental signals.

The comparison of the dispersed signals for all of the different waveguides produced similar results. The analytical signals normally had a similar shape as the experimental signal with some discrepancies. These discrepancies are not unexpected. For most comparisons the model considered 5000 different frequencies and up to 9 modes. A slight variation in the material properties affects both the phase velocities and the normal stress functions. However, the discrepancies seem to be related to the relative amplitudes of the modes. The arrival times of the dispersed signals agreed well between the experiments and the model. Also, the length of the dispersed signals agreed well. For the 5 MHz pulse the arrival times of all of the pulses calculated by the model were exactly the same as the arrival times of the pulses observed in the experiments. However, the shapes of the pulses are only similar with obvious differences. These comparisons imply the phase information in the model is accurate, but the amplitudes of the modes may be off.

The TRM experiments and the spectrograms indicate similar results. The ability of the analytical signal to create a signal with compact support in the time domain was demonstrated with the TRM experiments despite the discrepancies between the experimental and analytical dispersed signals. These observations are consistent with previous time reversal research that has shown that only the phase information is needed in the time reversal mirror to create a signal with compact support in the time domain (Montaldo *et al.* 2001). Therefore, the TRM experiments imply the phase velocity information seems to be accurate regardless of the accuracy of the amplitude information.

The best indication that the amplitude information is not perfect appears in the spectrograms. The spectrograms of the dispersed signals calculated from the analytical model show that the higher modes contain energy at frequencies not observed in the spectrograms of the experimental dispersed signals. Specifically, the spectrograms in Fig. 4.10 and 4.11 show there is extra energy in the third mode of the analytical signal.

The experimental comparisons with the analytical model indicate that for these waveguides the phase information is accurate. This implies the material properties of the waveguide used in the analytical model are accurate. The accuracy of the material properties would imply the normal stresses should also be accurate. Therefore, the discrepancies in the amplitude information may be due to the assumptions of the end conditions. Both the excitation transducer and the receiving transducer have been idealized. There may be aspects of the experimental system that are not captured in the analytical model. Meitzler (1961) observed mode coupling between the first axially symmetric mode and certain flexural modes at frequencies where the phase velocity of the first axially symmetric mode was the same as the phase velocity of one of the flexural modes in long wires. The measured signals displayed a reduction in the peak amplitude and an increase in the duration of the pulse. The waveguides considered in this research are not as long; however, there may be some excited flexural modes that contribute to the measured signal, which are not accounted for in the analytical model. However, the information from the model is adequate to produce results that generally capture the physics of wave propagation in cylindrical waveguides.

This model assumes linear elastic homogeneous isotropic materials. If these criteria are not satisfied then calculated signals may not agree well with experiments. A possible extension of this work could consider the use of modes sensitive to anisotropy to characterize the radial material properties of the waveguide.

CHAPTER 5: PHYSICAL INSIGHTS

The ability of the analytical model to capture the physics of the wave propagation allows the model to be used to explore the behavior of axially symmetric wave propagation in the waveguide. The contribution of each propagating mode can be determined from the transfer functions of the modes, which have already indicated that different modes dominate over certain frequency ranges. It is the interactions of the modes that describe the experimentally observed phenomena.

5.1. Trailing Pulses

When the end of a solid cylindrical bar is excited by a high frequency pulse the measurement of the transmitted signal at the opposite end of the bar is characterized by the appearance of several secondary pulses of similar shape trailing the main pulse as shown in Fig. 5.1. These secondary pulses are known as trailing pulses, and were first observed by Mason and McSkimin (1947). They explained the appearance of the trailing pulses by considering the transverse wave reflected from an incident longitudinal wave.

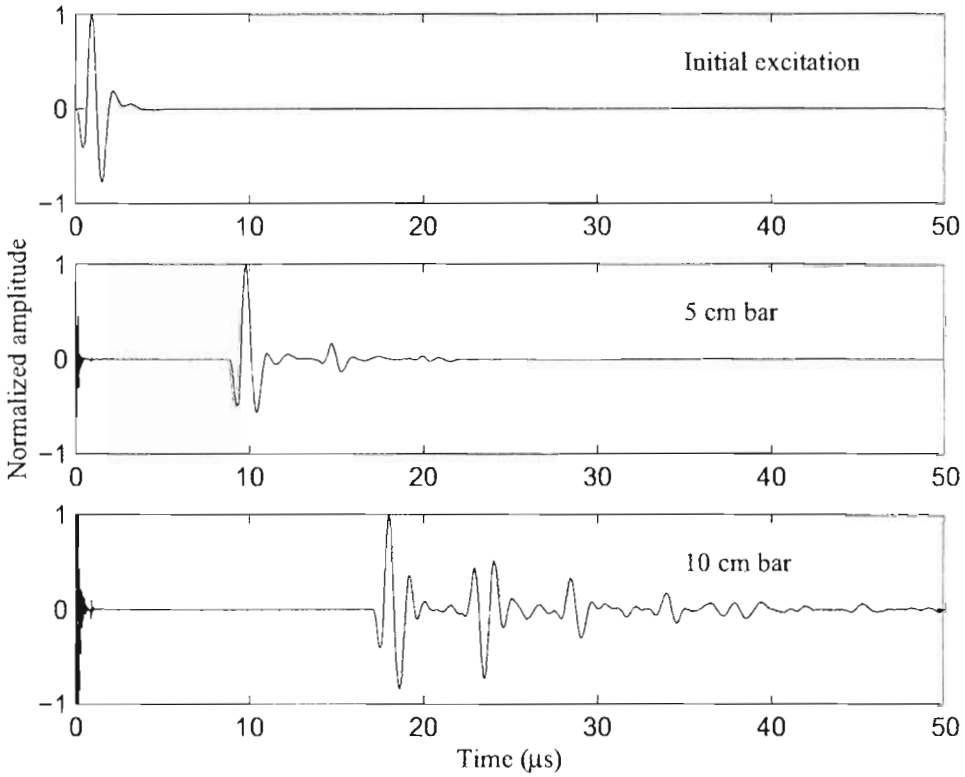

Fig. 5.1. Comparison of a 1MHz pulse excitation with the measured signals from two different length bars.

A longitudinal wave at glancing incidence on the traction free boundary of the cylinder reflects a longitudinal wave and a transverse wave to satisfy the boundary conditions. The angle of the transverse wave with the wall of the bar is considerable, such that the transverse wave propagates across the diameter of the bar over a relatively short length of the bar, Fig. 5.2. On the opposite side of the cylinder the transverse wave reflects a transverse wave and a new longitudinal wave, which propagates in the same direction as the original longitudinal wave and corresponds to the first observed trailing pulse after the main pulse. The time delay of the trailing pulse behind the first pulse is the time for the transverse wave to propagate across the diameter of the bar. The transverse wave continues to excite additional longitudinal waves at each reflection with the cylinder wall. The longitudinal waves appear as additional trailing pulses in the measured signals of Fig 5.1. Although these wave interactions occur for any excitation, distinct trailing pulses are generally observed in experiments where the excitation signal has sufficient bandwidth such that the pulse length is less than the time delay between pulses.

A complete description of axially symmetric wave propagation in infinite solid cylinders is given by the solutions of Pochhammer (1876) and Chree (1889). However, the relationship of the solutions with trailing pulses has not been considered extensively. McSkimin (1956) approximated the cylinder as a fluid waveguide by considering only the dilatational components of the Pochhammer-Chree solutions. The approximation was used to determine the effective loss from the mode conversion at the boundary, so the main pulse could be used to measure attenuation. Using the approximation of a fluid waveguide introduced by McSkimin, Redwood (1959) conducted a more rigorous analysis, which also considered inward traveling transverse waves. Redwood further suggested that the Pochhammer-Chree solutions do not predict the existence of trailing pulses or the observed amplitudes of the pulses.

Trailing pulses have been observed for pulse excitations consisting of a single cycle as well as for pulse excitations consisting of several hundred cycles. In the latter case, the excitation signal has a bandwidth that is very narrow, and Redwood focused on this case. From experimental observations of high frequency excitation signals in waveguides (a radius to wavelength ratio, a/λ, of the order of 10) Redwood concluded the first pulse in the series of trailing pulses travels with a velocity close to that of longitudinal waves in an infinite medium, c_L. If the pulse were to be described by the Pochhammer-Chree theory, then the signal would have to be propagating in one of the higher modes. However, Redwood noticed the

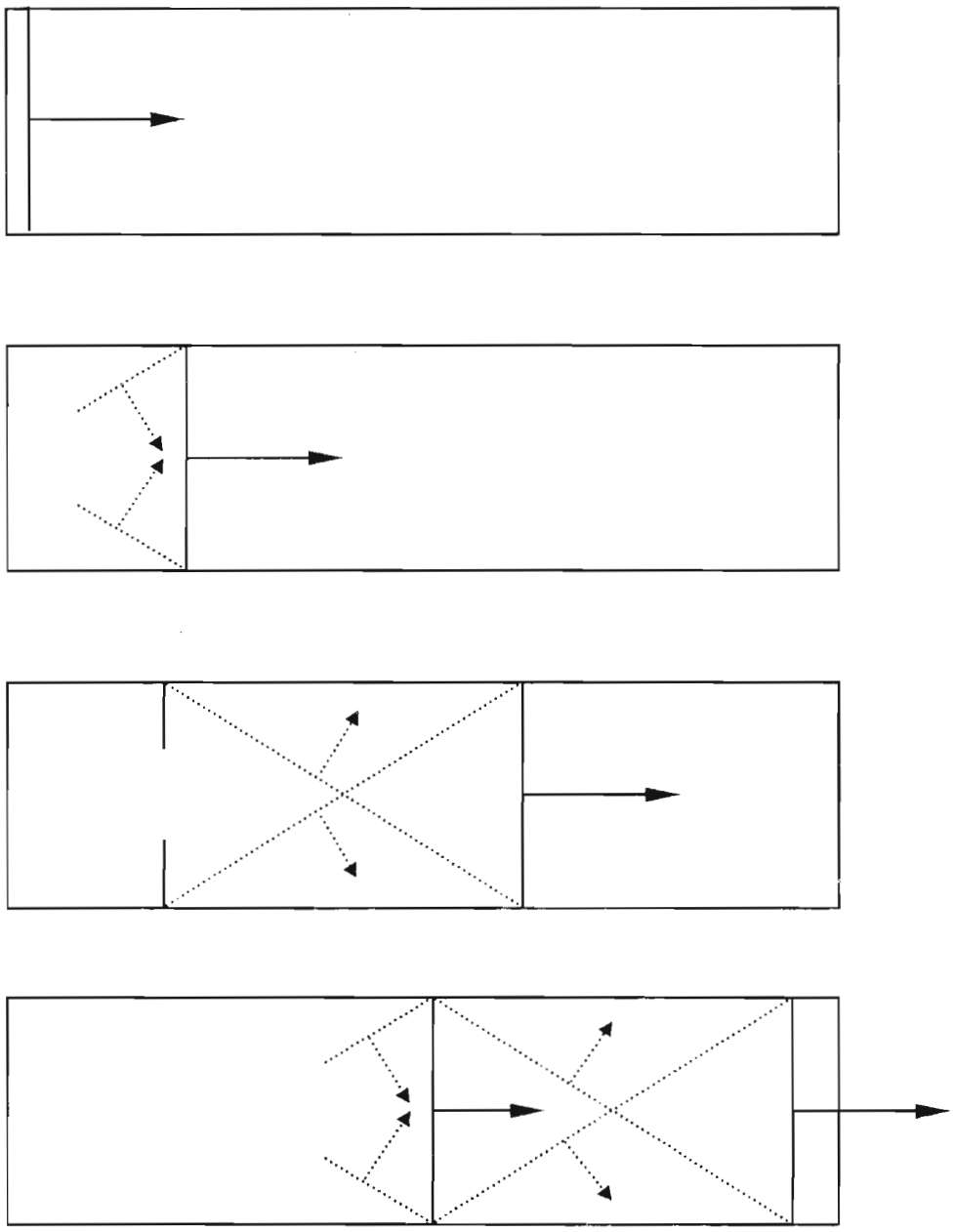

Fig. 5.2. Propagation of a compressional wave (solid) excites a trailing shear wave (dashed), which excites additional longitudinal and shear waves.

dispersion curves predict the arrivals of the pulses will change as the phase velocity and group velocity change with frequency, while in the experiments, the pulses arrived at the same times independent of frequency. Redwood concluded the Pochhammer-Chree solutions could predict neither the observed loss in amplitude of the main signal nor the presence of any trailing pulses and developed the modified solution.

However, these conclusions are based solely on the phase velocity curves and are incorrect. For the case of trailing pulses, the idea of the first pulse in the series propagating in a single higher mode is wrong. A new look at the relationship of trailing pulses to the Pochhammer-Chree theory is needed, and the advances of computer technology allow a more detailed analysis to be made. The semi-analytical model based on the Pochhammer-Chree solutions allows the contribution of each individual mode to be determined. The individual modal contributions make clear the relationship of the Pochhammer-Chree solutions to trailing pules.

A closer look at the excitation signal and the transfer functions of the propagating modes reveals the relationship of the Pochhammer-Chree solutions to the observed behavior of trailing pulses. Fig. 5.3 compares the frequency spectrum of the excitation signal used in Fig. 5.1 (top) with the transfer functions of the modes of the cylindrical bar (middle) and the group velocity curves (bottom). In the graphs of the transfer functions and the group velocity curves, each line corresponds to a different propagating mode. It is apparent from the middle graph that the magnitude of the transfer function of each mode is largest over a small range of frequencies. In effect a mode dominates over a specific frequency range. This is consistent with Zemanek's (1962) findings and other explanations. Zemanek noted that the axial displacement is in phase over a range of frequencies where the mode's group velocity is near the longitudinal wave speed. The same behavior is observed for the normal stress. The experiments and the model used a uniform excitation across the radius of the cylindrical bar, which most excites the modes whose normal stress functions are in phase. The averaging over the area of the receiving transducer further emphasizes the modes that are in phase. These two boundary conditions produce the shape of the transfer functions of the modes.

The frequency spectrum of the excitation pulse overlaps the transfer functions of multiple modes, which implies the pulse excites multiple propagating modes in the bar. But how do the trailing pulses relate to the propagating modes? Qualitatively the shape of each of the trailing pulses is similar to the

excitation pulse. This would imply that the magnitude of the frequency spectrum of each of the trailing pulses is similar to that of the excitation pulse. Therefore, each of the trailing pulses contains energy from each of the propagating modes. Additionally, each mode has a similar range of group velocities, so all of the modes should arrive at nearly the same time.

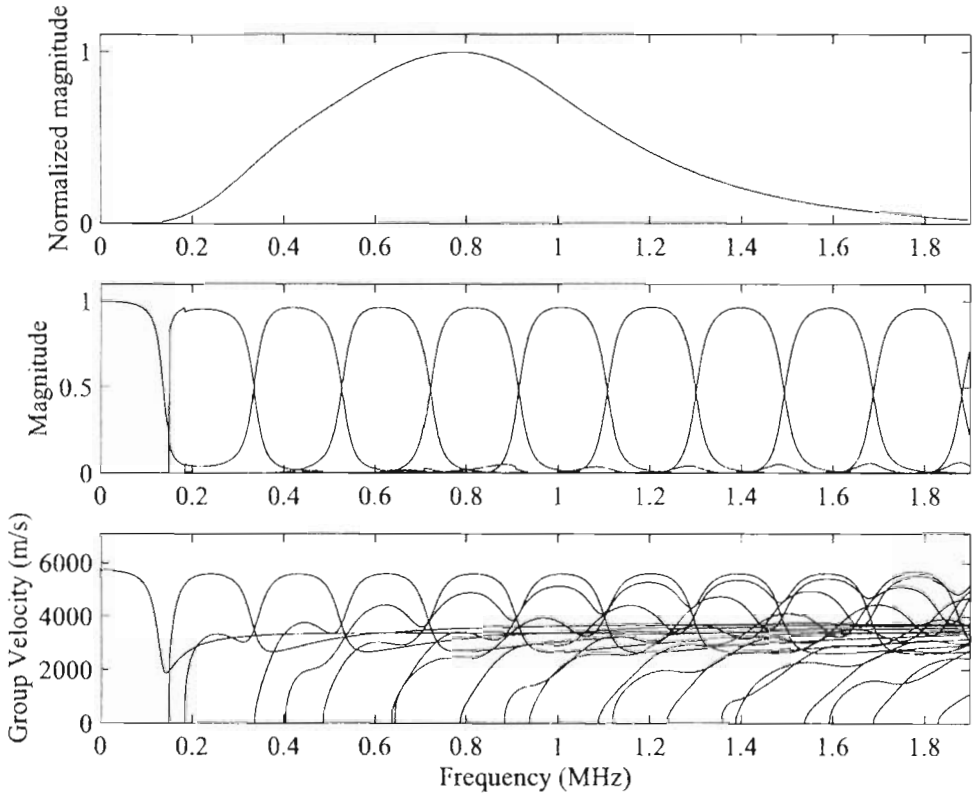

Fig. 5.3. Comparison of the magnitude of the frequency spectrum of the excitation signal (top) with transfer functions of the modes (middle) and the group velocity curves (bottom).

The nature of the model allows these behaviors to be verified. The inverse discrete Fourier transform is a linear operator, so the summation of the modes in the dispersion function can occur after the inverse transform operation instead of before as shown above. Therefore, the contribution of each mode can be determined in the time domain and the frequency domain. Fig. 5.4 shows the time representation and the frequency representation of the propagating modes for a pulse propagated in a 0.2 m long 25 mm diameter waveguide. The second mode through the ninth mode are dominant in the frequency spectrum of the excitation signal and contribute to the dispersed signal. In the figure, the temporal signals appear on the left and the magnitudes of the spectral signals appear on the right. The bottom left graph is the summation

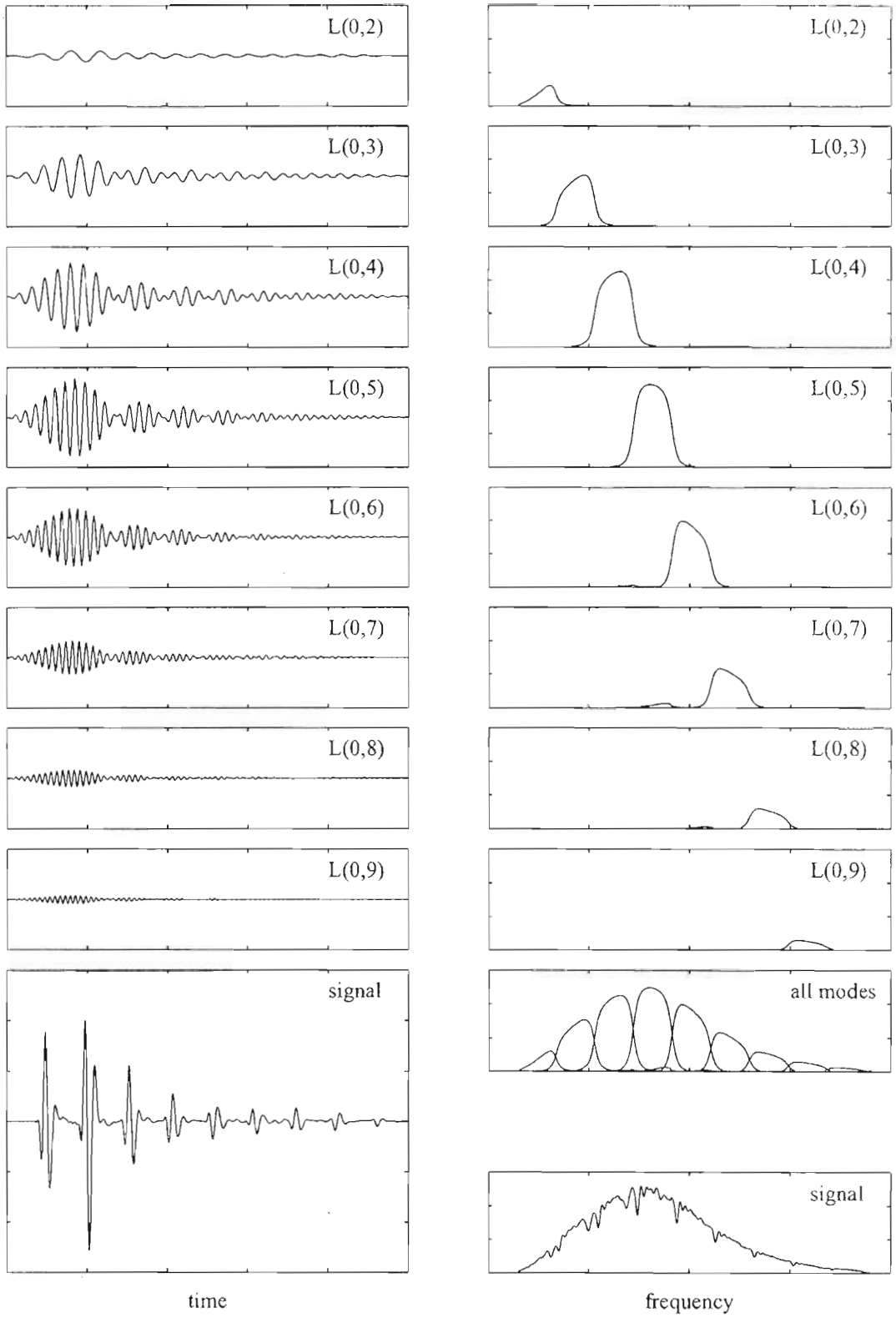

Fig. 5.4. Contributions of the individual modes for the trailing pulses observed in a 0.2 m long 25 mm diameter fused quartz rod. Temporal signals are on the left and spectral signals are on the right.

of the temporal signals, and the bottom right graph is the magnitude of the dispersion function. The spectral signals of all of the modes are plotted in the penultimate graph on the right.

The temporal signals in Fig. 5.4 confirm that each of the propagating modes contributes energy to each of the trailing pulses. It is the interference pattern of the modal signals that produces the observed trailing pulses. The relationship of trailing pulses to the Pochhammer-Chree solutions is more apparent, but considerably more complicated than described by Redwood. However, Redwood based his arguments on observations of trailing pulses from pulse excitations of many cycles, i.e. a sine burst, which have a narrower bandwidth than a pulse excitation.

The observation of trailing pulses from narrow band sine burst excitations can be explained by considering the frequency spectrum of a sine burst. An increase in the number of cycles in a sine burst increases the magnitude of the frequency spectrum very close to the frequency of the sine wave. The bandwidth is defined as the range of frequencies with magnitudes within a certain decibel drop of the maximum magnitude, so an increase in the number of cycles in a sine burst narrows the bandwidth of the signal. Fig. 5.5 compares the frequency spectra of a 10 cycle sine burst and a 20 cycle sine burst with different scales. From Fig. 5.5 it is apparent the 20 cycle sine burst has a narrower band frequency spectrum than the 10 cycle sine burst. However, the magnitudes of the frequencies away from the center frequency remain the same. The magnitudes of these frequencies are sufficient to create the characteristics of trailing pulses.

As an illustration, the calculated signals for two 1 MHz sine burst excitations in a 0.25 m long 25 mm diameter quartz bar are shown. The modal components of a 10 cycle sine burst are presented in Fig. 5.6, and the modal components of a 20 cycle sine burst are presented in Fig. 5.7. Both figures use the same scale, and in both signals the trailing pulses overlap because the length in time of the sine burst is greater than the time between trailing pulses. The peak of the frequency spectrum coincides with the maximum magnitudes of the transfer function of the sixth mode, which has by far the largest amplitude signal of the propagating modes. However, in both signals other propagating modes are very important in composing the shape of the propagating signal.

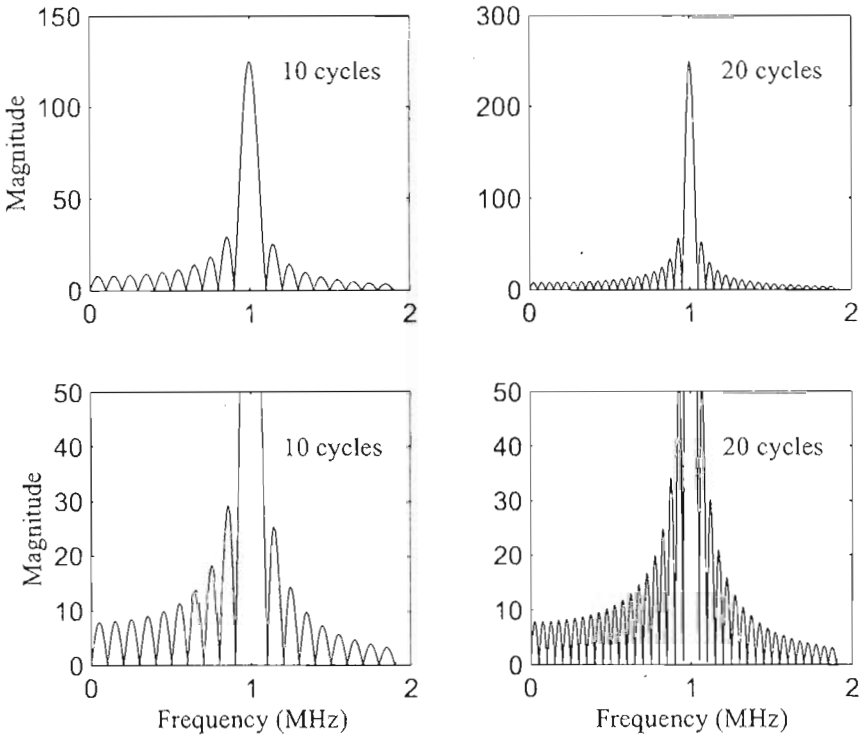

Fig. 5.5. Comparison of the frequency spectrums of sine bursts.

A comparison of Fig. 5.6 and Fig. 5.7 shows the beginnings of the temporal signals of the corresponding modes are the same for both excitations, which is expected since the beginnings of the excitations are the same. The remaining portions of the corresponding temporal signals are different due to the different interference of the two excitations. The amplitudes of the temporal signals do not change noticeably with the increase in the number of cycles; only the magnitudes of the frequency components directly above and below the center frequency change. The magnitudes of the frequency components away from the center frequency are only changed by the phase components. For a further increase in the number of cycles in the sine burst the same effects will occur, and the same modes will contribute to the signal.

A smooth variation of the group velocity with frequency is one of the experimental observations on which Redwood (1959) based his conclusions. The modal decomposition indicates that more than one mode is excited with a sine burst. These modes have a similar range of group velocities, so a shift in the center frequency up or down will simply put more energy into the neighboring modes with the same group velocities. Therefore, the arrival time of the signal will not change.

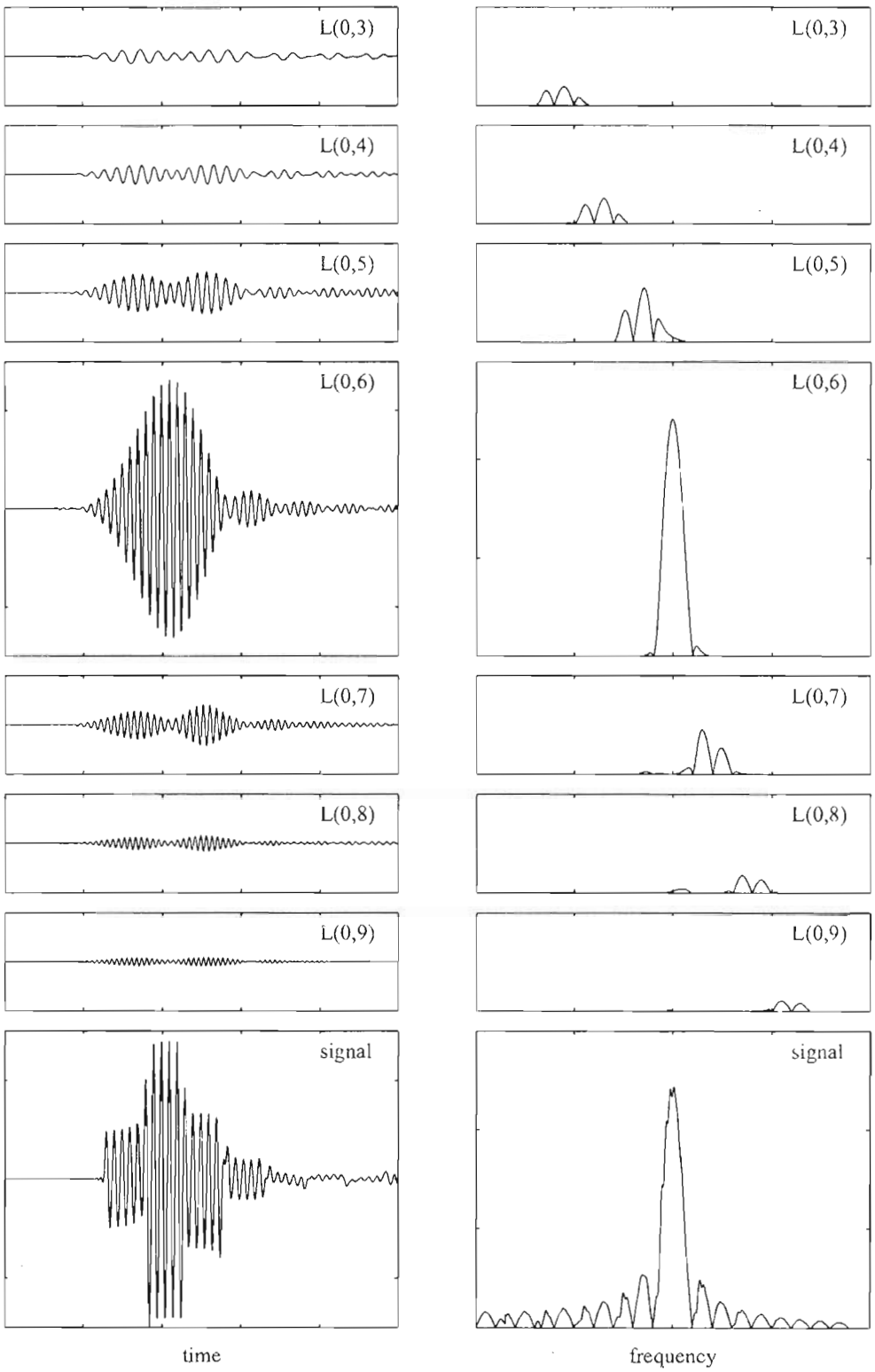

Fig. 5.6. Contributions of the individual modes for a 10 cycle sine burst propagated through a 0.25 m long 25 mm diameter quartz bar. Temporal signals are on the left and spectral signals are on the right.

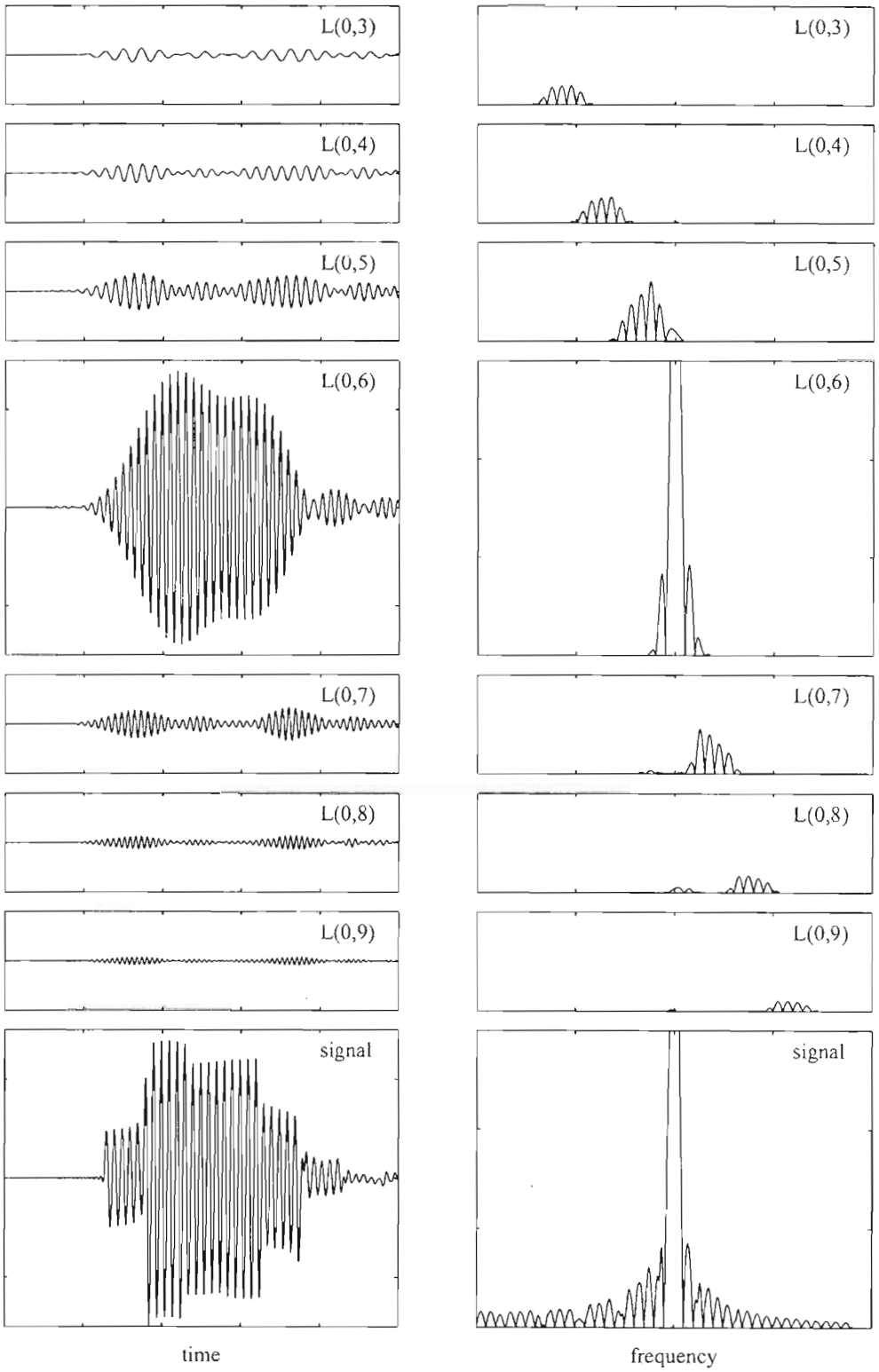

Fig. 5.7. Contributions of the individual modes for a 20 cycle sine burst propagated through a 0.25 m long 25 mm diameter quartz bar. Temporal signals are on the left and spectral signals are on the right.

A signal such as a Gaussian modulated sine wave has much less energy in the frequencies away from the frequency of the sine wave. Meitzler (1965) used a 2.5 MHz Gaussian excitation with a bandwidth of 10 kHz in a 2.12 m long 1.44 mm diameter wire of Isoelastic alloy to demonstrate the backward wave motion of the third axially symmetric mode. For the wire, this was a sufficiently narrow band signal to exhibit the variation of the group velocities of the first three modes over the narrow frequency range predicted by the Pochhammer-Chree solutions. In this case, although multiple modes are excited, over the narrow frequency range the modes do not have the same group velocities. As such, the pulses in the received signals correspond to individual modes. However, for the modes to be separated in time, long cylinders are required due to the large time signatures of the narrow band signal. Meitzler's cylinder had a length to diameter ratio, L/d, of almost 1500 where as Redwood based his conclusions on bars with a L/d of less than 10.

5.2. Excitation of a Single Mode

The propagation of a single nondispersive mode in a cylindrical bar is of interest in ultrasonic NDE and the SHPB. The propagation of a single nondispersive mode allows information from a sample to be transmitted though the cylinder without changing. Previously only the first mode has been considered because it is described by one-dimensional theory and is the only mode excited for low frequency signals. However, the use of the first mode limits the diameter of the waveguide and the frequencies that can be used. From the transfer functions and group velocity curves the low frequencies over which the first mode is nondispersive are apparent. The transfer functions and group velocities also show that all of the higher modes are nondispersive over a small frequency range. Over this frequency range the other modes have considerably smaller amplitude. Zemanek (1962) qualitatively observed this by just considering the group velocity curves and normal stresses of the modes. The transfer functions provide a quantifiable prediction of the amplitude of the propagating modes at a frequency. Therefore, with a sufficiently narrow band excitation, it should be possible to propagate a single mode at higher frequencies with little dispersion.

5.2.1. Frequency Dependence

It is quite interesting that excitations that are centered on certain frequencies will propagate nondispersively while others will be very dispersive. A series of analytical calculations are presented to

show the change of a Gaussian excitation propagated through a cylinder for different frequencies. The nondispersive and dispersive frequency ranges can be found be considering the transfer functions of the waveguide, which are specific to the diameter of the waveguide and the end conditions. Of most interest are the peaks of the transfer functions of the modes, which have a group velocity close to the longitudinal wave speed and are the least dispersive. The intersection of the transfer functions of the modes are also of interest because at these frequencies the signals are most dispersive. Fig 5.8 shows the transfer functions and the group velocity of modes. Table 5.1 lists the frequencies of the peaks of the transfer functions and their group velocities. Table 5.2 lists the frequencies of the intersections of the transfer functions of two neighboring modes and the group velocities of the modes.

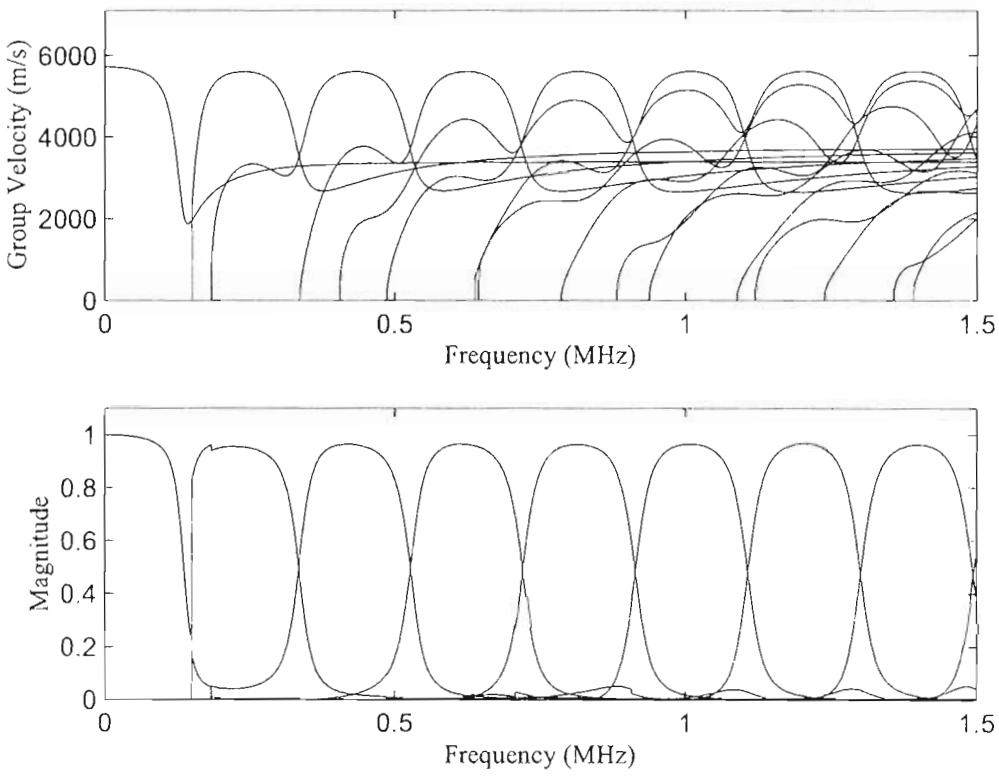

Fig. 5.8. Group velocities (top) and transfer functions (bottom) of the propagating modes.

Mode	Frequency (Hz)	Amplitude	Group Velocity (m/s)
1	0.00	1.0000	5720.76
2	222015.38	0.9559	5576.12
3	418853.76	0.9644	5586.41
4	614166.26	0.9648	5592.71
5	815200.81	0.9634	5602.08
6	1007843.02	0.9655	5604.62
7	1203536.99	0.9665	5607.69
8	1398849.49	0.9628	5609.86
9	1594161.99	0.9615	5611.48
10	1788330.08	0.9596	5614.02

Table 5.1. Frequencies of the peaks of the transfer functions of the modes and the corresponding group velocities.

Frequency (Hz)	Mode	Group Velocity (m/s)	Mode	Group Velocity (m/s)
149917.60	1	1956.17	2	2320.43
334930.42	2	3525.49	3	3524.99
527572.63	3	3663.14	4	3744.56
721359.25	4	3657.62	5	3935.36
914382.93	5	3676.87	6	4096.29
1107406.62	6	3692.98	7	4262.49
1300811.77	7	3691.47	8	4436.35
1494216.92	8	3692.05	9	4599.56
1687622.07	9	3694.82	10	4747.53
1881027.22	10	3699.79	11	4878.66

Table 5.2. Frequencies of the intersections of the transfer functions of the modes and the corresponding group velocities.

Two frequency ranges were considered in the analytical calculations. The first set of calculations considered the frequency range of 240 kHz to 420 kHz. This range of frequencies contains the peaks of the second and third mode and the intersection of the second and the third mode for a 25 mm diameter fused quartz cylinder. The second set of experiments considered the frequency range 1000 kHz to 1200 kHz, which contains the peaks of the sixth and seventh modes and their intersection for a 25 mm diameter fused quartz cylinder. Over each frequency range a 25 mm diameter, 0.252 m long fused quartz waveguide was considered in the analytical model with a Gaussian excitation.

A Gaussian signal is similar to a sine burst, but the start and end of the burst are gradual, and the frequency spectrum of the Gaussian signal can be very narrow. The downside of the Gaussian signal is the shape is neither flat nor compact in time. All of the Gaussian signals were defined by the equation,

$$x_r(t) = \exp[-0.5((t-\mu)/\sigma)^2]\sin(2\pi t f)\,, \tag{5.1}$$

where x_r is the time representation of the reference signal used in the model, μ is the location of the pulse in time, σ is the standard deviation, and f is the center frequency of the signal. For all of the Gaussian signals only the center frequency changed, so the envelope of the signals defined by the Gaussian distribution is the same. The standard deviation was chosen so the frequency spectrums of the signals defined by a 40 dB drop in amplitude were plus or minus 100 kHz around the center frequency. This is a sufficiently narrow spectrum that, when centered at the frequency associated with the peak amplitude of a single mode, will fall within the transfer function of the mode and predominantly excite the mode. The propagated signal of this mode should have little dispersion because the group velocity of the signal is nearly constant. The Gaussian signals centered at 240 kHz, 420 kHz, 1000 kHz, and 1200 kHz meet this criterion, and correspond to the frequencies of the peaks of the transfer functions of the second, third, sixth and seventh modes respectively. Fig. 5.9 compares the propagated signals for the different Gaussian signals.

The calculated signals illustrate the varying amounts of dispersion for the different frequencies. In both frequency ranges the signals increase in length as the frequency changes from the peak of a transfer function to the intersection of two transfer functions, and decrease in length as the frequency approaches the peak of the next mode. The four frequencies corresponding to the peaks of the transfer functions maintain their shape and arrive at a time corresponding to a group velocity near the longitudinal wave speed. At 330 kHz both the second and third modes are nearly equally excited and the group velocity of both modes is approximately 3525 m/s. This is substantially slower than the longitudinal wave speed, so the signal should appear later in time than the Gaussian excitations at the frequencies near the maximum of modes. However, there is still energy that arrives at the time corresponding to waves with the longitudinal wave speed. Although the Gaussian is a narrow band signal, there is still appreciable energy away from the center frequency that includes frequencies with group velocities near the longitudinal wave speed. The same phenomenon is observed in the second range of frequencies at 1100 kHz, the intersection of the sixth and seventh mode.

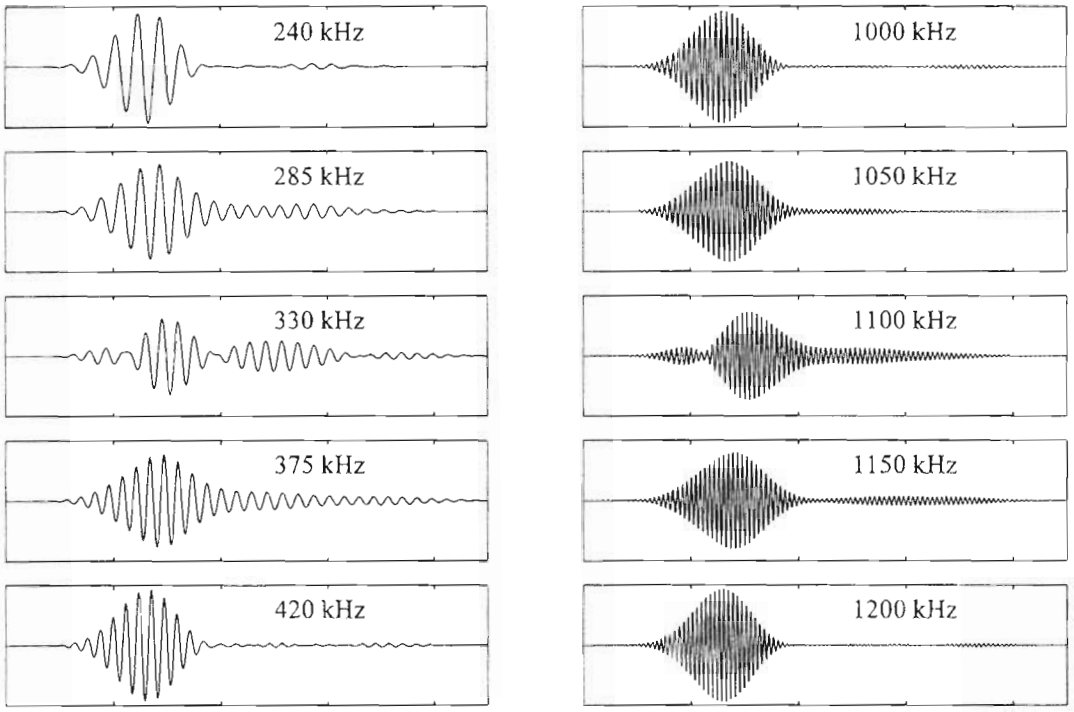

Fig. 5.9. Comparison of the calculated signals from a Gaussian excitation over a range of frequencies corresponding to the second and third modes (left graphs) and the sixth and seventh modes (right graphs).

5.2.2. Distance

The analytical results show the amount of dispersion in the frequencies centered at the peaks of the transfer functions. There does appear to be some energy trailing the main pulse over the same time period as the more dispersive signals. The Gaussian excitations were considered in a set of experiments to observe the change of the signal with distance. Four frequencies, 335 kHz, 420 kHz, 1000 kHz, and 1107 kHz were considered for two different lengths, 0.25 m and 0.5 m. The excitation signal is compared to the measured dispersed signals for the two length bars for each frequency in Figs. 5.10 to 5.13.

For the longer lengths, more dispersion is apparent at all of the frequencies. For 335 kHz and 1107 kHz this is not unexpected because two modes are equally excited and there is a large amount of variation in the group velocity. However, the frequencies associated with the peaks of the transfer functions are also more dispersive, and there is energy that trails the main pulse. There are two factors that contribute to this dispersion, the excitation of the neighboring modes and the variation of the group velocity

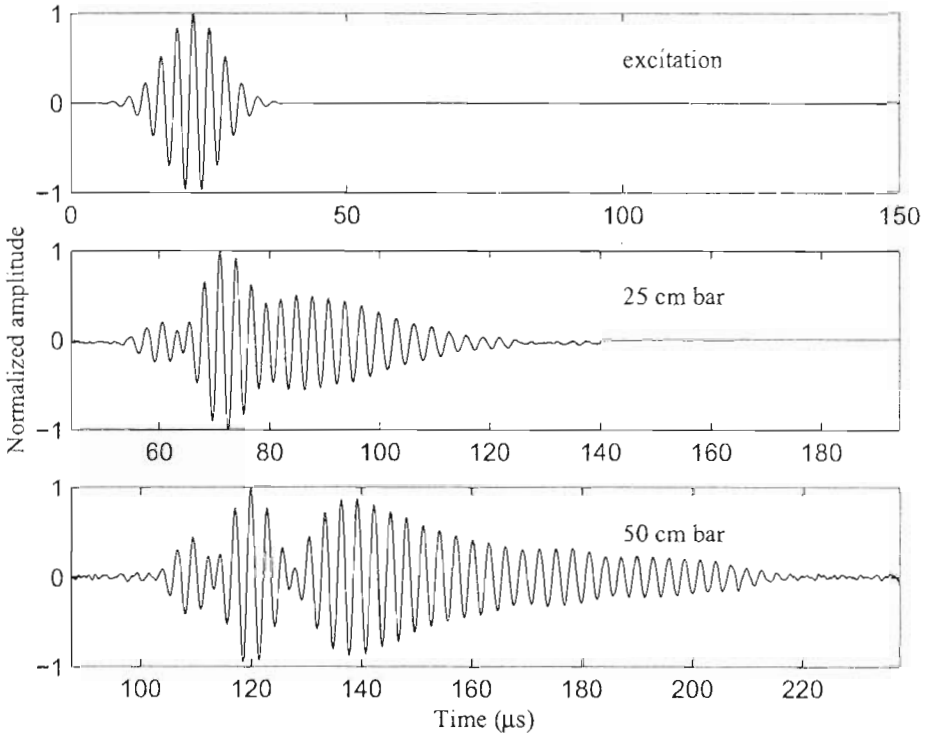

Fig. 5.10. Comparison of a Gaussian signal centered at 335 kHz (top) propagated through two length bars.

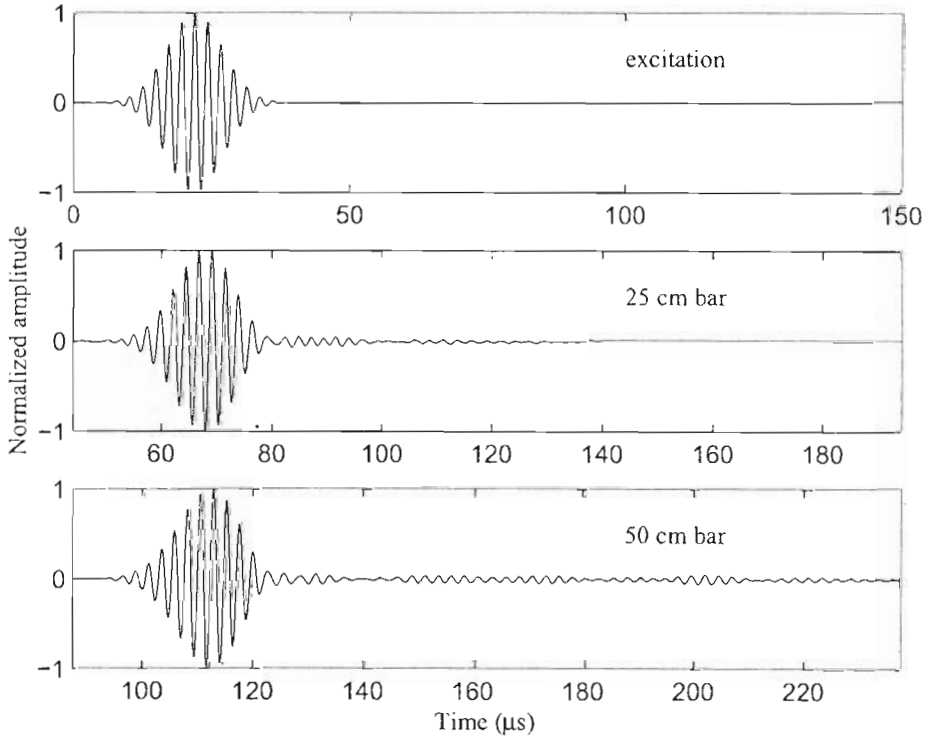

Fig. 5.11. Comparison of a Gaussian signal centered at 420 kHz (top) propagated through two length bars.

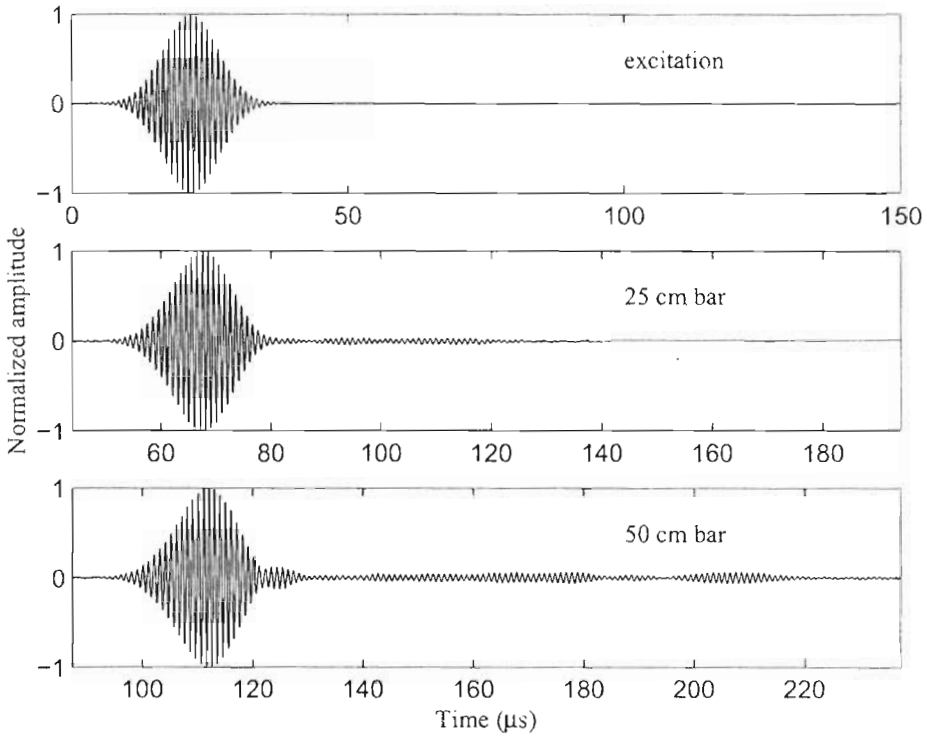

Fig. 5.12. Comparison of a Gaussian signal centered at 1000 kHz (top) propagated through two length bars.

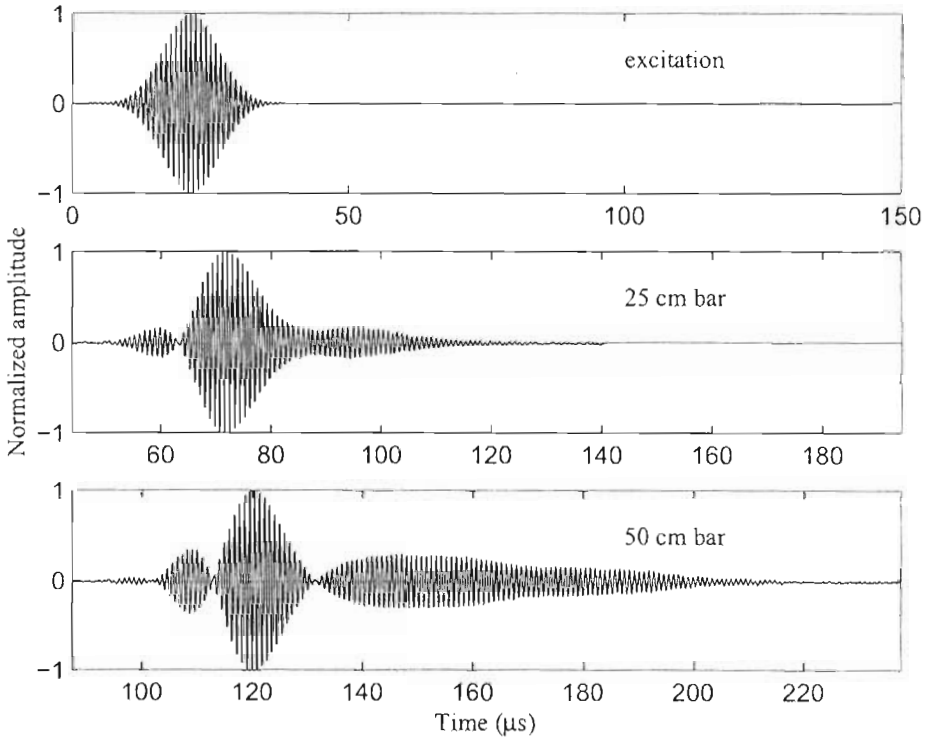

Fig. 5.13. Comparison of a Gaussian signal centered at 1107 kHz (top) propagated through two length bars.

of the predominantly excited mode. With an annular array transducer, it is theoretically possible to excite a single mode without exciting the neighboring modes by adjusting the radial pressure distribution with frequency. However, the group velocities of the mode with frequency do not change, so the signal will still be slightly dispersive. A narrower band signal can reduce both of these effects, but a narrower band signal corresponds to a longer signal in the time domain. The techniques for obtaining data using a narrow band Gaussian require very careful analysis of the signals to ensure accurate data.

A pulse is a much simpler signal to analyze; however, the use of a pulse excitation produces trailing pulses in the observed signals. For the narrow band Gaussian excitation, trailing pulses are also excited, and as in the sine bursts, the trailing pulses overlap because of the long time signature. However, the unique shape of the signal and the frequency content of the signal minimize the appearance of the trailing pulses. The superposition of the excitation signal and the trailing pulses maintain the shape of the excitation signal. Some of the energy does appear behind the signal at long lengths, because the superposition of the signals is not totally effective. A narrower band signal will be more effective. but with the consequences previously discussed. For reference, the pulse excitation is compared to the Gaussian excitation, Fig. 5.14, in a 25 mm diameter fused quartz rod at two different lengths 0.25 m and 0.5 m, Figs 5.15 and 5.16 respectively. The main energy of the narrow band signal maintains its shape with some energy trailing the main signal. The main energy of the pulse signal expands in time and covers a similar length of time as the Gaussian excitation. With proper experimental techniques the narrow band Gaussian excitation might be an effective signal for obtaining information using cylindrical waveguides. However, time-reversal is a more attractive choice because of its effectiveness to produce a pulse response in a waveguide.

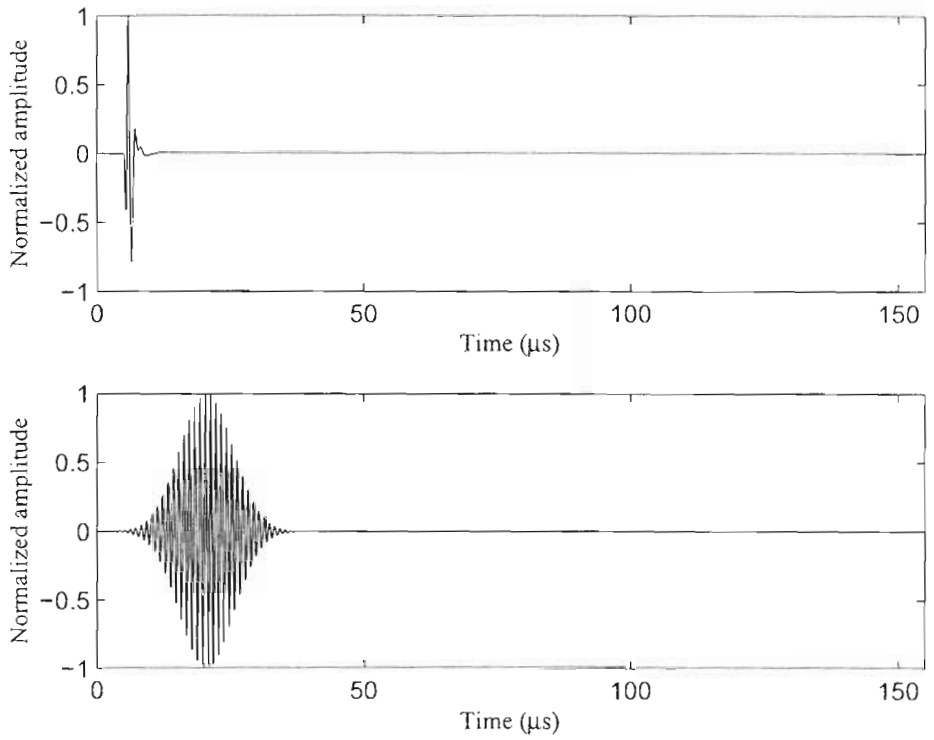

Fig. 5.14. Comparison of the broadband pulse excitation (top) and the narrow band Gaussian excitation (bottom). Both excitations are centered at 1 MHz.

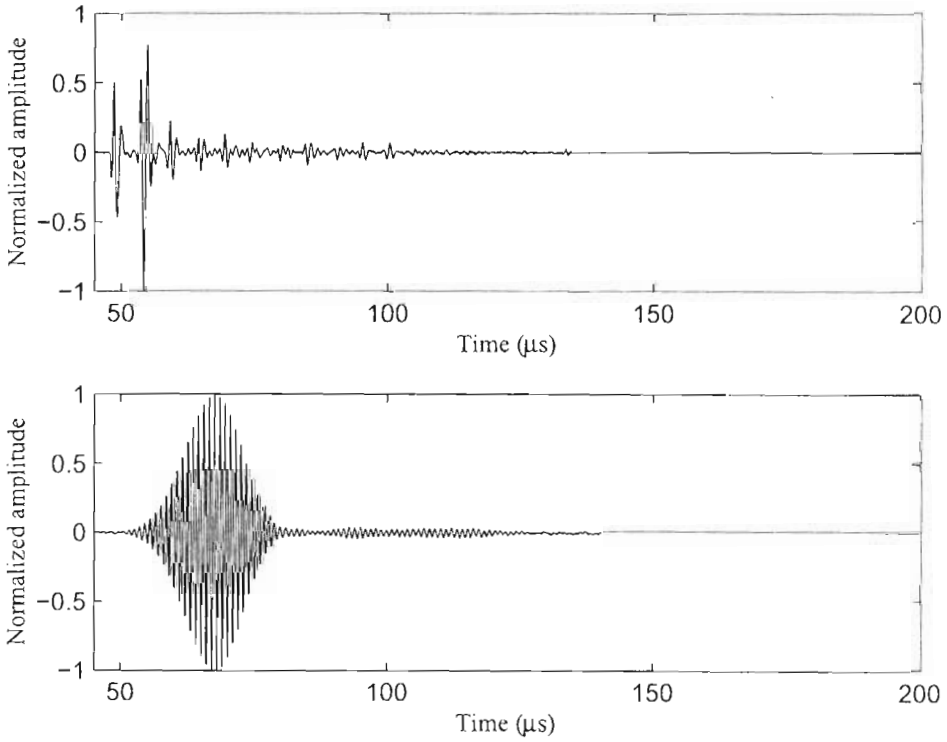

Fig. 5.15. Comparison of narrow band and broadband excitations propagated in 0.25 m long bar.

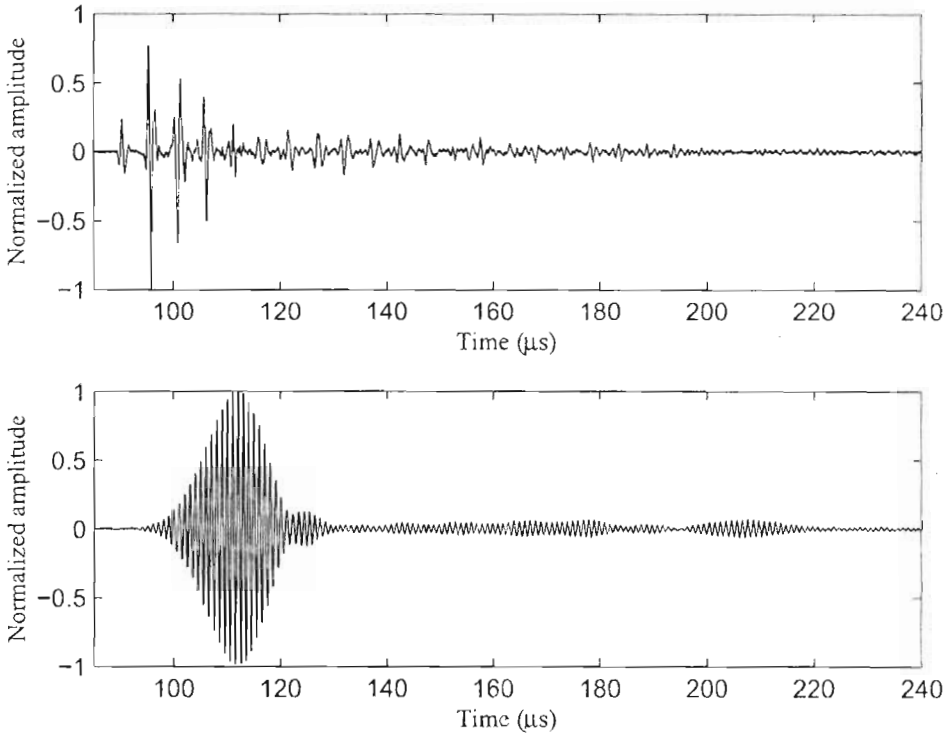

Fig. 5.16. Comparison of narrow band and broadband excitations propagated in 0.5 m long bar.

CHAPTER 6: CONCLUSIONS

6.1. Summary

An analytical model for wave propagation in cylindrical waveguides has been presented. The model uses the phase velocities and normal stresses of the Pochhammer-Chree theory to calculate the dispersed signal measured at the end of the waveguide. The analytical model is designed around a general experimental configuration and considers three parts, the excitation of the ultrasonic signal into the waveguide, the propagation of the signal in the waveguide and the reception of the ultrasonic signal. The frequency dependence of the solutions generates a transfer function for each propagating mode. The magnitude of the transfer function at each frequency is determined by the boundary conditions on the ends of the waveguide. The phase shift is calculated from the phase velocity and the length of the waveguide. The sum of these transfer functions of the modes is the transfer function of the waveguide, which can be used to predict the change of a signal.

The ability of the model to accurately capture the general physics of multiple mode wave propagation was demonstrated in the time, frequency, and joint-time frequency domain. Additionally, using time-reversal, the calculated dispersed signal is shown to produce a signal with compact time domain in a dispersive waveguide. A range of diameter to wavelength ratios was considered for comparison to the model. For wavelengths less than the radius of the cylinder discrepancies may be observed between the model and experiments. However, this configuration is not commonly encountered in ultrasonics.

The transfer functions generated by the model confirm previous conclusions and provide new insight into the propagation of multiple modes. For this experimental configuration the transfer functions show each mode is dominant over a different range of frequencies. The range of frequencies over which a mode is dominant corresponds to frequencies where the group velocity of the mode is near the longitudinal wave speed in an unbounded medium. Over these frequencies the other modes have a much smaller or negligible magnitude. The transfer functions further indicate that broadband signals are composed of multiple modes. It is found that observed trailing pulses contain energy from multiple propagating modes, it is the superposition of the modes that creates the trailing pulses. The information from the transfer

functions also shows that a sufficiently narrow band signal can excite a single higher order mode with little dispersion.

6.2. Suggestions for Future Work

The other motivation for this work was the split Hopkinson pressure bar (SHPB). The transfer functions for the SHPB are different because of the use of strain-gages instead of contact transducers. Future work would modify the analytical model to consider the SHPB experimental configuration, which could provide a useful tool for predicting the experimental signals and determining the influence of higher modes. This model would also have the potential to remove the dispersion of multiple propagating modes from the data using time reversal.

For NDE the potential of time reversal with cylindrical waveguides is enormous. The experimental abilities are good for even a single element contact transducer. The ability of the model allows time reversal to be extended to situations where the necessary reversed signal is not available experimentally. Industrial and commercial applications could take advantage of the ability of time reversal in cylindrical waveguides using techniques like those presented in Section 3.2.3. The field of NDE might also be able use a single propagating mode effectively. Research needs to determine if it is possible to propagate a single mode and obtain meaningful data.

REFERENCES

Achenbach, J.D. (**1999**). *Wave Propagation in Elastic Solids* (North Holland, Amsterdam).

Adem, J. (**1954**). "On the axially-symmetric steady wave propagation in elastic circular rods," Q. Appl. Math. **12**, 261-275.

Al-Mousawi, M.M. (**1986**). "On experimental studies of longitudinal and flexural wave propagations: an annotated bibliography," Appl. Mech. Rev. **39**, 853-865.

Bacon, D.R., Chivers, R.C., and Som, J.N. (**1993**). "The acousto-optic interaction in the interferometric measurement of ultrasonic transducer surface motion," Ultrasonics **31**, 321-325.

Bancroft, D. (**1941**). " The velocity of longitudinal waves in cylindrical bars," Phys. Rev. **59**, 588-593.

Chree, C. (**1889**). "The equations of an isotropic elastic solid in polar and cylindrical coordinates, their solution and application," Trans. Cambridge Phil. Soc. **14**, 250-369.

Christie, D.G. (**1955**). "Reflection of elastic waves from a free boundary," Phil Mag. **46**, 527-541.

Curtis, C.W. (**1953**). "Plastic deformation and fracture of metals at high rates of strain," Ann. Rep. OOR Contr. No. DA-36-034-ORD-969, Lehigh Univ., Bethlehem, Pa.

Davies, R.M. (**1948**). "A critical study of the Hopkinson Pressure Bar," Phil. Trans. Royal Soc. **A240**, 375-457.

Eliot, F.C., and Mott, G. (**1968**). "Elastic waves propagation in circular cylinders having hexagonal crystal symmetry," J. Acoust. Soc. Am. **44**, 423-430.

Fama, M.E. (**1972**). "Radial eigenfunctions for the elastic circular cylinder," Q. Jl. Mech. appl. Math. **25**, 479-495.

Field, G.S. (**1931**). "Velocity of sound in cylindrical rods," Can. J. Res. **5**, 619-624.

Fink, M. (**1997**). "Time reversed acoustics", Physics Today **50**, 34-40

Folk, R., Fox, G., Shook, C.A., and Curtis, C.W. (**1958**). "Elastic strain produced by sudden application of pressure to one end of a cylindrical bar. I. Theory," J. Acoust. Soc. Am. **30**, 552-558.

Follansbee, P.S., and Frantz, C. (**1983**). "Wave propagation in the split Hopkinson pressure bar," J. Eng. Mat. Tech. **105**, 61-66.

Fox, G., and Curtis, C.W. (**1958**). "Elastic strain produced by sudden application of pressure to one end of a cylindrical bar. II. Experimental observations," J. Acoust. Soc. Am. **30**, 559-563

Fraser, W.B. (**1975**). "An orthogonality relation for the modes of wave propagation in an elastic circular cylinder," J. Sound Vibrat. **43**, 568-571

General Electric Advanced Materials. (**2004**). *Quartz Properties* [Online]. Available: http://www.gequartz.com/en/properties.htm (2004, April 27).

Goldberg, I.S., and Folk, R.T. (**1993**). "Solutions to time-dependent pure-end condition problems of elasticity: pressure-step wave propagation and end-resonance effects," SIAM J. of Appl. Math. **53**, 1264-1292

Gong, J.C., Malvern, L.E., and Jenkins, D.A. (**1990**). "Dispersion investigation in the split Hopkinson pressure bar," J. Eng. Mat. Tech. **112**, 309-314.

Graff, K.F. (**1975**). *Wave Motion in Elastic Solids*, (Dover Publications, New York).

Gray, G.T. (**2000**). "Classic split-Hopkinson pressure bar testing," *ASM Handbook Vol. 8 Mechanical Testing and Evaluation*, (ASM International, Metals Park, Ohio).

Greenberg, M.D. (**1978**). *Foundations of Applied Mathematics*, (Prentice Hall, Englewood Cliffs, NJ).

Gregory, R.D., and Gladwell, I. (**1989**). "Axisymmetric waves in a semi-infinite elastic rod," Q. Jl Mech. Appl. Math **42**, 327-337.

Hearmon, R.F.S. (**1984**). "The elastic constants of crystals and other anisotropic materials," *Landolt-Börnstein – Numerical Data and Functional Relationships in Science and Technology* (Springer-Verlag, Berlin), Group III, Vol. 18.

Hejase, H.A.N. (**1993**). "On the use of Davidenko's method in complex root search," IEEE. Trans. Microwave Theory Tech. **41**, 141-143.

Hopkinson, B. (**1914**). "A method of measuring the pressure produced in the detonation of high explosives or by the impact of bullets," Phil. Trans. R. Soc. (London) **A213**, 437-456.

Ing, R.K., and Fink, M. (**1998**). "Time-reversed lamb waves," IEEE Trans. Ultrason., Ferroelect., Freq. Contr. **45**, 1032-1043.

Jen, C.K., Piche, L., and Bussiere, J.F. (**1990**). "Long isotropic buffer rods," J. Acoust. Soc. Am. **88**, 23-25.

Jen, C.-K, Franca, D.R., Sun, Z., and Ihara, I. (**2001**). "Clad polymer buffer rods for polymer process monitoring," Ultrasonics. **39**, 81-89

Jen, C.K., Heering, Ph. de, Sutcliffe, P., and Bussiere, J.F. (**1991**). "Ultrasonic monitoring of the molten zone of single-crystal germanium," Mater. Eval. **49**, 701-705.

Jen, C.K., Cao, B., Nguyen, K.T., Loong, C.A., and Legoux, J.-G. (**1997**). "On-line ultrasonic monitoring of a die-casting process using buffer rods," Ultrasonics **35**, 335-344.

Jones, O.E., and Norwood, F.R. (**1967**). "Axially symmetric cross-sectional strain and stress distributions in suddenly loaded cylindrical elastic bars," J. Appl. Mech. **34**, 718-724.

Kennedy, L.W., and Jones, O.E. (**1969**). "Longitudinal wave propagation in a circular bar loaded suddenly by a radially distributed end stress," J. Appl. Mech. **36**, 470-478.

Kohl, T., Datta, S.K., and Shah, A.H. (**1992**). "Axially symmetric pulse propagation in semi-infinite hollow cylinders," AIAA J. **30**, 1617-1624.

Kolsky, H. (**1949**). "An investigation of the mechanical properties of materials at very high rates of loading," Proc. Phys. Soc. (London) **62B**, 676-700.

Kolsky, H. (**1963**). *Stress Waves in Solids*, (Dover Publications, New York).

Krautkramer, J., and Krautkramer, H. (**1983**). *Ultrasonic Testing of Materials*, (Springer-Verlag, Berlin).

Lerch, T.P., Schmerr, L.W., and Sedov, A. (**1998**). "Ultrasonic beam models: An element edge approach," J. Acoust. Soc. Am. **104**, 1256-1265.

Love, A.E.H. (**1944**). *A Treatise on the Mathematical Theory of Elasticity, 4th Ed.*, (Dover Publications, New York).

Mason, W.P., and McSkimin, H.J. (**1947**). "Attenuation and scattering of high frequency sound waves in metals and glasses," J. Acoust. Soc. Am. **19**, 464-473.

McSkimin, H.J. (**1956**). "Propagation of longitudinal waves and shear waves in cylindrical rods at high frequencies," J. Acoust. Soc. Am. **28**, 484-494.

Meitzler, A.H. (**1961**). "Mode coupling occuring in the propagation of elastic pulses in wires," J. Acoust. Soc. Am. **33**, 435-445.

Meitzler, A.H. (**1965**). "Backward-wave transmission of stress pulses in elastic cylinders and plates," J. Acoust. Soc. Am. **38**, 835-842.

Miklowitz, J. (**1966**). "Elastic wave propagation," In *Applied Mechanics Surveys*, (Spartan Books, Washington DC), 809-839.

Montaldo, G., Roux, P., Derode, A., Negreira, C., and Fink, M. (**2001**). "Generation of very high pressure pulses with 1-bit time reversal in a solid waveguide," J. Acoust. Soc. Am. **110**, 2849-2857.

Niethammer M., and Jacobs, L.J. (**2001**). "Time-frequency representations of Lamb waves," J. Acoust. Soc. Am. **109**, 1841-1847.

Oliver, J. (**1957**). "Elastic wave dispersion in a cylindrical rod by a wide-band short-duration pulse technique," J. Acoust. Soc. Am. **29**, 189-194.

Onoe, M., McNiven, H.D., and Mindlin, R.D. (**1962**). "Dispersion of axially symmetric waves in elastic rods," J. Appl. Mech. **28**, 729-734.

Papadakis, E.P., Oakley, C.G., Selfridge, A., and Maxfield, B. (**1999**). "Fabrication and characterization of transducers," In *Ultrasonic Instruments and Devices*, (Academic Press, San Diego), 472-557.

Peterson, M.L. (**1997**). "A method for increased accuracy of the measurement of phase velocity," Ultrasonics **35**, 17-29.

Peterson, M.L. (**1994**). "A signal processing technique for measurement of multi-mode waveguide signals: an application to monitoring of reaction bonding in silicon nitride," Res. Nondestr. Eval. **5**, 239-256.

Peterson, M.L. (**1999**). "Prediction of longitudinal disturbances in a multi-mode cylindrical waveguide," Exp. Mech. **39**, 36-42.

Pierce, A.D. (**1981**). *Acoustics: An Introduction to Its Physical Principles and Applications*, (McGraw-Hill, New York).

Pilant, W.L. (**1960**). "The propagation of elastic waves in thin plates," Ph.D. Diss., Univ. Cal., Los Angeles.

Pochhammer, L. (**1876**). "Über die Fortpflanzungsgeschwindigkeiten kleiner Schwingungen in einem unbegrenzten isotropen Kreiscylinder," J. Reine Angew. Math. **81**, 324-336.

Power, L.D., and Childs, S.B. (**1971**). "Axisymmetric stresses and displacements in a finite circular bar," Int. J. Engng. Sci. **9**, 241-255.

Puckett, A.D., and Peterson, M.L. (**2002**). "Fidelity of an analytical time-reversal mirror," in *Review of Progress of Quantitative Nondestructive Evaluation*, edited by D.O. Thompson and D.E. Chimenti (American Institute of Physics, New York), Vol. 21, 945-952.

Puckett, A.D., and Peterson, M.L. (**2003**). "Technique for determining the pressure distribution on the face of a contact ultrasonic transducer," Experimental Techniques **27**(4), 37-39.

Puckett, A.D., and Peterson, M.L. (**2003**). "A time-reversal mirror in a solid circular cylindrical waveguide using a single, time-reversal element," Acoustic Research Letters Online **4**, 31-36.

Rattanawangcharoen, N., Shah, A.H., and Datta, S.K. (**1994**). "Reflection of waves at the free edge of a laminated circular cylinder," J. Appl. Mech. **61**, 323-329.

Redwood, M., and Lamb, J. (**1957**). "On the propagation of high frequency compressional waves in isotropic cylinders," Proc. Phys. Soc. (London) **B70**, 136-143.

Redwood, M. (**1960**). *Mechanical Waveguides*, (Pergamon Press, New York).

Redwood, M. (**1959**). "Velocity and attenuation of a narrow-band, high frequency compressional pulse in a solid wave guide," J. Acoust. Soc. Am. **31**, 442-448.

Roesler, F.C. (**1955**). "Glancing angle reflection of elastic waves from a free boundary," Phil. Mag. **46**, 517-526.

Schmerr, L.W. (**1998**). *Fundamentals of Ultrasonic Nondestructive Evaluation*, (Plenum Press, New York).

Scruby, C.B., and Drain, L.E. (**1990**). *Laser Ultrasonics*, (Adam Hilger, Bristol).

Skalak, R. (**1957**). "Longitudinal impact of a semi-infinite circular elastic bar," J. Appl. Mech. **24**, 59-64.

Talisa, S.H. (**1985**). "Application of Davidenko's method to the solution of dispersion relations in lossy waveguiding systems," IEEE Trans. Microwave Theory Tech. **MTT-33**, 967-971.

Thurston, R.N. (**1978**). "Elastic waves in rods and clad rods," J. Acoust. Soc. Am. **64**, 1-37.

Tu, L.Y., Brennan, J.N., and Sauer, J.A. (**1955**). "Dispersion of ultrasonic pulse velocity in cylindrical rods." J. Acoust. Soc. Am. **27**, 550-555.

Tyas, A., and Watson, A.J. (**2000**). "Experimental evidence of Pochhammer-Chree strain variations in elastic cylinders," Exp. Mech. **40**, 331-337.

Vales, F., Moravka, S., Brepta, R., and Cerv, J. (**1996**). "Wave propagation in a thick cylindrical bar due to longitudinal impact," JSME Int. J. **39A**, 60-70.

Zemanek, J. (**1972**). "An experimental and theoretical investigation of elastic wave propagation in a cylinder," J. Acoust. Soc. Am. **51**, 265-283.

Zemanek, J. (**1962**). "An experimental and theoretical investigation of elastic wave propagation in a cylinder," Ph.D. Diss., Univ. Cal., Los Angeles.

APPENDIX A. TIME REVERSAL

The property of time invariance allows a signal with compact support in the time domain to be generated from a multiple mode dispersive waveguide. The excitation signal necessary to generate a compact signal is found by exciting the waveguide with the desired signal and measuring the dispersed signal. Alternatively, the dispersed signal can be calculated using the MATLAB code in Appendix D. The dispersed signal reversed in time is the excitation signal that will generate the desired signal with compact support in the time domain. Any end reflections should not be included in the reversed signal. The complex nature of the excitation signal requires the arbitrary wave generator and a power amplifier to excite the signal. The MATLAB code for programming the function generator follows.

```
%*********************************************************************
%  Program to write reversed dispersed signal to Waveform Generator
%*********************************************************************

% Open dispersed signal, amplitude only if analytical, amplitude and time if experimental

[signal] = textread('C:\WINDOWS\Desktop\Research\quartz010_nu18_2Mhz.dat');

% Specify time step and length of the signal of interest
tstep=2e-8;
n=length(signal);
n=1500; %length of dispersed signal without reflections
N=2^14; %length of programmed signal
signal=signal(1:n);
volt=signal;
volt=volt-volt(1); % remove dc offset
volt=[volt.';zeros(N-n,1)]; % add zeros, so the signal is N data points
volt=flipud(volt); %reverse the signal in time
volt=volt/max(abs(volt)); % normalize signal
V=abs(fft(volt)); % magnitude of the frequency spectrum

% Plot of signals to verify correctness before writing to waveform generator
figure
subplot(2,1,1)
plot((0:N-1),volt);
subplot(2,1,2)
plot(0:1/(N*tstep):1/(16*(tstep)),V(1:N/16+1));
pause

% Write signal to waveform generator
file='tempdata.txt';
fid=fopen(file,'w+');
count=fprintf(fid,'data\t volatile\t, %4.3f\t, ', volt(1));
for i=2:1:N-1
    count=fprintf(fid,'%4.3f\t, ', volt(i));
end
count=fprintf(fid,'%4.3f\n', volt(N));
fclose(fid);
format=textread(file,'%c','whitespace',' ').';
format;

g=gpib('ni',0,10);
g.OutputBufferSize = N*8;
g.Timeout=1000;
fopen(g)
fprintf(g,format);

fprintf(g,'data:copy sigtr'); % sigtr is the name of the signal, which can change
fprintf(g,'func:user sigtr');
fprintf(g,'func user');
fprintf(g,'appl:user %10.2f, .01, -.005',1/(N*tstep));

fclose(g)
delete(g)
clear g
```

APPENDIX B. TRANSDUCER FACE MAPPING

Chapter 3 describes the procedure for mapping the face of a transducer. This appendix contains the MATLAB code for performing the cross correlation and displaying the pressure distribution across the diameter. Three signals were taken at each data point, so the file name of each signal contains two numbers. The first number represents the point along the diameter, and the second number is which of the three signals, for example *hor19_1.dat*. A separate file, in this case, 'hor3dist.dat' contains the distance of each measurement point.

```
%************************************************************************
% This program performs the cross correlation for all of the signals.
% Only the amplitude and time delay of a specific peak is calculated.
% The amplitude variation and the time delay variation are plotted
% for the horizontal data from the transducer.
%************************************************************************

% read in distances at which signals were acquired
[dist] = textread('C:\WINDOWS\Desktop\Research\hor3dist.dat');

% read in reference signal
[signalref] = textread('C:\WINDOWS\Desktop\Research\hor19_1.DAT');

tstep=signalref(2,1)-signalref(1,1); % specify time step
M=length(signalref(:,2)); % determine length of the reference signal
N=5500;
refspect=fft(signalref(:,2)); % Find freqeuncy spectrum of reference signal
freqstep=1/signalref(M,1); % frequency step of reference signal
refspect(1)=0; % remove dc offset of reference signal
refspect(61:M-60)=0; % filter out high frequency noise
signalref(:,2)=real(ifft(refspect)); % Generate filtered reference signal

range=100; % the number of points considered in the cross correlation
for n=1:35 % number of points on the radius at which signals were taken
    for m=1:3 % number of signals taken at each point
        file='file.txt';
        fid=fopen(file,'w+');
        fprintf(fid,'C:\\WINDOWS\\Desktop\\Research\\hor%02i_%1i.DAT',n,m);
        fclose(fid);
        filename=textread(file,'%c','whitespace','\t').'; % open one of the signals
        [signaltemp] = textread(filename);
        tempspect=fft(signaltemp(:,2));
        tempspect(1)=0;
        tempspect(61:N-60)=0;
        signaltemp(:,2)=real(ifft(tempspect)); % filtered signal
        for k=-range:range
            clear temp
            clear ref
            if k<0
                temp=signaltemp(1-k:N,2);
                ref=signalref(1:N+k,2);
            elseif k>0
                temp=signaltemp(1:N-k,2);
                ref=signalref(1+k:N,2);
            else
                temp=signaltemp(:,2);
                ref=signalref(:,2);
            end
            temp=temp(1:N-range);
```

```
            ref=ref(1:N-range);
            C(range+1+k)=sum(temp.*ref); % cross correlation
        end
        [MAX(n,m),I(n,m)]=max(C); % find max of the cross correlation, value and indices
        fprintf(1,'num=%-2i %1i\n',n,m);
    end
end
tdelay=(I-(range+1))*tstep; % convert indices to time delay
amp=MAX/MAX(19,1); % find relative amplitude
ampaverage=mean(amp,2); % find average
ampmax=max(amp,[],2); % error bars
ampmin=min(amp,[],2); % error bars
taverage=mean(tdelay,2);
tmax=max(tdelay,[],2);
tmin=min(tdelay,[],2);

dist=dist-0.68; % Shift origin to the center of the transducer

% Plotting statements
figure
subplot(2,1,1)
errorbar(dist*25.4,ampaverage,abs(ampaverage-ampmin),abs(ampaverage-ampmax),'k');
hold on
pos=get(gca,'position');
set(gca,'Ylabel',text('String','Relative Amplitude','FontSize',10),...
    'Xlabel',text('String','Distance(mm)','FontSize',10),...
    'FontSize',10)
set(gca,'position',[pos(1)-0.2*pos(1) pos(2) pos(3) pos(4)],'YLim',[0 1.5]);

subplot(2,1,2)
ax(1) = newplot;
errorbar(dist*25.4,taverage*1e6,abs(taverage-tmin)*1e6,abs(taverage-tmax)*1e6,'k');
set(gcf,'nextplot','add')
set(ax(1),'box','on')
xlim1 = get(ax(1),'xlim');
ylim1 = get(ax(1),'ylim');
ax(2) = axes('position',get(ax(1),'position'));
set(ax(2),'YAxisLocation','right','color','none', ...
          'xgrid','off','ygrid','off','box','off');
xlim2 = xlim1;
ylim2 = ylim1;
set(ax,'xlim',[min(xlim1(1),xlim2(1)) max(xlim1(2),xlim2(2))])
set(get(ax(1),'Ylabel'),'String','Time delay (\mus)','FontSize',10,...
    'Color','k')
set(ax(1),'Ycolor','k','FontSize',10)
ylimits = [-0.15 0.15];
set(ax(1),'YLim',ylimits);
pos=get(ax(1),'position');
set(ax(1),'position',[pos(1)-0.2*pos(1) pos(2) pos(3) pos(4)]);
set(get(ax(2),'Ylabel'),'String','Distance (mm)','FontSize',10,...
    'Color','k')
set(ax(2),'Ycolor','k','FontSize',10,...
    'YLim',[ylimits(1)*333000/1e6 ylimits(2)*330000/1e6])
set(ax(2),'position',[pos(1)-0.2*pos(1) pos(2) pos(3) pos(4)]);
xlabel('Distance (mm)','FontSize',10)
set(ax(2),'ytick',[-0.025 0 0.025]);
set(ax(1),'ytick',[-.15 0 .15]);
```

APPENDIX C. DISPERSION CURVES

Dispersion curves for the propagating modes as well as the evanescent modes are required for the analytical model. The MATLAB files necessary for the propagating modes follow. POCHPROP.M specifies the material properties of the waveguide. It also specifies the time step, frequency step, and therefore, the number of points in the discrete transform pair. POCHCUTOFF.M finds the cutoff frequencies of all of the modes below the frequency of interest. POCHSTARTFREQ.M calculates the first two points for the each dispersion curve. POCHDISPCURV.M calculates the dispersion curves (wavenumber and frequency) for the propagating modes. The program uses a bisection method to determine the wavenumber at each frequency and the following subroutines. POCHKEVAL.M determines the slope between the two points in the bisection. POCHFREQEVAL.M evaluates the frequency equation with the current wavenumber. The frequency equation should equal zero. POCHBISECT.M performs the bisection using the specified values. If the two points in the bisection are both positive or both negative POCHKFIND.M iterates to find the wavenumber.

The imaginary modes require the similar files except the wavenumber is imaginary. POCHPROP.M is needed to specify the material properties. POCHDISPCURVIMAG.M calculates the imaginary portion of the dispersion curves. The beginning and ending frequencies are specifies along the wavenumber. The files POCHKFINDIMAG.M and POCHBISECTIMAG.M are called in the POCHDISPCURVIMAG.M.

The evanescent modes require a different numerical method for finding the complex wavenumbers. For these dispersion curves, Davidenko's method was used (see Talisa 1985 and Hejase 1993). Davidenko's requires an initial guess to find the wavenumber. The paper by Onoe et al. provides a means of finding the initial guesses for each of the modes. However, sometimes other guesses are required. POCHPROP.M is needed to specify the material properties. The file POCHDISPCURVCMPLX.M steps through the desired frequencies and writes the real and imaginary portions of the wavenumber to a file. The function DAVIDENKO.M is called to find the wavenumber. It was found that for some of the modes, primarily the first mode, the signs of the variables drealdt and dimagt needed to be switched for the solution to converge.

```
%*********************************************************************
%                POCHPROP.M
%*********************************************************************
% lambda - Lame constant
% mu - lame constant
% cd - dilitational wave speed in unbounded media
% ct - tranverse wave speed in unbounded media
% cb - longitudinal wave speed in infinitesimally thin bar
%*********************************************************************

lambda = nu*E/((1+nu)*(1-2*nu));
mu = E/(2*(1+nu));
cd = sqrt((lambda+2*mu)/rho);
ct = sqrt(mu/rho);
cb = sqrt(E/rho);

%*********************************************************************
%                NUMERICAL PARAMETERS
%*********************************************************************
% num - the number of modes to calculate dispersion curves.  It is
%       based on the highest frequency and the cutoff frequencies.
% success - the number of times in a row that Newton's method
%           must meet tolerance for the iteration to stop
% tol - the tolerance on Newton's method
% maxiter - the maximum iterations of Newton's method
% deltat - time step, based on input file or desired time step
% N - number of data points
% deltaf - frequency step in Hz
% wstep - freqeuncy step in radians
%*********************************************************************

success=4;
tol=0.001;
maxiter=1000;
deltat=1/50000000;
N=2^17;
deltaf=1/(N*deltat);
wstep=deltaf*2*pi;

save properties

%*********************************************************************
%                end of script
%*********************************************************************
```

```
%*********************************************************************
%                          POCHCUTOFF.M
%*********************************************************************
% This Matlab file computes the cutoff frequencies for all the
% modes with a cutoff frequency under the highest frequency(high).
%
% The frequency equations are those derived by Redwood(1960)
% pg. 145 eqns. 6.24 and 6.25.  The former calculates the
% dilitational modes and the latter the transverse modes.
%
% Newton's method is employed to iterate to the final solutions.
% There will be several duplicates and triplicates, and those are
% removed.  Finally, the dilitational and transverse modes are put
% together, sorted, and the first num modes are selected.
%
% Written by Anthony Puckett, February 2001.
%
%*********************************************************************
% Initialize Variables
%*********************************************************************

%*********************************************************************
% Dilitational Modes
%*********************************************************************
% The cutoff frequencies for the dilitational modes are found
% and the duplicates are removed.
%
% freqd - cutoff frequency equation for the dilitational modes
% dfreqd - the derivative of freqd
% subd - a substitution to make the line shorter
% broots - the roots of the dilatational cutoff frequency eqn.
% freqsdil - the cutoff frequencies of the dilitatinal modes
%*********************************************************************

%*********************************************************************
% Roots found by iterating
%*********************************************************************
xstep=0.01;
oldfreqd=1.5;
count=1;

for x=xstep:xstep:180
    freqd=x*(bessel(0,x)/bessel(1,x))-2*(ct/cd)^2;
    if sign(oldfreqd)-sign(freqd)==2
        dilroots(count)=x;
        count=count+1;
    end
    oldfreqd=freqd;
end

%*********************************************************************
% Roots found more precisely by bisection method
%*********************************************************************
clear x
goodcount=0;
iter=0;
oldx=0;
for n=1:1:count-1
    x1=dilroots(n)-xstep;
    x2=dilroots(n);
    while goodcount<success & iter<200
        deltax=(x2-x1)/2;
        x=x1+deltax;
        freqd=x*(bessel(0,x)/bessel(1,x))-2*(ct/cd)^2;

        if abs(oldx-x)<0.00001 & abs(freqd)<0.0001
            goodcount=goodcount+1;
        else
            goodcount=0;
        end
```

```
        if freqd>0
            x1=x;
        elseif freqd==0
            goodcount=4;
        else
            x2=x;
        end
        iter=iter+1;
        oldx=x;
    end
    dilroots(n)=x;
    goodcount=0;
    iter=0;
end

%*********************************************************************
% Calculate the cutoff frequencies from the roots.
%*********************************************************************

for n=1:1:length(dilroots)
  freqsdil(n,1)=dilroots(n)*cd/(a*2*pi);
  freqsdil(n,2)=1;
end

%*********************************************************************
% Transverse Modes
%*********************************************************************
% The cutoff frequencies for the transverse modes are found
% and the duplicates are removed.
%
% freqt - cutoff frequency equations for the transverse modes
% tranroots - the roots of the dilitational cutoff frequency eqn.
% freqstran - the cutoff frequencies of the dilitatinal modes
%*********************************************************************

%*********************************************************************
% Roots found by iterating
%*********************************************************************
xstep=0.01;
oldfreqt=1.5;
count=1;

for x=xstep:xstep:300
    freqt=bessel(1,x);
    if abs(sign(oldfreqt)-sign(freqt))==2
        tranroots(count)=x;
        count=count+1;
    end
    oldfreqt=freqt;
end

%*********************************************************************
% Roots found more precisely by bisection method
%*********************************************************************
clear x
goodcount=0;
iter=0;
oldx=0;
for n=1:1:count-1
    x1=tranroots(n)-xstep;
    x2=tranroots(n);
    while goodcount<success & iter<200
        deltax=(x2-x1)/2;
        x=x1+deltax;
        freqt=bessel(1,x);

        if abs(oldx-x)<0.00001 & abs(freqt)<0.0001
            goodcount=goodcount+1;
        else
            goodcount=0;
        end
```

```
        if freqt>0
            x1=x;
        elseif freqt==0
            goodcount=4;
        else
            x2=x;
        end
        iter=iter+1;
        oldx=x;
    end
    tranroots(n)=x;
    goodcount=0;
    iter=0;
end

%*********************************************************************
% Calculate the cutoff frequencies from the roots.
%*********************************************************************

for n=1:1:length(tranroots)
  freqstran(n,1)=tranroots(n)*ct/(a*2*pi);
  freqstran(n,2)=2;
end

%*********************************************************************
% Combine cutoff frequencies, sort
%*********************************************************************
freqstot=[0 1;freqsdil;freqstran];

freqstot=sortrows(freqstot,1);

%*********************************************************************
% Print Cutoff Frequencies
% num - total number of modes with cutoff frequencies below highfreq
%*********************************************************************

n=2;
while freqstot(n,1) < highfreq;
    if freqstot(n,2)==1
        fprintf(1,'The cut off frequency for mode %1i is %9.2f %s\n',...
            n,freqstot(n,1),'Hz.     dilitational');
    else
        fprintf(1,'The cut off frequency for mode %1i is %9.2f %s\n',...
            n,freqstot(n,1),'Hz.     transverse');
    end
    n=n+1;
end
num=n-1;

%*********************************************************************
% end of script
%*********************************************************************
```

```
%*********************************************************************
%                          POCHSTARTFREQ.M
%*********************************************************************
% This Matlab file computes the starting frequency and
% wavenumber for each mode to ensure that none of the dispersion
% curves are duplicated or absent.
%
% Written by Anthony Puckett, February 2001.
%
%*********************************************************************
%              Initialize Variables
%*********************************************************************

load properties

%*********************************************************************
%               Calculate Start Frequencies and Wave Numbers
%*********************************************************************
% The start frequency for the first mode is based on the fact
% cp=cb at small k.  The start frequency for higher modes is
% calculated by the cutoff frequency plus wstep rad/s.
%
% Wave numbers are determined by incrementing the wave number
% until the frequency equation changes sign and does not
% correspond to a singularity.
%
% propstart - wave number for first two frequencies of each mode
% pochkfind - function to find k for a frequency
%*********************************************************************
for n=1:1:num
    kinc=0.01;
    if n==1
        kinc=0.001;
        w=wstep;
        k=kinc;
    else
        w=(ceil((2*pi*freqstot(n,1))/wstep))*wstep+2*wstep;
        k=kinc;
    end
    [k,kinc]=pochkfind(w,cd,ct,a,kinc,k);
    [k,kinc]=pochkfind(w,cd,ct,a,kinc,k-3*kinc);
    propstart(n,1)=k-kinc;
    propstart(n,2)=w;
    propstart(n,3)=kinc/3;

%*********************************************************************
%               Calculate Next Frequencies and Wave Numbers
%*********************************************************************
% The frequencies and wave numbers for the first frequency step
% are calculated.  The new frequency equals the old frequency
% plus wstep rad/s.  New wave numbers are found the same way as previous.
%*********************************************************************
    if n==1
        kinc=0.001;
    else
        kinc=0.01;
    end
    w=w+wstep;
    k=propstart(n,1);
    [k,kinc]=pochkfind(w,cd,ct,a,kinc,k);
    [k,kinc]=pochkfind(w,cd,ct,a,kinc,k-3*kinc);
    propstart(n,4)=k-kinc;
    propstart(n,5)=w;
    propstart(n,6)=kinc/3;
    fprintf(1,'For mode %2i kstart=%8.3f
wstart=%10.2f\n',n,propstart(n,1),propstart(n,2));
end

%*********************************************************************
% end of script
%*********************************************************************
```

```
%*********************************************************************
%                        POCHDISPCURV.M
%*********************************************************************
% This Matlab file computes the dispersion curves for the first
% num modes for the given material properties.
%
% The dispersion curves are calcuted by stepping the frequency, w
% and using a bisection method to find the wavenumber.
%
% Written by Anthony Puckett, February 2001.
%
%*********************************************************************
%              Initialize Variables
%*********************************************************************

load properties

%*********************************************************************
% Plotting Commands
%*********************************************************************
% Phase velocity and group velocity figures are created with lines
% indicating transverse and dilatational phase velocities.
%*********************************************************************
plotcurves=1;
if plotcurves==1
figure(1)
xlabel('f')
ylabel('cp /cb')
axis([0 1.5*freqstot(num,1) 0 2.5])
cpvs=0:1.5*freqstot(num,1)/1000:1.5*freqstot(num);
plot(cpvs,ct/cb,'-r',cpvs,cd/cb,'-r')
hold on
figure(2)
xlabel('f')
ylabel('cg /cb')
axis([0 1.5*freqstot(num,1) 0 2.5])
cpvs=0:1.5*freqstot(num,1)/1000:1.5*freqstot(num);
plot(cpvs,ct/cb,'-r',cpvs,cd/cb,'-r')
hold on
end

%*********************************************************************
% Variables
%*********************************************************************
% a - radius
% cb - wave speed in a long bar
% cd - dilatational wave speed
% counter - variable to keep track of iteration
% ct - transverse wave speed
% deltakstep - change in kstep
% dk - difference between kprev and k
% dwdk - matrix containing all of the group velocities for a specific mode
% freqroots - matrix containing all of the frequencies for a specific mode
% highfreq - highest frequency, specified by user
% k - wavenumber
% k1 - lower wavenumber used in bisection method
% k1prev - previous value of k1
% k2 - upper wavenumber used in bisection method
% kinc - increment of k used in pochkfind.m
% kprev - previous value of k
% kstepprev - previous value of kstep
% omega - matrix containing all of the frequencies for a specific mode
% pochbisect - function to find wavenumber by bisection method
% pocheval - function to evaluate k1 and k2 and determine if there is a root between the
values
% pochkfind - function to find wavenumber by iterating
% propstart - wavenumbers and frequencies for first two frequencies of each mode
% results - matrix that contains the wavenumber and phase velocity information of all the
modes
% slope - a value from function pocheval.m to indicate k1 and k2 contain root
% w - frequency
```

```
% wavenum - matrix containing all of the wavenumbers for a specific mode
% wend - end frequency, same for all modes
% wstart - start frequency, different for each mode
% wstep - frequency step
%*****************************************************************

%*****************************************************************
% Calculate wavenumbers
%*****************************************************************
% For each mode the frequency is incremented. For each freqeuncy
% increment, wstep,the wavenumber, k, is calculated.  k1 and k2
% are calculated based on the starting values calculated in
% pochstartfreq, in the matrix propstart.
%
%*****************************************************************

kinc=0.01;
wend=ceil(highfreq*2*pi/wstep)*wstep;
for n=4:1:4
    k1=propstart(n,1)-3*propstart(n,3);
    k2=propstart(n,1)+3*propstart(n,3);
    k1prev=k1;
    dk=kinc;
    wstart=propstart(n,2);
    clear freqroots;
    clear wavenum;
    clear dwdk;
    clear omega;
    ctcount=0;
    crcount=0;
    counter=1;
    offset=round(propstart(n,2)/wstep);
    for w=wstart:wstep:wend

        %*********************************************************
        % Find wavenumber.  If bisection method does not
        % converge, recalculate starting values and find
        % wavenumber again.
        %*********************************************************
        slope=pochkeval(w,cd,ct,a,k1,k2);
        [k,iter,slope]=pochbisect(w,cd,ct,a,kinc,k2,k1,slope);
        if slope==0
            fprintf(1,'Did not converge.  slope=%-2i\n',slope);
            if w==wstart
                kprev=k1;
            end
            k=kprev;
            kinc=dk/100;
            [k,kinc]=pochkfind(w,cd,ct,a,kinc,k);
            if (k>(5*dk+kprev))&(counter~=2)
                k=kprev+dk;
                fprintf(1,'k = kprev + dk\n')
            else
                k1=k-2*kinc;
                k2=k+kinc;
                slope=pochkeval(w,cd,ct,a,k1,k2);
                fprintf(1,'slope=%-2i\n',slope);
                [k,iter,slope]=pochbisect(w,cd,ct,a,kinc,k2,k1,slope);
            end
        end

        %*********************************************************
        % Progress statement, displays mode and frequency
        %*********************************************************
        fprintf(1,'w=%-8i  k=%-6.4f  iter=%-3i  counter=%-5i  mode=%-2i\n',...
               w,k,iter,counter,n);

        %*********************************************************
        % Write values of wavenumber and phase velocity to
        % martix 'results'.
        %*********************************************************
```

```
        freqroots(counter)=real(w);
        wavenum(counter)=real(k);
        results(counter+offset-1,1+2*(n-1))=wavenum(counter);
        results(counter+offset-1,2*n)=freqroots(counter)/wavenum(counter);
        iters(counter)=iter;

        %*********************************************************
        % Calculate parameters for next step
        %*********************************************************
        if counter==1
            k1=propstart(n,4)-2*propstart(n,6);
            k2=propstart(n,4)+2*propstart(n,6);
            k1prev=k1;
            kprev=k;
            kstepprev=abs(propstart(n,4)-propstart(n,1));
        else
            dw=wstep;
            dk=k-kprev;
            dwdk(counter-1)=(dw/dk)/cb; %group velocity
            omega(counter-1)=freqroots(counter);
            kstep=k-kprev;
            kprev=k;
            k=k+kstep;
            deltakstep=abs(kstep-kstepprev);
            if (deltakstep/kstep)<0.01
                deltakstep=0.01*kstep;
            end
            k1=k-10*deltakstep;
            k2=k+10*deltakstep;
            k1prev=k1;
            kstepprev=kstep;
        end
        counter=counter+1;
    end
    figure(1) % plot phase velocity curve
    plot(freqroots/(2*pi), (freqroots./(wavenum))/sqrt(E/rho),'k')
    figure(2) % plot group velocity curve
    plot(omega/(2*pi),dwdk,'k')
    pause(2)
end

%*********************************************************************
% Write data to file.  k and cp
%*********************************************************************
wrtfile=1;
if wrtfile==1;
    file='format.txt';
    fid=fopen(file,'w+');
    for i=1:1:num-1
        count=fprintf(fid,'%%12.4f\\t %%10.6f\\t ');
    end
    count=fprintf(fid,'%%12.4f\\t %%10.6f\\n');
    fclose(fid);
    format=textread(file,'%c','whitespace','\t').';

    fid=fopen('quartz25_nu16_2Mhz.dat','w');
    fprintf(fid,format,results.');
    fclose(fid);
end

hold off


%*********************************************************************
% end of script
%*********************************************************************
```

```
%*********************************************************************
%                          POCHKEVAL.M
%*********************************************************************
% This Matlab file evaluates the values of k1 and k2 to determine
% if the slope is positive or negative.  If the values of k1 and k2
% are not on either side of zero, the slope is set equal to zero.
%
% Written by Anthony Puckett, February 2001.
%
%*********************************************************************
%              Variables
%*********************************************************************
% k - wavenumber.
% kinc - k increment. This is made smaller at first in order to
%        make sure small wave number roots are found.
% ksize - used to adjust the the size od kinc.
% value - real value of the frequency equation.
% freq - Pochhammer frequency equation, should equal zero
%*********************************************************************
function slope=pochkeval(w,cd,ct,a,k1,k2)

freqk1=pochfreqvalue(w,cd,ct,a,k1);

freqk2=pochfreqvalue(w,cd,ct,a,k2);

if sign(real(freqk2))-sign(real(freqk1))==2
    slope=1;
elseif sign(real(freqk2))-sign(real(freqk1))==-2
    slope=-1;
else
    slope=0;
end

%*********************************************************************
% end of script
%*********************************************************************
```

```
%*********************************************************************
%                          POCHFREQVALUE.M
%*********************************************************************
% This Matlab file calculates the value of Pochhammer-Chree freq.
% equation for a specific frequency and wavenumber.
%
% Written by Anthony Puckett, February 2001.
%
%*********************************************************************
%              Variables
%*********************************************************************
% freq - Pochhammer frequency equation evaluated at k
%*********************************************************************
function freq=pochfreqvalue(w,cd,ct,a,k)

p=sqrt((w^2/cd^2)-k^2);
q=sqrt((w^2/ct^2)-k^2);
freq=k^2*q*besselj(0,q*a)/besselj(1,q*a)-0.5*((w/ct)^2)/a+...
    (0.5*(w/ct)^2-k^2)^2*(besselj(0,p*a)/(p*besselj(1,p*a)));

%*********************************************************************
% end of script
%*********************************************************************
```

```
%*********************************************************************
%                          POCHBISECT.M
%*********************************************************************
% This Matlab file uses a bisection method to find the wavenumber
% for a specific frequency and mode.
%
% Written by Anthony Puckett, February 2001.
%
%*********************************************************************
%              Variables
%*********************************************************************
% deltak - difference between k1 and k2, used to find k
% k1 - lower point of bisection
% k2 - upper point of bisection
% freq - Pochhammer frequency equation, should equal zero
%*********************************************************************
function [k,iter,slope]=pochbisect(w,cd,ct,a,kinc,k2,k1,slope)

oldk=0;
iter=0;
goodcount=0;
while goodcount<4 & iter<300
    deltak=k2-k1;
    deltak=0.5*deltak;
    k=k1+deltak;
    freq=pochfreqvalue(w,cd,ct,a,k);

    if abs(oldk-k)<0.0001 & abs(freq)<1
        goodcount=goodcount+1;
    else
        goodcount=0;
    end

    if slope==1;
        if freq<0
            k1=k;
        elseif freq==0
            goodcount=4;
        else
            k2=k;
        end
    elseif slope==-1
        if freq>0
            k1=k;
        elseif freq==0
            goodcount=4;
        else
            k2=k;
        end
    else
        goodcount=4;
    end

    iter=iter+1;
    oldk=k;
end

if iter==300
    freq1=pochfreqvalue(w,cd,ct,a,k);
    freq2=pochfreqvalue(w,cd,ct,a,k+deltak);
    freq3=pochfreqvalue(w,cd,ct,a,k+2*deltak);
    if (sign(freq3-freq2)-sign(freq2-freq1))~=0
        slope=0;
    else
        slope=slope;
    end
end

%*********************************************************************
% end of script
%*********************************************************************
```

```
%*********************************************************************
%                          POCHKFIND.M
%*********************************************************************
% This Matlab file increments the value of k until a root is
% found.
%
% Written by Anthony Puckett, February 2001.
%
%*********************************************************************
%              Variables
%*********************************************************************
% k - wavenumber.
% kinc - k increment. This is made smaller at first in order to
%        make sure small wave number roots are found.
% ksize - used to adjust the the size of kinc.
% value - real value of the frequency equation.
% freq - Pochhammer frequency equation, should equal zero
%*********************************************************************
function [k,kinc]=pochkfind(w,cd,ct,a,kinc,k)

value(3)=1;
value(2)=1;
value(1)=1;
count=3;
while ~((abs(sign(value(count))-sign(value(count-1)))==2)&...
      ((sign(value(count)-value(count-1))-sign(value(count-1)-value(count-2)))==0))
    count=count+1;
    freq=pochfreqvalue(w,cd,ct,a,k);
    value(count)=real(freq);
    if count==500
        kinc=kinc*20;
    end
    k=k+kinc;
sign(value(count)-value(count-1))-sign(value(count-1)-value(count-2)));
end
%*********************************************************************
% end of script
%*********************************************************************
```

```
%*********************************************************************
%                        POCHDISPCURVIMAG.M
%*********************************************************************
% This MATLAB file computes the imaginary portion of a dispersion
% curve for the given material properties.
%
% The dispersion curves are calcuted by stepping the frequency, w
% and using a bisection method to find the wavenumber.
%

% Written by Anthony Puckett, February 2001.
%
%*********************************************************************
%              Initialize Variables
%*********************************************************************

load properties
clear i;

    startk=450*i; % initial k
    wstart=1863*wstep; % start frequency
    wend=2548*wstep; % end frequency
    clear freqroots;
    clear wavenum;
    clear compval;
    counter=1;
    for w=wstart:wstep:wend
        if counter==1
            k=startk;
            pochkfindimag
            pochbisectimag
            freqroots(counter)=real(w);
            wavenum(counter)=imag(k);
            fprintf(1,'w=%-8i  k=%-6.4f  iter=%-3i  counter=%-5i  mode=%-2i\n',...
               w,imag(k),iter,counter,n);
            kprev=k;
        elseif counter==2
            k=startk;
            pochkfindimag
            pochbisectimag
            freqroots(counter)=real(w);
            wavenum(counter)=imag(k);
            fprintf(1,'w=%-8i  k=%-6.4f  iter=%-3i  counter=%-5i  mode=%-2i\n',...
               w,imag(k),iter,counter,n);
            oldkstep=k-kprev;
            kprev=k;
        elseif counter==3
            k=startk;
            pochkfindimag
            pochbisectimag
            freqroots(counter)=real(w);
            wavenum(counter)=imag(k);
            fprintf(1,'w=%-8i  k=%-6.4f  iter=%-3i  counter=%-5i  mode=%-2i\n',...
               w,imag(k),iter,counter,n);
            kstep=k-kprev;
            kprev=k;
            k=k+kstep;
            deltakstep=i*abs(imag(kstep-oldkstep));
            k1=k-10*deltakstep;
            k2=k+10*deltakstep;
            oldk=k1;
            oldkstep=kstep;
        else
            ksize=1;
            pochbisectimag;
            if iter>199
                k=0;
                pochkfindimag;
                k1=k-3*kinc/ksize;
                k2=k+3*kinc/ksize;
                pochbisectimag;
```

```
            end
            fprintf(1,'w=%-8i  k=%-6.4f  iter=%-3i  counter=%-5i  mode=%-2i\n',...
               w,imag(k),iter,counter,n);
            freqroots(counter)=real(w);
            wavenum(counter)=imag(k);
            kstep=k-kprev;
            kprev=k;
            k=k+kstep;
            deltakstep=i*abs(imag(kstep-oldkstep));
            k1=k-10*deltakstep;
            k2=k+10*deltakstep;
            oldk=k1;
            oldkstep=kstep;
        end
        compval(counter,1)=w;
        compval(counter,2)=wavenum(counter);
        counter=counter+1;
    end
    figure(1)
    plot(freqroots, wavenum)

%*********************************************************************
% Write imaginary wavenumber
%*********************************************************************
fid=fopen('C:\WINDOWS\Desktop\Research\matlab code\dispersion
model\steel_10\imagk5c_5r_st10.dat','w');
fprintf(fid,'%12.4f  %10.6f\n',compval.');
fclose(fid);
%*********************************************************************
% end of script
%*********************************************************************
```

```
%*********************************************************************
%                          POCHKFINDIMAG.M
%*********************************************************************
% This Matlab file increments the value of k until a root is
% found.
%
% Written by Anthony Puckett, February 2001.
%
%*********************************************************************
%              Variables
%*********************************************************************
% k - wavenumber.
% kinc - k increment. This is made smaller at first in order to
%        make sure small wave number roots are found.
% ksize - used to adjust the the size od kinc.
% value - real value of the frequency equation.
%*********************************************************************
clear j
value(3)=1;
value(2)=1;
value(1)=1;
count=3;
kinc=0.2*j;

% The while statement requires the sign of the slope to not change
% when the sign of the frequency equation does change.  This eliminates
% poles from the roots.

while ~((abs(sign(value(count))-sign(value(count-1)))==2)&((sign(value(count)-...
       value(count-1))-sign(value(count-1)-value(count-2)))==0))
    count=count+1;
    p=sqrt((w^2/cd^2)-k^2);
    q=sqrt((w^2/ct^2)-k^2);

    freq1=k^2*q*besselj(0,q*a)/besselj(1,q*a);
    freq2=-0.5*((w/ct)^2)/a;
    freq3=(0.5*(w/ct)^2-k^2)^2*(besselj(0,p*a)/(p*besselj(1,p*a)));
    freq=freq1+freq2+freq3;
    freqsign=sign(real(freq));
    value(count)=real(freq);
    if count==500
        kinc=0.05*j;
    end
    k=k+kinc;
end

k1=k-4*kinc;
k2=k+2*kinc;
%*********************************************************************
% end of script
%*********************************************************************
```

```
%*********************************************************************
%                          POCHBISECTIMAG.M
%*********************************************************************
% This Matlab file uses a bisection method to find the wavenumber
% for a specific frequency and mode.
%
% Written by Anthony Puckett, February 2001.
%
%*********************************************************************
%              Variables
%*********************************************************************
% deltak - difference between k1 and k2, used to find k
% k1 - lower point of bisection
% k2 - upper point of bisection
%*********************************************************************
oldk=0;
iter=0;
goodcount=0;
while goodcount<success & iter<300
    deltak=k2-k1;
    deltak=0.5*deltak;
    k=k1+deltak;
    p=sqrt((w^2/cd^2)-k^2);
    q=sqrt((w^2/ct^2)-k^2);
    freq1=k^2*q*besselj(0,q*a)/besselj(1,q*a);
    freq2=-0.5*((w/ct)^2)/a;
    freq3=(0.5*(w/ct)^2-k^2)^2*(besselj(0,p*a)/(p*besselj(1,p*a)));
    freq=freq1+freq2+freq3;

    if abs(oldk-k)<0.001*kratio & abs(freq)<kratio
         goodcount=goodcount+1;
    else
         goodcount=0;
    end

    if freqsign==1
        if freq<0
         k1=k;
        elseif freq==0
            goodcount=4;
        else
            k2=k;
        end
    else
        if freq>0
         k1=k;
        elseif freq==0
            goodcount=4;
        else
            k2=k;
        end
    end
    iter=iter+1;
    oldk=k;
end
%*********************************************************************
% end of script
%*********************************************************************
```

```
%*****************************************************************
%                        POCHDISPCURVCMPLX.M
%*****************************************************************
% This MATLAB file computes the complex portion of a dispersion
% curve for the given material properties.
%
% The dispersion curves are calcuted by stepping the frequency, w
% and using a bisection method to find the wavenumber.
%

% Written by Anthony Puckett, February 2001.
%
%*****************************************************************
%              Initialize Variables
%*****************************************************************

load properties

counter=1;
clear waver;
clear wavei;
clear compval;
clear freqrad;

kr=415.3232;
ki=3119.30;
oldk=kr+ki*j;
wend=4000*wstep;
tlen=1e12;
for w=wstep:wstep:wend
    iter=1;
    goodcount=0;
    while goodcount<success & iter<100
        [t,y] = ode15s(@davidenko,[0 tlen],[kr; ki],[],w,cd,ct,a);
        kr=y(length(t),1);
        ki=y(length(t),2);
        k=kr+ki*j;
        if abs(oldk-k)<0.001
            goodcount=goodcount+1;
        else
            goodcount=0;
        end
        oldk=k;
        iter=iter+1;
    end
    fprintf(1,'w=%-8i  kreal=%-6.4f  kimag=%-6.4f  counter=%-5i  iter=%-4i\n',...
       w,kr,ki,counter, iter);
    freqrad(counter)=w;
    waver(counter)=kr;
    if ki<0
        ki=-ki;
    end
    wavei(counter)=ki;
    compval(counter,1)=w;
    compval(counter,2)=kr;
    compval(counter,3)=ki;
    counter=counter+1;
end
figure(1)
plot(freqrad,waver,freqrad,wavei);

%*****************************************************************
% Write complex wavenumber
%*****************************************************************
fid=fopen('complexk89_q10.dat','w');
fprintf(fid,'%12.4f   %10.6f  %10.6f\n',compval.');
fclose(fid);
%*****************************************************************
% end of script
%*****************************************************************
```

```
%*********************************************************************
%                              DAVIDENKO.M
%*********************************************************************
% This MATLAB file uses Davidenko's method to find the complex
% wavenumbers for the evanescent modes.
%*********************************************************************

function dydt=davidenko(t,y,w,cd,ct,a)

k=y(1)+j*y(2);

p=sqrt((w^2/cd^2)-k^2);
q=sqrt((w^2/ct^2)-k^2);
dpdk=-k./sqrt((w^2/cd^2)-k^2);
dqdk=-k./sqrt((w^2/ct^2)-k^2);
dq2dk=-2*k;

freq1=k^2*q*besselj(0,q*a)/besselj(1,q*a);
freq2=-0.5*((w/ct)^2)/a;
freq3=(0.5*(w/ct)^2-k^2)^2*(besselj(0,p*a)/(p*besselj(1,p*a)));
freq=freq1+freq2+freq3;

d1freq1=k*2*q*besselj(0,q*a)/besselj(1,q*a);
d2freq1=k^2*dqdk*besselj(0,q*a)/besselj(1,q*a);
d3freq1=-k^2*dqdk*a*q;
d4freq1=k^2*dqdk*a*q*(-besselj(0,q*a))*0.5*(besselj(0,q*a)-...
        besselj(2,q*a))/(besselj(1,q*a))^2;

dfreq2=0;

d1freq3=2*(0.5*(w/ct)^2-k^2)*(-2)*k*(besselj(0,p*a)/(p*besselj(1,p*a)));
d2freq3=(0.5*(w/ct)^2-k^2)^2*(-dpdk/p^2)*besselj(0,p*a)/besselj(1,p*a);
d3freq3=(0.5*(w/ct)^2-k^2)^2*(-dpdk*a*p);
d4freq3=(0.5*(w/ct)^2-k^2)^2*dpdk*a*(-besselj(0,p*a))*0.5*(besselj(0,p*a)-...
        besselj(2,p*a))/(besselj(1,p*a))^2;

dfreq1=d1freq1+d2freq1+d3freq1+d4freq1;
dfreq3=d1freq3+d2freq3+d3freq3+d4freq3;
dfreq=dfreq1+dfreq2+dfreq3;

drealdt=-(1/((real(dfreq))^2+(imag(dfreq))^2))*(real(freq)*real(dfreq)+...
        imag(freq)*imag(dfreq));
dimagdt=(1/((real(dfreq))^2+(imag(dfreq))^2))*(real(freq)*imag(dfreq)-...
        imag(freq)*real(dfreq));

dydt=[ drealdt;dimagdt ];

%*********************************************************************
% end of script
%*********************************************************************
```

APPENDIX D. ANALYTICAL MODEL

The analytical model uses the dispersion curves to calculate the phase velocities and stress functions for each of the modes. The file VELOCITIES.M combines the real, imaginary, and complex wavenumbers into a single set of dispersion curves. A lot of manual effort is required to determine the frequencies where each dispersion curve changes from complex to real or imaginary. The higher modes change from complex to imaginary many times before becoming real.

The linear nature of the model allows the components of the transfer functions from the end conditions to be calculated separately from the components from the propagation. Therefore, the end conditions can be calculated for a specific diameter and material waveguide separate from the propagation, which is based on the length of the bar. The calculation of the propagation does not require nearly as much computation as the end conditions, so different length bars can be considered easily.

The MATLAB code for determining the transfer functions of the waveguides, as well as finding the dispersed signals is included. The programs for the consideration of the propagating and evanescent modes are presented as well as the programs for considering just the propagating modes. In both cases POCHPROP.M should be run first to make sure the necessary material properties are available.

The files for consideration of the real and evanescent modes are presented first. VELOCITIES_Q10_NU16_COMPLEX.M provides the complex dispersion curves for a 10 mm diameter fused quartz rod. The file Q10_EXCITE_5MODE_COMPLEX.M calculates the transfer functions of the end conditions, and the file Q10_DISPSIGCALC_COMPLEX.M calculates the dispersion function and the dispersed signal. The files for the consideration of just the propagating modes are then presented, VELOCITIES_Q25_NU16.M, Q25_EXCITE_7MODE.M, Q25_DISPSIGCALC.M.

```
%*********************************************************************
%                      VELOCITIES_Q10_NU16_COMPLEX.M
%*********************************************************************
%   This program puts the necessary information in a matrix called
%   modes for the analytical dispersion program.  The values for
%   the real, complex, and imaginary modes are read into the program.
%*********************************************************************

%   Read files containing dispersion curves
[mode1] = textread('quartz010_nu16_complex_mode01.dat');
[mode2] = textread('quartz010_nu16_complex_mode02.dat');
[mode3] = textread('quartz010_nu16_complex_mode03.dat');
[mode4] = textread('quartz010_nu16_complex_mode04.dat');
[mode5] = textread('quartz010_nu16_complex_mode05.dat');
[mode6] = textread('quartz010_nu16_complex_mode06.dat');
[mode7] = textread('quartz010_nu16_complex_mode07.dat');
[mode8] = textread('quartz010_nu16_complex_mode08.dat');

[mode23_complex] = textread('complexk23_q10.dat');
[mode45_complex] = textread('complexk45_q10.dat');
[mode67_complex] = textread('complexk67_q10.dat');
[mode89_complex] = textread('complexk89_q10.dat');
[mode3_imag] = textread('imagk3i_3r_q10.dat');
[mode4_imag] = textread('imagk4c_4r_q10.dat');
[mode5_imag] = textread('imagk5c_5r_q10.dat');

%  Combination of modes.  Only the wavenumbers are recorded.  All files
%  and modes have the same frequency step.  Odd columns are the real
%  part of the wavenumber and even columns are the imaginary part.

clear modes
nrow=5000;

modes(1:nrow,1,1)=mode1(1:nrow,1);
modes(1:nrow,1,2)=0;

modes(1:936,2,1)=mode23_complex(1:936,2);
modes(1:936,2,2)=mode23_complex(1:936,3);
modes(937:nrow,2,1)=mode2(937:nrow,1);
modes(937:nrow,2,2)=0;

modes(1:936,3,1)=-mode23_complex(1:936,2);
modes(1:936,3,2)=mode23_complex(1:936,3);
modes(937:nrow,3,1)=mode3(937:nrow,1);
modes(937:nrow,3,2)=0;
modes(977:1199,3,1)=0;
modes(977:1199,3,2)=mode3_imag(:,2);

modes(1:2186,4,1)=mode45_complex(1:2186,2);
modes(1:2186,4,2)=mode45_complex(1:2186,3);
modes(2187:2196,4,1)=0;
modes(2187:2196,4,2)=mode4_imag(:,2);
modes(2197:nrow,4,1)=mode4(2197:nrow,1);
modes(2197:nrow,4,2)=0;

modes(1:2186,5,1)=-mode45_complex(1:2186,2);
modes(1:2186,5,2)=mode45_complex(1:2186,3);
modes(2187:2647,5,1)=0;
modes(2187:2647,5,2)=mode5_imag(:,2);
modes(2648:nrow,5,1)=mode5(2648:nrow,1);
modes(2648:nrow,5,2)=0;

modes(1:nrow,6,1)=mode6(1:nrow,1);
modes(1:nrow,6,2)=0;
modes(1:2905,6,1)=mode67_complex(1:2905,2);
modes(1:2905,6,2)=mode67_complex(1:2905,3);

modes(1:nrow,7,1)=mode7(1:nrow,1);
modes(1:nrow,7,2)=0;
modes(1:2905,7,1)=-mode67_complex(1:2905,2);
modes(1:2905,7,2)=mode67_complex(1:2905,3);
```

```
modes(1:nrow,8,1)=mode8(1:nrow,1);
modes(1:nrow,8,2)=0;
modes(1:3898,8,1)=mode89_complex(1:3898,2);
modes(1:3898,8,2)=mode89_complex(1:3898,3);

modes(1:3898,9,1)=-mode89_complex(1:3898,2);
modes(1:3898,9,2)=mode89_complex(1:3898,3);

clear mode1
clear mode2
clear mode3
clear mode4
clear mode5
clear mode6
clear mode7
clear mode8
clear mode23_complex
clear mode45_complex
clear mode67_complex
clear mode89_complex
clear mode3_imag
clear mode4_imag
clear mode5_imag

%*********************************************************************
% end of script
%*********************************************************************
```

```
%*********************************************************************
%                      Q10_EXCITE_5MODE_COMPLEX.M
%*********************************************************************
%   This program calculates the transfer
%   function for the end conditions
%*********************************************************************
%   The least squares method is used in the expansion to determine
%   the relative mode amplitudes.
%
%   Only 5 modes are considered for the expansion. Modes with
%   imaginary wavenumbers are not considered in the expansion.
%*********************************************************************
load properties;

%   The dispersion curves are specified
%   by the program velocities_q10_nu16_complex.

velocities_q10_nu16_complex
[A B C]=size(modes);
mode=B;
clear XD
clear XD1
clear x
clear i
clear dfunc
clear DISP
clear modemag
clear excamp
clear modeamp
clear modeint
clear C
hfreq=5000; % Highest frequency in terms of the frequency step
timestep=deltat;
modelow=1;
modehigh=5;
tol(1:8)=1e-6; % tolerance for the integration
points=50; % number of points along the radius in the expansion

%   The amplitude is calculated at each frequency.
for h=1:1:hfreq
    w=h*wstep;
    clearvar

    %   The number of propagating modes is calculated at each frequency.

    propmode=5;
    for j=2:mode
        if w >= freqstot(j,1)*2*pi
            propmode=j;
        end
        if propmode < 5
            propmode=5;
        end
    end

    %   The wavenumber is acquired for each mode at each frequency.
    for j=1:propmode
        wnum(j)=modes(h,j,1)+i*modes(h,j,2);
    end
    fprintf(1,'step=%-8i  modelow=%-2i   modehigh=%-2i    count=%-3i\n',...
        h,modelow,modehigh,count);

    if propmode<6
        modelow=1;
        modehigh=5;
    end

    %   Construct matrix of tzz
    clear tzz
    clear tzzsmall
    imagemode(1:propmode)=0;
```

```
    for m=modelow:modehigh
        k=wnum(m);
        if imag(k)~=0 & real(k)~=0 %complex wavenumbers
            p=sqrt((w^2/cd^2)-k^2);
            q=sqrt((w^2/ct^2)-k^2);
            A=(q^2-k^2)*bessel(1,q*a)/(-2*i*k*p*bessel(1,p*a));
            for n=1:points/2;
                PI(n,1)=1;
                r=(n-1)*a/(points/2-1);
                tauz=-A*bessel(0,p*r)*(lambda*(k^2+p^2)+2*mu*k^2)+...
                        bessel(0,q*r)*i*q*2*mu*k;
                tzz(n,m)=(tauz);
            end
            for n=points/2+1:points
                PI(n,1)=0;
                r=(n-points/2-1)*a/(points-points/2-1);
                taurz=-mu*(A*2*i*k*p*bessel(1,p*r)+(q^2-k^2)*bessel(1,q*r));
                tzz(n,m)=taurz;
            end
        elseif imag(k)~=0 % modes with imaginary wavenumbers are ignored
            tzz(:,m)=0;
            imagemode(m)=1;
        else
            p=sqrt((w^2/cd^2)-k^2);
            q=sqrt((w^2/ct^2)-k^2);
            A=(q^2-k^2)*bessel(1,q*a)/(-2*i*k*p*bessel(1,p*a));
            % normal stress
            for n=1:points/2;
                PI(n,1)=1;
                r=(n-1)*a/(points/2-1);
                tauz=-A*bessel(0,p*r)*(lambda*(k^2+p^2)+2*mu*k^2)+...
                        bessel(0,q*r)*i*q*2*mu*k;
                tzz(n,m)=(tauz);
            end
            % shear stress
            for n=points/2+1:points
                PI(n,1)=0;
                r=(n-points/2-1)*a/(points-points/2-1);
                taurz=-mu*(A*2*i*k*p*bessel(1,p*r)+(q^2-k^2)*bessel(1,q*r));
                tzz(n,m)=taurz;
            end
            normdivs(m)=1;
            phashift(m)=angle(tzz(1,m)); % calculate phase shift
            tzz(:,m)=tzz(:,m)*exp(-i*phashift(m)); % remove phase shift and imaginary
component
             modeint(h,m)=quadl(@lsintegrate,0,a,tol(m),[0],wnum(m),phashift(m),...
                normdivs(m),w,cd,ct,mu,a,lambda); % calculate receiving end condition
            tol(m)=abs(modeint(h,m)*1e-6);
            modeint(h,m)=modeint(h,m)/(pi*a^2);
        end
    end

    % normalize stresses and receiving end conditions
    normdivstauz(h)=max(max(abs(tzz)));
    modeint(h,:)=modeint(h,:)/normdivstauz(h);
    tzz=tzz/normdivstauz(h);

    % Calculate mode amplitudes, imaginary modes are not included in the expansion
    tzzcount=1;
    clear tzzsmall
    clear Csmall
    clear modeloc
    for m=modelow:modehigh
        if imagemode(m)==0
            tzzsmall(:,tzzcount)=tzz(:,m);
            modeloc(tzzcount)=m;
            tzzcount=tzzcount+1;
        end
    end

    Csmall=(inv(tzzsmall.'*tzzsmall))*tzzsmall.'*PI; % Least squares
```

```
    for m=1:length(modeloc)
        excamp(h,modeloc(m))=Csmall(m);
    end

    for m=1:1:modehigh
        if imag(wnum(m))==0 & imagemode(m)==0;
            modeamp(h,m)=modeint(h,m)*excamp(h,m);
        end
    end
    [maxmodeint maxmodeind]=max(modeamp(h,:));
    if maxmodeind > 2
        modelow=maxmodeind-2;
        modehigh=maxmodeind+2;
    end

end

figure
plot((1:hfreq)*deltaf,excamp(1:hfreq,:))

%   Write excitation transfer function to file.

writesignal=0;
if writesignal==1
    file='format.txt';
    fid=fopen(file,'w+');
    for i=1:1:propmode-1
        count=fprintf(fid,'%8.4e\\t ');
    end
    count=fprintf(fid,'%8.4e\\n');
    fclose(fid);
    format=textread(file,'%c','whitespace','\t').';
    fid=fopen('q10_nu16_exciteamp_5mode_complex.dat','w');
    fprintf(fid,format,excamp.');
    fclose(fid);
end


figure
plot((1:hfreq)*deltaf,abs(modeamp(1:hfreq,1:modehigh)))

%   Write end condition transfer function to file.

writesignal=1;
if writesignal==1
    file='format.txt';
    fid=fopen(file,'w+');
    for i=1:1:modehigh-1
        count=fprintf(fid,'%8.4e\\t ');
    end
    count=fprintf(fid,'%8.4e\\n');
    fclose(fid);
    format=textread(file,'%c','whitespace','\t').';
    fid=fopen('q10_nu16_modeamp_5mcomplex.dat','w');
    fprintf(fid,format,real(modeamp).');
    fclose(fid);
end

%*********************************************************************
% end of script
%*********************************************************************
```

```
%*********************************************************************
%                        Q10_DISPSIGCALC_COMPLEX.M
%*********************************************************************
%   This program calculates the phase shift of each mode and uses
%   the transfer functions of the end conditions to calculate
%   the dispersed signal
%*********************************************************************
%   Only the propagating modes are considered in the propagation.
%*********************************************************************
clear all
load properties;

%   Specify the dispersion curves
velocities_q10_nu16_complex
[A B C]=size(modes);
mode=B;
clear XD
clear XD1
clear x
clear i
clear dfunc
clear DISP
clear modemag
clear C
clear count
D=48*0.0254;
hfreq=5000;
timestep=deltat;

% Read in the transfer functions of the end conditions
[C]=textread('q10_nu16_modeamp_5mcomplex_trz.dat');

% Specify the excitation signal, already in the frequency spectrum
[trandata] = textread('refsig.dat');
refsig=trandata(:,1)+i*trandata(:,2);
XR=refsig;

%   The amplitude is calculated at each frequency.
for h=1:1:hfreq
    w=h*wstep;
    clearvar

    %   The number of propagating modes is calculated at each frequency.

    propmode=length(C(1,:));

    %   The wavenumber is acquired for each mode at each frequency.
    count=0;
    for j=1:propmode
        if modes(h,j,2)==0 & modes(h,j,1)~=0
            count=count+1;
            wnum(count)=modes(h,j,1);
        end
    end
    fprintf(1,'step=%-8i  count=%-3i  ',h,count);

    %   Sum the REAL part of the modes at each frequency

    for m=1:1:count
        phvel(m)=w/real(wnum(m));
        if real(wnum(m))==0;
            Q(m)=0;
        else
            Q(m)=exp(-i*h*(D/phvel(m)/deltat)*(2*pi/N));
        end
        modtranfunc(h,m)=Q(m)*C(h,m);
        fprintf(1,'%-3i  ',m)
        modexfunc(h,m)=abs(modtranfunc(h,m));
    end
    fprintf(1,'\n')
    dfunc(h)=sum(modtranfunc(h,:));
```

```
    dfuncfile(h,1)=real(dfunc(h));
    dfuncfile(h,2)=imag(dfunc(h));

    %   Multiply frequency spectrum of input signal by the
    %   transfer function of the waveguide.
    XD(h+1)=dfunc(h)*XR(h+1);
end

%   Take the inverse transform.
XD=[XD.';zeros(N-hfreq,1)];
xd=ifft(XD);

num=count;
%   Write dispersed signal and dispersion function and transfer functions to files.
writesignal=1;
if writesignal==1
    fid=fopen('q10_nu16_1MHz_complex_trz.dat','w');
    fprintf(fid,'%8.4e\n',xd.');
    fclose(fid);
    fid=fopen('q10_nu16_dispxfunc_complex_trz.dat','w');
    fprintf(fid,'%8.4e    %8.4e\n',dfuncfile.');
    fclose(fid);

    file='format.txt';
    fid=fopen(file,'w+');
    for i=1:1:num-1
        count=fprintf(fid,'%%8.4e\\t  ');
    end
    count=fprintf(fid,'%%8.4e\\n');
    fclose(fid);
    format=textread(file,'%c','whitespace','\t').';
    fid=fopen('q10_nu16_modexfunc_complex_trz.dat','w');
    fprintf(fid,format,modexfunc.');
    fclose(fid);
end

figure
subplot(2,1,1);
plot(deltat:deltat:length(xd)*deltat,xd);
l=axis;
axis([0 (2^14-1)*deltat l(3) l(4)]);


%**********************************************************************
% end of script
%**********************************************************************
```

```
%*********************************************************************
%                        VELOCITIES_Q25_NU16.M
%*********************************************************************
%   This program puts the necessary information in a matrix called
%   'modes' for the analytical model.  Only the real modes are
%   considered
%*********************************************************************

%   Read files containing dispersion curves
[results] = textread('quartz025_nu16_4Mhz.dat');

%  Combination of modes.  Only the wavenumbers are recorded.
%  All files and modes have the same frequency step.
%  Odd columns are the real part of the wavenumber and even
%  columns are the imaginary part.

clear modes
nrow=10000;
[matlen matwid]=size(results);
for n=1:matwid/2
    modes(:,n,1)=results(1:nrow,2*n-1);
    modes(:,n,2)=zeros(nrow,1);
end
clear results

%*********************************************************************
% end of script
%*********************************************************************
```

```
%*********************************************************************
%                        Q25_EXCITE_7MODE.M
%*********************************************************************
%   This program calculates the transfer
%   function for the end conditions
%*********************************************************************
%   The least squares method is used in the expansion to determine
%   the relative mode amplitudes.
%
%   Only the real modes are considered in the expansion with a
%   maximum of 7 modes considered.
%*********************************************************************
load properties;

%   The dispersion curves are specified
velocities_q25_nu16_smooth
[A B C]=size(modes);
mode=B;
clear XD
clear XD1
clear x
clear 1
clear dfunc
clear DISP
clear modemag
clear C
hfreq=10000; % highest frequency
timestep=deltat;
modelow=1;
modehigh=0;

%   The amplitude is calculated at each frequency.
for h=1:1:hfreq
    w=h*wstep;
    clearvar

    %   The number of propagating modes is calculated at each frequency.

    propmode=1;
    for j=2:mode
        if w >= freqstot(j,1)*2*pi+2*wstep
            propmode=j;
        end
    end

    %   The wavenumber is acquired for each mode at each frequency.
    count=0;
    for j=1:propmode
        count=count+1;
        wnum(count)=modes(h,j,1);
    end

    fprintf(1,'step=%-8i  modelow=%-2i   modehigh=%-2i    count=%-3i\n',...
        h,modelow,modehigh,count);

    if count<8
        modelow=1;
        modehigh=count;
    elseif modehigh==0
        modelow=1;
        modehigh=count;
    end

    %   Construct matrix of tzz
    clear tzz
    clear tzzsmall
    for m=modelow:modehigh
        k=wnum(m);
        c=w/k;
        p=sqrt((w^2/cd^2)-k^2);
        q=sqrt((w^2/ct^2)-k^2);
```

```
        A=(q^2-k^2)*bessel(1,q*a)/(-2*i*k*p*bessel(1,p*a));
        for n=1:100;
            PI(n,1)=1;
            r=(n-1)*a/(100-1);
            tauz=-A*bessel(0,p*r)*(lambda*(k^2+p^2)+2*mu*k^2)+bessel(0,q*r)*i*q*2*mu*k;
            tzz(n,m)=(tauz);
        end
        phashift(m)=angle(tzz(1,m));
        tzz(:,m)=tzz(:,m)*exp(-i*phashift(m)); % remove phase shift and imaginary
                                               % component of stress
        normdivs(m)=real(max(tzz(:,m)));
        tzz(:,m)=real(tzz(:,m)/normdivs(m)); % normalize
    end

    % Calculate the average stress over the end of the cylinder

    for m=modelow:modehigh
       modeint(h,m)=quadl(@lsintegrate,0,a,1e-10,[0],wnum(m),...
              phashift(m),normdivs(m),w,cd,ct,mu,a,lambda);
       modeint(h,m)=modeint(h,m)/(pi*a^2);
    end
    [maxmodeint maxmodeind]=max(modeint(h,:));

    %   Calculate the relative amplitudes of each mode.

    clear C
    if count>7
        tzzsmall=tzz(:,modelow:modehigh);
        Csmall=(inv(tzzsmall.'*tzzsmall))*tzzsmall.'*PI;
        excamp(h,1:count)=0;
        excamp(h,modelow:modehigh)=Csmall.';
        modelow=maxmodeind-3;
        modehigh=maxmodeind+3;
    else
        C=(inv(tzz.'*tzz))*tzz.'*PI;
        excamp(h,1:count)=C.';
    end
end

figure
plot((1:hfreq)*deltaf,excamp)

%   Write excitation transfer functions to file.

writesignal=1;
if writesignal==1
    file='format.txt';
    fid=fopen(file,'w+');
    for i=1:1:propmode-1
        count=fprintf(fid,'%8.4e\\t ');
    end
    count=fprintf(fid,'%8.4e\\n');
    fclose(fid);
    format=textread(file,'%c','whitespace','\t').';
    fid=fopen('q25_nu16_exciteamp_sm7modeLS.dat','w');
    fprintf(fid,format,excamp.');
    fclose(fid);
end

for m=1:1:modehigh
    modeamp(:,m)=modeint(:,m).*excamp(:,m);
end

figure
plot((1:hfreq)*deltaf,modeamp)

%   Write transfer functions of the both end conditions to file.

writesignal=1;
if writesignal==1
    file='format.txt';
```

```
    fid=fopen(file,'w+');
    for i=1:1:modehigh-1
        count=fprintf(fid,'%%8.4e\\t ');
    end
    count=fprintf(fid,'%%8.4e\\n');
    fclose(fid);
    format=textread(file,'%c','whitespace','\t').';
    fid=fopen('q25_nu16_modeamp_sm7modeLS.dat','w');
    fprintf(fid,format,modeamp.');
    fclose(fid);
end

%*********************************************************************
% end of script
%*********************************************************************
```

```
%*********************************************************************
%                        Q25_DISPSIGCALC.M
%*********************************************************************
%   This program calculates the phase shift and transfer functions
%   for each mode and the dispersed signal.
%*********************************************************************
%   Only the real modes are considered.
%*********************************************************************
clear all
load properties;

%   The dispersion curves are specified
velocities_q25_nul6_smooth
[A B]=size(modes);
mode=B;
clear XD
clear XD1
clear x
clear i
clear dfunc
clear DISP
clear modemag
clear C
clear count
D=0.200; % length of waveguide
hfreq=5000;
timestep=deltat;

[C]=textread('q25_nul6_modeamp_sm9modeLS.dat');

%   The input signal and FFT of the signal is specified.
[trandata] = textread('refsig.dat');
refsig=trandata(:,1)+i*trandata(:,2); % Excitation signal, xr in the model
XR=refsig;

%   The amplitude is calculated at each frequency.
for h=1:1:hfreq
    w=h*wstep;
    clearvar

    %   The number of propagating modes is calculated at each frequency.

    propmode=1;
    for j=2:mode
        if w >= freqstot(j,1)*2*pi
            propmode=j;
        end
    end

    %   The wavenumber is acquired for each mode at each frequency.
    count=0;
    for j=1:propmode
        if j>propmode
        elseif modes(h,j)<=0;
        else
            count=count+1;
            wnum(count)=modes(h,j);
        end
    end
    fprintf(1,'step=%-8i  count=%-3i  ',h,count);


    %   Calculates the phase shift of each mode

    for m=1:1:count
        phvel(m)=w/real(wnum(m));
        if real(wnum(m))==0;
            Q(m)=0;
        else
            Q(m)=exp(-i*h*(D/phvel(m)/deltat)*(2*pi/N));
        end
```

```
        modtranfunc(h,m)=Q(m)*C(h,m);
        modedisp(h+1,m)=modtranfunc(h,m)*XR(h+1);
        modexfunc(h,m)=abs(modtranfunc(h,m));
    end
    fprintf(1,'\n')
    dfunc(h)=sum(modtranfunc(h,:));
    dfuncfile(h,1)=real(dfunc(h));
    dfuncfile(h,2)=imag(dfunc(h));

    %   Multiply frequency spectrum of input signal by the
    %   transfer function of the waveguide.
    XD(h+1)=dfunc(h)*XR(h+1);
end

%   Take the inverse transform.
XD=[XD.';zeros(N-hfreq,1)];
xd=ifft(XD);

num=count;
%   Write dispersed signal and dispersion functions to file.
writesignal=0;
if writesignal==1
    fid=fopen('q25_len200_nu16_1MHz.dat','w');
    fprintf(fid,'%8.4e\n',real(xd.'));
    fclose(fid);
    fid=fopen('q25_len200_nu16_dispxfunc.dat','w');
    fprintf(fid,'%8.4e    %8.4e\n',dfuncfile.');
    fclose(fid);

    file='format.txt';
    fid=fopen(file,'w+');
    for i=1:1:num-1
        count=fprintf(fid,'%%8.4e\\t  ');
    end
    count=fprintf(fid,'%%8.4e\\n');
    fclose(fid);
    format=textread(file,'%c','whitespace','\t').';
    fid=fopen('q25_len200_nu16_modexfunc.dat','w');
    fprintf(fid,format,modexfunc.');
    fclose(fid);
end

% Plotting statements for trailing pulses figure.
modesumw=[zeros(hfreq,1)];
figure
set(gcf,'Units','inches','Position',[1 -2 (4/5)*6 (4/5)*9])
for m=2:10
    modesumw(1:hfreq)=modesumw(1:hfreq)+modedisp(1:hfreq,m);
    modesig(:,m)=ifft([modedisp(1:hfreq,m);zeros(N-hfreq,1)]);

    subplot(11,2,2*m-3);
    plot(deltat:deltat:length(modesig)*deltat,modesig(:,m),'k');
    l=axis;
    axis([3e-5 8e-5 -0.05 0.05]);
    set(gca,'yticklabel',{},'xticklabel',{},'Units','inches','Position',...
        [(4/5)*.25 (4/5)*(9-(m-1)*0.625-(m-1)*0.125) (4/5)*2.5 (4/5)*0.625])
    file='file.txt';
    fid=fopen(file,'w+');
    fprintf(fid,'L(0,%1i)',m);
    fclose(fid);
    textlabel=textread(file,'%c','whitespace','\t').';
    text(7e-5,0.03,textlabel,'FontSize',8,'FontName','times')%,'FontWeight','Bold')
    subplot(11,2,2*(m-1));
    plot(0:wstep/(2*pi):wstep/(2*pi)*(hfreq-1),abs(modedisp((1:hfreq),m)),'k');
    l=axis;
    axis([l(1) l(2) 0 15]);
    set(gca,'yticklabel',{},'xticklabel',{},'Units','inches','Position',...
        [(4/5)*3.25 (4/5)*(9-(m-1)*0.625-(m-1)*0.125) (4/5)*2.5 (4/5)*0.625])
    text(1.6e6,12,textlabel,'FontSize',8,'FontName','times')%,'FontWeight','Bold')
end
```

```
modesumt=ifft([modesumw(1:hfreq);zeros(N-hfreq,1)]);

subplot(11,2,19);
plot(deltat:deltat:length(modesumt)*deltat,modesumt,'k');
l=axis;
axis([3e-5 8e-5 -0.15 0.15]);
set(gca,'yticklabel',{},'xticklabel',{},'Units','inches','Position',...
        [(4/5)*.25 (4/5)*(9-12*0.625-4*0.125) (4/5)*2.5 (4/5)*1.875])
text(7e-5,0.13,'signal','FontSize',8,'FontName','times')%,'FontWeight','Bold')
xlabel('time','FontSize',8,'FontName','times')
subplot(11,2,20);
plot(0:wstep/(2*pi):wstep/(2*pi)*(hfreq-1),abs(modedisp(1:hfreq,:)),'k');
l=axis;
axis([l(1) l(2) 0 15]);
set(gca,'yticklabel',{},'xticklabel',{},'Units','inches','Position',...
        [(4/5)*3.25 (4/5)*(9-10*0.625-4*0.125) (4/5)*2.5 (4/5)*0.625])
text(1.5e6,12,'all modes','FontSize',8,'FontName','times')%,'FontWeight','Bold')
subplot(11,2,22);
plot(0:wstep/(2*pi):wstep/(2*pi)*(hfreq-1),abs(modesumw((1:hfreq))),'k');
l=axis;
axis([l(1) l(2) 0 15]);
set(gca,'yticklabel',{},'xticklabel',{},'Units','inches','Position',...
        [(4/5)*3.25 (4/5)*(9-12*0.625-4*0.125) (4/5)*2.5 (4/5)*0.625])
text(1.6e6,12,'signal','FontSize',8,'FontName','times')%,'FontWeight','Bold')
xlabel('frequency','FontSize',8,'FontName','times')

%*********************************************************************
% end of script
%*********************************************************************
```

APPENDIX E. TRANSFER FUNCTIONS

The transfer functions of the modes are a combination of the excitation end conditions and reception end conditions, each of which is represented by a set of transfer functions. The shape of these transfer functions vary depending on what scheme is used to normalize the stress functions. For this research the stress function of each mode was divided by the maximum stress of the mode. However, regardless of how the stress functions are normalized, the multiplication of the transfer functions of excitation end conditions and the transfer functions of the reception end conditions will always create the same transfer functions for the modes. Fig. E1. shows the excitation transfer functions and reception transfer functions for the stress functions normalized by the maximum value of the stress.

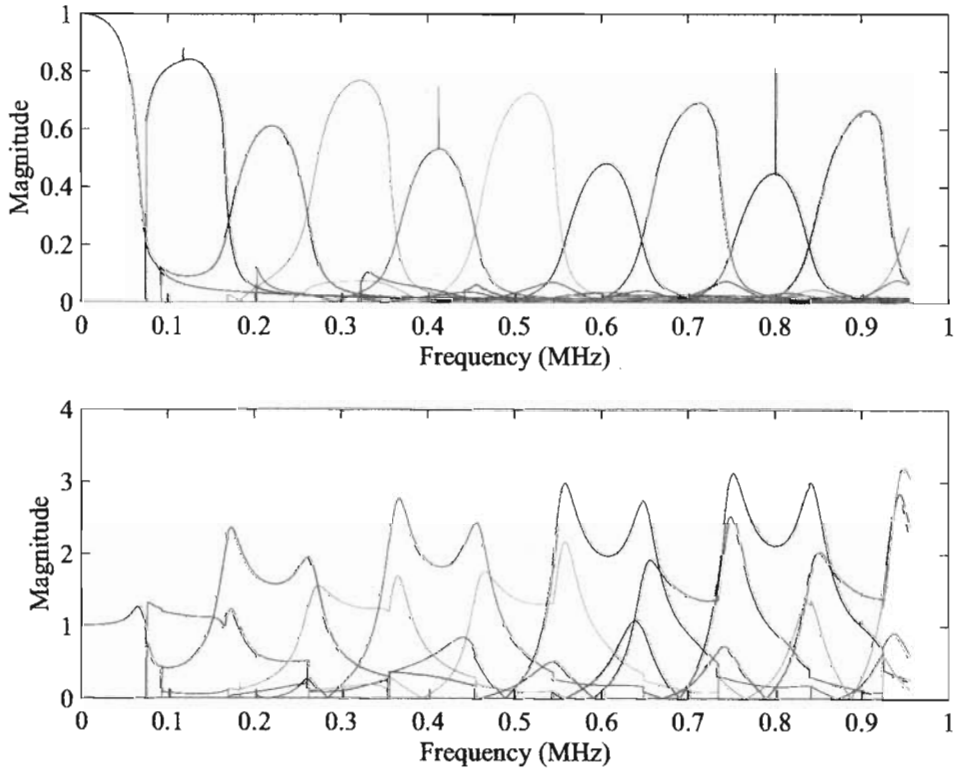

Fig. E1. Transfer functions of the excitation (left) and reception (right) end conditions.

If the excitation end conditions change then the transfer functions of the excitation end conditions change as do the transfer functions of the modes. Fig. E2 shows the transfer functions for a number of different pressure distributions of the excitation. The magnitudes of the transfer functions change because the maximum amplitudes of each pressure distributions is the same and not the average pressure. Therefore,

there is less energy in the nonuniform pressure distributions. A closer look at the versine pressure distribution shows some interesting results, Fig. E3. There are two noticeable differences between the transfer functions from the versine distribution and the transfer functions from the uniform distribution. First, the transfer functions of the versine distribution have a wider bandwidth with a different shape. Second, the location of the transfer function of each mode is shifted to the left. Both of these are due to the shape of the versine. The versine pressure distribution is closest in shape to a Bessel function, which appears in the stress functions of the modes. It is crucial that the boundary conditions on the bar ends are well understood for accurate comparison to experiments.

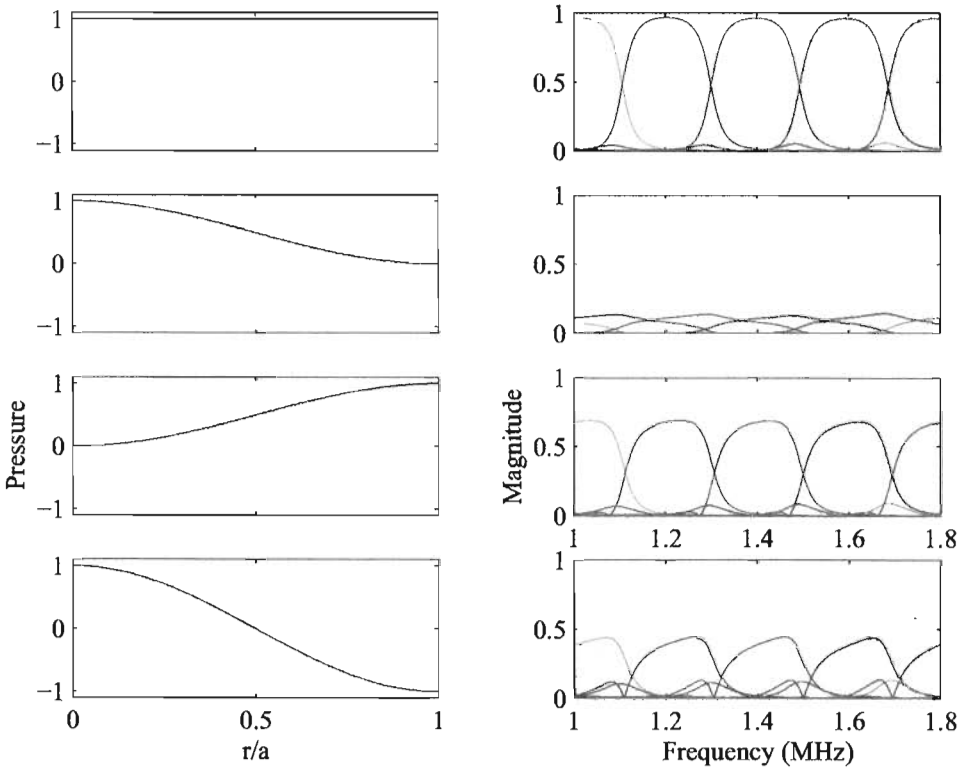

Fig. E2. Comparison of the transfer functions (right) for different pressure distributions (right) for the excitation. Top to bottom the pressure distributions are uniform, versine, haversine, and cosine.

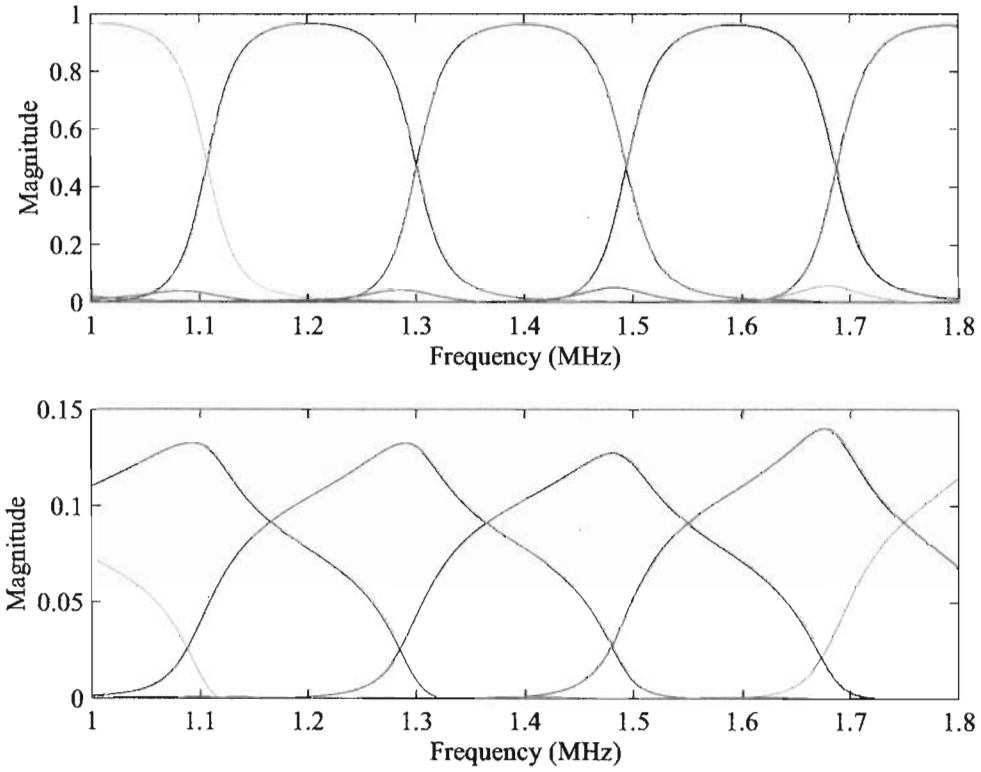

Fig. E3. Comparison of the transfer functions of the modes for a uniform pressure distribution (top) and a versine pressure distribution (bottom).

BIOGRAPHY OF THE AUTHOR

Anthony Puckett was born and raised in Los Alamos, New Mexico. He graduated from Los Alamos High School in 1993 and enrolled in the Department of Mechanical Engineering at Colorado State University. He spent his sophomore year studying Mechanical Engineering at the University of Bath in Bath, England. In 1998 Anthony received his Bachelor of Science degree in Mechanical Engineering with a minor in mathematics from Colorado State University, and in 2000 he received his Master's of Science degree in Mechanical Engineering. His Master thesis research on finite element modeling of axially symmetric waves in cylindrical waveguides was conducted at Los Alamos National Laboratory. In the winter of 2001 he entered the Mechanical Engineering graduate program at the University of Maine.

During his tenure at the University of Maine Anthony has published journal articles in *Ultrasonics*, *Acoustic Research Letters Online* and *Experimental Techniques*. Anthony has also coauthored a number of conference papers. Anthony is a member of the Acoustical Society of America (ASA), the American Society of Mechanical Engineers (ASME), and the Society for Experimental Mechanics (SEM). He is also a member of the mechanical engineering honor society Pi Tau Sigma, the engineering honor society Tau Beta Pi, and the multidisciplinary honor society Phi Kappa Phi.

After receiving his degree, Anthony will be traveling back to New Mexico for a postdoctoral position at Los Alamos National Laboratory. Anthony is a candidate for the Doctor of Philosophy degree in Mechanical Engineering from The University of Maine in May, 2004.